# Reference dosimetry of HDR Ir-192 sources using radiochromic film

Saad Aldelaijan

Medical Physics Unit

McGill University, Montreal

May 2010

A thesis submitted to McGill University in partial fulfillment of the requirements of the degree of Master of Science

# Table of Contents

## Abstract

A protocol of establishing radiochromic film based reference dosimetry for high dose rate Ir-192 brachytherapy source was assessed and described. A comparison between calibration curves created in water and Solid Water$^{TM}$ are provided. Solid Water$^{TM}$ was shown to be a viable alternative to water in establishing calibration curve for Ir-192 radiation beam. A Monte Carlo correction factor was calculated to convert the *dose to water* into *dose to Solid Water$^{TM}$* and the experimental methods that we performed agreed with the Monte Carlo results where the ratio $(D_{SW}/D_W)^{Ir\text{-}192}$ was found to be 0.9808 ± 0.14% (1σ). EBT-2 GAFCHROMIC$^{TM}$ film model was also investigated for absorption properties and found to be a less sensitive than its predecessor (EBT-1) in terms of net change of absorbance, but that did not affect the dosimetric value that this film possesses. A dose error assessment method has been described for EBT-2 film model (and is applicable to other types as well) that can establish the time error constraints on the post-irradiation scanning time that will still provide an acceptable dose error for clinical applications if the protocol employing the shorter post-irradiation scanning time is implemented in the clinic. We show that for two post-irradiation scanning times of 30 minutes and 24 hours the 1% dose error can be granted if the scanning time window is less than ± 5 minutes and ± 2 hours, respectively. Performance of EBT-2 model was also evaluated in water and it was concluded that a suggested correction protocol is necessary for immersion times that exceed 2 hours. This correction was tested with the calibration curve created from water setup and found to be effective when compared to the dose-corrected calibration curve in Solid Water$^{TM}$.

## Résumé

Un protocole d'établir film radiochromique dosimétrie de référence en fonction de débit de dose élevé source Ir-192 curiethérapie été évalués et décrits. Une comparaison entre les courbes d'étalonnage créé dans l'eau et Solid WaterTM sont fournis. Solid Water$^{TM}$ s'est révélée être une alternative viable à l'eau dans l'établissement de la courbe d'étalonnage pour les Ir-192 faisceau de rayonnement. Un facteur de correction de Monte Carlo a été calculé pour convertir la dose à l'eau en dose à Solid WaterTM et les méthodes expérimentales que nous avons réalisé d'accord avec les résultats de Monte Carlo où le ratio $(D_{SW}/D_W)^{Ir\text{-}192}$ a été trouvé à 0.9808 ± 0.14% (1σ). EBT-2 modèle GAFCHROMIC$^{TM}$ film a également été étudiée pour les propriétés d'absorption et jugé être un moins sensible que son prédécesseur (EBT-1) en termes de variation nette de l'absorbance, mais cela n'a pas d'incidence sur la valeur dosimétrique que ce film possède. Une méthode d'évaluation des doses d'erreur a été décrit pour le modèle EBT-2 film (et est applicable à d'autres types ainsi) qui permet d'établir les contraintes de temps d'erreur sur le post-irradiation temps de balayage, qui va encore donner une erreur de dose acceptable pour des applications cliniques, si le protocole emploie le plus court post-irradiation de numérisation temps est mis en œuvre dans la clinique. Nous montrons que pour deux post-irradiation de numérisation fois de 30 minutes et 24 heures, la dose d'erreur de 1% peut être accordée si la fenêtre de temps de balayage est inférieure à ± 5 minutes et de ± 2 heures, respectivement. Performance de la EBT-2 modèle a également été évaluée dans l'eau et il a été conclu un protocole de correction proposé est nécessaire pour que les temps d'immersion supérieure à 2 heures. Cette correction a été testé avec la courbe de calibration créée à partir d'installation de l'eau et ont été jugés efficaces par rapport à la courbe de calibration corrigée en fonction de la dose Solid Water$^{TM}$.

## Acknowledgment

In the beginning I would like to thank Almighty Allah for his blessings, guidance, mercy and support through all hardships.

I would like to extend my sincere thanks to my supervisor Dr. Slobodan Devic for being such a patient and kind teacher. Without his guidance and vision, this project would not have reached its goals within the time frame of submission. Dr. Devic is a pioneer in the radiochromic film dosimetry and all experimental procedures and radiochromic film dosimetry training that I received at the Jewish General Hospital (JGH) was under his supervision. I also would like to express my gratitude for him and all of his family for treating me like one of them.

I would like to thank my co-supervisor and academic director of the medical physics unit at McGill University, Dr. Jan Seuntjens for all of his support, ideas, encouragement, patience and for maintaining this program.

My sincere thanks and gratitude is passed to Dr. Ervin Podgorsak who developed this solid program and it was my honor to attend his classes during my first year. It has been a unique experience that was forged by his guidance and encouragement. I also would like to thank all my teachers: Dr. Wamied Abdel-Rahman, Dr. Francois Deblois, Mr. Michael Evans, Mr. William Parker, Dr. Gyorgy Hegyi, Dr. Bruce Spike, Dr. Andrew Reader, Dr. Christian Janicki, Mr. Horacio Patrocinio, Dr. Russell Ruo, Ms. Marylene Brodeur, Samy El-Jaby, Dr. Wieslaw Wierzbicki, Dr. Shirley Lehnert, Eng. Pierre Leger and Dr. Ernst Meyer, may he rest in peace. All thanks goes to Ms. Margery Knewstubb and Ms Titjana Nisic for their unlimited support, warm welcoming and smiles.

I would also like to thank all the medical physics staff and the radiation oncology staff at the Jewish General Hospital for their tremendous support. I would like to specifically thank Dr. Deblois, Dr. Devic and Mrs. Nicole Gendron for welcoming me in the department and all of their support in giving

me an open access to all the equipments that I needed. I would like to thank Mrs. Nada Tomic and Mr. Li-Heng Liang for their ideas and suggestions. I would like to thank Eng. Philippo Piccolo and Mr. Daniel Dufault for letting me use their lab in the construction of some materials that we needed and for their constructive ideas.

I would like to sincerely thank Dr. Abdel-Rahman and his family for all the support they have given and the great times we had together. I would also like to thank him for all the time he invested in teaching me and suggesting a lot of ideas that helped us a lot in reaching our goals. I would like to thank Dr. Arman Sarfehnia for all of his support in Monte Carlo simulations. He never hesitated to help me given the narrow time frame I had. I would like to thank him also with Dr. Seuntjens, Dr. Abdel-Rahman and Eng. Robin van Gils for their help in constructing the setups of the experiments we needed to perform.

I would like to thank my friends and colleagues whom have been supportive and added a flavor to the times we spent together: Hurriyah Mohammed, Jonathan Thebaut, Sangkyu Lee, Krum Asiev, Dr. John Kildea, Ileana Jelescu, Joseph Holmes, Matt Giles, Andrew Alexander, Eunah Chung, Dr. Emily Poon, Ayman Oweidah and Dr. Abdullah Alsuhaibani. I would like to thank Ismail AlDahlawi and his father for being such nice friends and family. He never hesitated to help me when first arrived in Montreal.

I also would like to thank my parents and family for their patience and prayers that kept me on the right way. I hope that they accept this work as my small gift and that it is going to make them proud for the rest of their lives. All the gratitude and thanks goes especially to my fiancée and best friend, Laila Alawda for her unlimited support and continuous encouragements.

In the end, I would like to acknowledge and thank the Saudi Food & Drug Authority (SFDA) and especially the Medical Devices Sector (MDS) for sponsoring and supporting me through my studies. I hope that those whom I forgot to mention, forgive my ignorance and accept my gratitude and apologies.

# Chapter 1: Introduction

## 1.1 General introduction

Current trends in treatment of cancer concentrate on the accuracy of treatment delivery to the tumor volume. This goal is important because sparing healthy tissues in general and vital sensitive organs in particular, are the dynamic motivators for all technologies we see in today's radiation oncology centers. Composite non-standard beams such as Intensity Modulated Radiation Therapy (IMRT), Adaptive radiotherapy, Cyber Knife™, and TomoTherapy™ require more than single point measurements to verify dose distributions. For these modalities, radiation beam delivery is modified in order to provide higher intensities inside malignant volumes. Such dose modifications may lead to an increase in dose gradients and physicists have to deal with the challenge of verifying such treatments before implementing them.

Generally, single point dosimeters such as ionization chambers are considered a very well established dosimetry system since primary dose standards for a lot of energies are available through national standard laboratories, while reference dosimetry can be achieved from ionization chambers that have calibration coefficients traceable to primary or secondary standards labs. Accuracy of such dosimeters is of the order of 0.5% and thus it has been the medical physicist's first choice in dosimetry. However, the implementation of these dosimeters in non standard beams poses many questions due to high dose gradients in one hand and dose volume averaging effect in the other hand, and one might need more than single position for dose measurements for such treatments.

Radiochromic films are very high resolution 2D dosimeters and one can verify the dose distribution in any given plane easily. Arrays of diodes or ionization chambers have also been introduced to the market with the intention of achieving a balance between precision and 2D dosimetry. However, such dosimeters fail to provide the high level of spatial resolution in dosimetry

required by non standard beams. One might argue that moving these detectors in one plane can increase the spatial resolution for that plane, but this increase would be in single plane only (1D) and it is subject to mechanical accuracy. In addition to the superior spatial resolution of radiochromic film, it has properties equivalent to those of water and has been shown to have a response independent of beam quality in a broad energy range, which makes it suitable candidate in the dosimetry of non standard beams. Radiochromic film industry has developed in clinical practices and has found use in a number of additional dosimetry applications: brachytherapy,[1, 2, 3, 4] total skin electron therapy (TSET),[5, 6] electron therapy,[7, 8] skin dose measurements,[9, 10] total body irradiation (TBI),[11] lung[12, 13] and breast[14] phantom measurements, stereotactic radiotherapy,[15, 16, 17] dosimetry characterization of proton therapy beams,[18] as well as dose verification during cell irradiation in radiobiological experiments.[19]

Among these techniques, brachytherapy has always been considered one of the most conformal dose distributions that one can use in cancer treatment. This technique involves inserting encapsulated radionuclide source(s) directly into or next to the designated treatment site. This allows physicians to deliver relatively high doses in the order of 50 Gy; a demand that is difficult to achieve directly and as quickly by other modalities without damaging healthy tissues. However, brachytherapy is used nowadays more in conjunction with external beam radiotherapy as a boost in order to achieve better healthcare outcomes.

Brachytherapy is performed during very limited time. Verification of treatment plans is a difficult task since for some types of implants the entire planning process is done mostly while the treatment applicators are already inserted into the patient. So, setting up any dosimetry system in the process seems impossible as long as the patient is still lying on the treatment couch. Dosimetry in such cases is carried out during commissioning process of both radionuclide source and the afterloader unit which is the machine used to drive the source(s) accurately to specified positions. This makes the accuracy that one

wants to achieve in the dosimetry of such system, a very important task. Testing various treatment setups during the commissioning procedure would be easier if 2D dosimetry could be performed and dose distribution was be recorded directly.

Thus, it is desirable to take advantage of properties of radiochromic films and use them in the dosimetry of high dose rate (HDR) Ir-192 sources in water in order to mimic the planning system, which according to TG-43 assumes water medium for everything. It is also advantageous to perform dosimetry measurements in the more convenient Solid Water™ medium which is less cumbersome experimentally. However, such demand requires establishing a dose conversion factor that accounts for the fact that the medium is Solid Water™ and not water and a general comparison between radiochromic film dosimetry in Solid Water™ and in water is required and this is the goal of this work.

Reaching this goal was not possible to implement at once as the new GAFCHROMIC™ film model (EBT-2) was just introduced early in 2009. We needed to test all the characteristics of the new film model and to find a mathematical model that best describes the behavior of this new film, especially for larger doses. It was also necessary to test the impact of performing radiochromic film dosimetry in water medium because film pieces would be immersed in water for relatively long times. Finally, it was desirable to establish a dosimetry protocol on how to perform dosimetry of HDR Ir-192 source in water and Solid Water™ mediums.

## 1.2 Literature review of dosimetry of HDR brachytherapy

### 1.2.1 Introduction to brachytherapy

Treatment of cancer that involves either direct contact of encapsulated radionuclide sources with volumes of interest or emplacement of these sources at short distances from the volumes to be treated are referred to as brachytherapy.[20] This kind of treatment results in continuous delivery of dose at different rates, which depends on the source specifications and distance between the source and treatment volume. Some of these sources include: Ir-192, Cs-137, Au-198, Co-60, I-125, Pd-103 and others that differ in nominal activity, effective energy, specific activity, physical description and half life. Table 1-1 summarizes the differences between these sources.[20]

Table.1-1: list of some isotopes used in brachytherapy treatments and their properties

| ***Source*** | ***Half Life*** | ***Effective Energy*** | ***HVL in mmPb*** | ***Physical description*** | ***Nominal activity*** | ***Specific Activity*** |
|---|---|---|---|---|---|---|
| ***Co-60*** | *5.26 y* | *1.25 MeV* | *11* | *Metal: Pellets* | *5000 Ci* | *1100 Ci/g* |
| ***Cs-137*** | *30 y* | *0.662 MeV* | *6.5* | *Powder: Needles, tubes or pellets* | *10 – 20 mCi* | *80 Ci/g* |
| ***Au-198*** | *2.7 d* | *0.41 MeV* | *2.5* | *Metal: seeds* | *0.4 mCi* | *250000 Ci/g* |
| ***Ir-192*** | *73.8 d* | *0.38 MeV* | *3* | *Metal: Seeds, wires* | *10 Ci* | *450 Ci/g* |
| ***I-125*** | *60 d* | *0.028 MeV* | *0.02* | *Powder: seeds* | *1 mCi* | *1739 Ci/g* |
| ***Pd-103*** | *17 d* | *0.021 MeV* | *0.01* | *Metal: seeds* | *1 mCi* | *7448 Ci/g* |
| ***Sr-90*** | *29 y* | *0.546 MeV* | *0.5* | *Metal* | *100 mCi* | *150 Ci/g* |

There are many configurations in which these sources could be utilized in brachytherapy treatments but they are mainly either intracavitary where the source is placed in body cavities close to the tumor volume or interstitial where the sources are implanted within the tumor volume. The sources are implanted through manually inserted catheters into the designated positions either manually or more conveniently by automatic afterloading systems. These systems have a radiological health advantage over manual procedures where it

prevents extra exposure to the operating staff, and it also has more consistency, capacity and reproducibility in daily treatment deliveries[21]. Remote afterloading systems consist of: (1) a shielded radioactive source chamber (safe) which includes the source(s) and (2) a mechanism for source delivery through transfer guide tubes and treatment applicators, (3) an operating control unit for the treatment delivery, and (4) a treatment planning system. [20]

The sources and delivery mechanisms fall into one of the following categories:

- Low Dose Rate (LDR): ranges between 0.4 and 2 Gy/hr
- Medium Dose Rate (MDR): ranges between 2 and 12 Gy/hr
- High Dose Rate (HDR): rates larger than 12 Gy/hr
- Pulsed Dose Rate (PDR): using HDR one minute per hour

The most commonly used source in HDR brachytherapy is Ir-192 because of its convenient effective energy with its relatively high specific activity. The advantage of such systems over LDR, MDR and PDR lies within the possibility to optimize dose distributions and convenience of treatments for the patient (outpatient treatments) but since it is a high dose rate radioactive source, much care has to be taken during the delivery process and a relaxed margin of error is highly unappreciated. [22, 23]

### 1.2.2 Comparison of brachytherapy and external beam radiotherapy

Brachytherapy comprises around 20% of the treatment carried in a typical radiation oncology department.[20] While external beam radiotherapy (EBRT) occupies the other 80% of the cases, brachytherapy is mostly used as a secondary treatment in conjunction with EBRT. Brachytherapy has the advantage in treatment of more localized tumors and it efficiently avoids skin dose which results in better patient's quality of life. However, this is not advantageous for larger or metastasized tumors. Brachytherapy has the advantage of reduced treatment times where long treatments resulting from extra fractionation are avoided and treatments are more conveniently carried out

on outpatient basis. However, it has the disadvantage of possibly needing an invasive intervention in order to implant the treatment catheters or seeds, whereas this is generally not necessary in the case of EBRT. It depends on the tumor site, stage, nature and size to decide which treatment combination(s) provide better outcomes for the patients and all treatment modalities should be used optimally where they are considered advantageous, be it solely or in conjunction with other modalities.

### 1.2.3 Brachytherapy dosimetry

The success of brachytherapy dose delivery relies on two main aspects: (1) the use of calibrated sources and (2) credibility of the dosimetric model used for dose calculations based on these calibrated source. This raises the importance of having a well established dosimetric system that is able to measure the dose precisely in a specific point or region from a given calibrated sources. This calibration process[24] is based on air-kerma strength ($S_K$) defined in the report of American Association of Medical Physicists Task Group # 43: Dosimetry of interstitial brachytherapy sources [25] as:

$$S_K = \dot{K}_\delta(d) \times d^2 \tag{1-1}$$

where $\dot{K}_\delta(d)$ denotes the air-kerma rate measured at distance $d$ along the transverse bisector of the source with energy cutoff ($\delta$) which is intended to exclude low energy and contaminant photons. This definition is valid at a single point in air placed into an infinite volume of vacuum which excludes by nature beam attenuation and scattering.

Ultimately, TG-43 protocol and its update provides a recipe by which one can convert the reference air-kerma strength, $S_K$, to dose to water, $D_w$, in Ir-192 and other sources at a point of interest through both calculated and measured factors. The TG-43 protocol is considered to be the reference dosimetry protocol in HDR brachytherapy where it gives a review of publications and a summary of recommendations on dosimetry of brachytherpay sources, and it also provides dose calculation formalism and

gives data sets for dosimteric parameters it describes. It also compares this formalism with measurements previously done by Interstitial Collaborative Working Group (ICWG).[26] The TG-43 involves direct use of measured or measurable dose distributions produced by a source in water since it is universally available and accepted as tissue-equivalent phantom. Other materials have shown acceptable behavior for dose measurements under full scattering conditions such as polystyrene, Solid Water™, polymethylmethacrylate and Lucite. [27] However, TG-43 does not provide an uncertainty budget for dose measurements and such analysis could be found in the literature.[1, 55]

### 1.2.4 Summary of AAPM TG-43 recommendations

According to Soares et al[24] recommendations of the members of TG-43 fall within three categories:

a) Recommendations on experimental techniques for dose measurements
   - Dose rate has to be measured around the source in a tissue-equivalent phantom.
   - $S_K$ is determined either by National Institute of Standards and Technology (NIST) measurements or by using an instrument that has a NIST traceable calibration coefficient (such as a well-type ionization chamber).
   - LiF thermoluminescent dosimeters (TLD) are recommended as dosimeters in the first update of TG-43.

b) Recommendations on theoretical techniques for dose calculations
   - It is recommended that various Monte Carlo codes such as EGS, MCNP and PTRAN utilize the modern cross-section libraries that are equivalent to NIST XCOM database.
   - Physical dimensions and elemental composition of the source capsule and internal components should be known accurately.
   - Utilize the NIST Wide-Angle Free-Air Chamber (WAFAC) geometry as opposed to point detector in $S_K$ calculation per history.

c) Recommendations on determination of consensus dosimetry data sets
   - A consensus dosimetry is formed by averaging theoretical and experimental data that are accepted for publication in a peer-reviewed scientific journal.
   - Physical dimensions and elemental composition of the source capsule and internal components should be known accurately.
   - Utilize the NIST Wide-Angle Free-Air Chamber (WAFAC) geometry as opposed to point detector in $S_K$ calculation per history.

### 1.2.5 Historical summary of important contributions to Ir-192 dosimetry

This historical review of Ir-192 is based on the review of various important contributing papers that added to this field of dosimetry and on the historical review provided in TG-43.[25]

In 1968, a major work has been done by Meisberger et al[28] where their contribution to the dosimetry of Ir-192 sources (and other sources) provided the basis for all upcoming studies and investigations that involved measurements in water. They have measured the effective water to air attenuation coefficient ratio for distances 10 to 100 mm from a cluster of seeds and they found 7% difference between calculation and measurement at 100 mm source and decided to average the measured and calculated data with preceding available data at that time. So, they created a third degree polynomial fit that estimates this ratio in the given distances and thus recommended their model for clinical calculations. It is also worth mentioning that they used Berger's et al[29] build up factors to calculate ratio of *exposure to water* to *exposure to air*.

In 1979, Webb and Fox[30] used Monte Carlo simulations to calculate dose rates as a function of distance from un-encapsulated Ir-192 source, where their results were useful in validating the averaging approach of Meisberger's selected values.

In 1981, Boyer et al[31] have measured exposure rate constants for the steel and platinum encapsulated Ir-192 sources with 4% uncertainty. Kocher et

al[32] showed that there is a high contribution of low energies in the spectrum of Ir-192 which increases self-absorption in the source cladding. Glasgow et al[33] reported 3% difference between exposure rate constants in the platinum and stainless steel encapsulation and showed that these values differ by 5-9% from un-encapsulated Ir-192 source.

In 1982, Dale[34] simulated the dose rate calculations in Monte Carlo and argued that data provided by Webb and Fox shows failure in accuracy reported at low energy for scattering events. Dale also reported dosimetric function calculations that differed significantly from both Meisberger and Webb and Fox data, but was challenged by Mayles and Turner that Dale[34] didn't use the latest spectrum and decay scheme of Ir-192 and his data must be increased by 9%, and when he applied this suggestion he found an agreement with the pre-opposed data.

In 1987, Nath et al[35] published the AAPM Task Group No. 32 (TG-32) report which defined source strength for all nuclides in terms of $S_K$. In 1988, Meli et al[27] published their review paper on the choice of phantom material for dosimetry of Ir-192 sources. They showed from Monte Carlo calculations that under full scattering conditions, polystyrene, Solid Water™, polymethylmethacrylate are viable equivalents of water. They also observed that water and Solid Water™ are still equivalent even in the absence of full scattering medium. They also reported that the accuracy in positioning is critical for sources because of the high dose gradients. They used 70 mm backscatter medium and their results showed good agreement with Meisberger's data set.

In 1990, Anderson et al[26] measured dose distributions for Pd-103, I-125 and Ir-192 seeds which were referred to as the measurements of ICWG and as explained earlier, were adopted for comparison in the 1995 first version of TG-43 report. Thomason et al[36] compared both stainless steel and platinum encapsulations for both Ir-192 and Cs-137. They found that 7% of photons are interacting with either source core or encapsulation, and 4-5% of photons

exiting the source capsule are scattered. They also showed that primary photons inside the source which exit and interact in Compton mode exhibits scattering towards all angles of up to $180^{o}$. They also showed that a source-to-detector distance of 30 mm is actually a very good choice since the fractional scatter is around 30% in both directions: along the long axis of the source (32%) and perpendicular to the bisector of the source (30%).

In 1991, Williamson et al[37] compared both measured and calculated dose rates in water near I-125 and Ir-192 seeds. They compared Monte Carlo results with NCI measured data in Solid Water™ and found 4.3% difference between water and Solid Water™ data for I-125 at 10 mm whereas it was nearly identical as they described it within ±2% for Ir-192. They showed this explicitly in their Figure 4 (not shown here) where they plotted the ratio of dose in Solid Water™ to dose in water for different energies from monoenergetic point sources and two different distances. It is evident from that figure that under 300 keV, this ratio becomes questionable. Their dose rate constants data differed by 1% from those of ICWG and Mesiberger. They also show that at 30 mm, the gradient of dose rate is almost constant in both measurements and simulations. Goetsch et al[38] introduced an interpolation procedure for calibration factors which were adopted by Accredited Dosimetry Calibration Laboratories (ADCL) where they interpolated the calibration factors at Ir-192 weighted average energy between Co-60 or Cs-137 and orthovoltage energies.

In 1995, Nath et al[25] established the AAPM Task Group No. 43 (TG-43) report which was explained previously. In 1998, Williamson et al[39] refined TG-43 for low energy photon emitting sources to adhere to specific conditions that are concerned mainly with the importance of traceability of $S_K$ to NIST WAFAC air-kerma calibration standard. Daskalov et al[40] introduced a Monte Carlo-aided dosimetry of the microSelectron-HDR source used in Nucletron remote afterloading devices in a lookup table for the 2D dose rate distribution over 1 to 70 mm distance range. They quote 5-8% difference in dose distributions from subsequent source designs. Their work demonstrates that the

TG-43 dose calculation model estimates the dose rates accurately within 2%. Their work was adopted in the Nucletron treatment planning system (Oncentra, Nucletron, Veenedaal, The Netherlands). Reynaert et al[41] provided methodology of ionometric calibration of sources directly in terms of dose rate in water for different distances using an NE2571 Farmer type ionization chamber. They calculated conversion factors that enables the conversion of air-kerma rate to a dose to water rate and compared their data with current accepted values, at the time, and found that they agree to within 1%. They confirmed their data with TLD measurements too.

In 2000, Raynaert et al[42] provided an in-phantom calibration technique for Ir-192 sources used for endovascular brachytherapy. They used their previous work to find dose to water and they determined $S_K$ as well. They also performed Monte Carlo simulations to find the depth dose distribution for distances between 0.6 mm and 100 mm in which they used to convert the absolute dose rate at 10 mm to the absolute dose rate at a reference point of 2 mm. These MC calculated depth doses were confirmed by radiochromic film measurements. Dose to water from their measurement was found to be agreeing within 2% with the source supplier's data.

In 2004, Rivard et al[43] provided the newest update of TG-43U1 where they updated the 1995 version with more source consensus datasets and introduced a revised air-kerma strength standard and issued guidance on extrapolating tabulated dose ratios to small and large distances beyond the provided data range. They also described the NIST WAFAC-based primary calibration standard and its role in clinical source calibration.

After 2004, a number of reports have been published about Ir-192 dosimetry but we will limit the search for those which involved the use of radiochromic films as dosimeters and I will present them in the next section as it provides more basis to our work.

## 1.3 Literature review of HDR Ir-192 dosimetry using radiochromic films

Many brachytherapy sources dosimetry studies have been conducted using radiochromic films (RCF). This is advantageous specially in validating the TG-43 calculated factors since the film is a 2D dosimeter by nature and one could measure the 2D dose distribution around the source at a given distance directly. Radiochromic films also show promise because of their water-equivalency which allows for in-water measurements of dose without worrying about perturbation effects. All the aspects and characteristics of radiochromic film dosimetry will be discussed in this section.

### 1.3.1 Background on radiochromic film use in Ir-192 dosimetry

Given the previous properties of radiochromic films, RCF dosimetry in brachytherapy has started since the introduction of the first radiochromic film model, HD-810 which was relatively insensitive to typical clinical doses but found interest in brachytherapy since its sensitivity range extends beyond 50 Gy up to 2500 Gy.

One of the first attempts to make use of these films was recorded by Sayeg and Gregory[44] in 1991 where they measured surface dose rates with HDR beta particle ophthalmic applicators. Soares[45] did a similar work at the same time but more interestingly accomplished dosimetry of three beta particle emitting ophthalmic applicators ($^{90}$Sr–$^{90}$Y and $^{106}$Ru–$^{106}$Rh and a concave applicator of $^{106}$Ru–$^{106}$Rh) in an international study with eight different detectors ten years later in 2001.[46] Radiochromic film was one of the detectors and they used two types of custom made films: less sensitive with 6 – 8 μm of active layer backed up with a polyethylene terephthalate (PTP) backing, while the other is fairly sensitive with 16 – 18 μm of active layer. Comparisons were made of absolute dose measurements determined at 1 mm from the source surface in water or water-equivalent plastic and relative dosimetry along and perpendicular to the source axes. The results of the inter-comparison indicate

that the various methods yield consistent absolute dosimetry results at the level of 10%–14% depending on the source. For relative dosimetry along the source axis at depths of 5 mm or less, the agreement was 3%–9% depending on the source and the depth.

In 2004, Chiu-Tsao et al[47] used double layered MD-55 radiochromic film (MD-55-2) to verify dose distributions around Ir-192 seeds at radial distances from 0.5 mm to 6 mm. They needed to measure doses accurately because in intravascular brachytherapy treatments of in-stent restenosis, the source can be as close as 0.5 mm to the arterial wall if not centered in the lumen and thus the assessment of dose at these distances was deemed necessary. They built their calibration curve that they used later for dosimetry, directly in Ir-192 beam inside a Solid Water™ phantom, with a separation of 11.12 mm between the film and center of the source. They also confirmed that dose rates along the transverse axes are within the error margin of previous Monte Carlo results.

Sharma et al[48] used High Sensitivity (HS) radiochromic films in 2004 to measure the anisotropy function for Ir-192 brachytherapy source. They showed that their measurements agree with previous experimental work (ionization chamber by Baltas et al[49] and TLD measurements by Anctil et al[50]) and Monte Carlo calculations by Williamson and Li[51]. Ionization chamber measurement agreed with MC within 3% while TLDs showed a difference of up to 5% from MC. Difference between RCF data (±3.2%) and other methods were within the uncertainty of measurements and calculation. However, it is worth mentioning that they used a double exposure technique where they set a dose of 2 Gy as the base line of their calibration curve and then used linear fit in-between for doses up to 10 Gy while the behavior of the HS film is by nature not linear in terms of optical density and dose.

Using Monte Carlo code, GEANT4, Poon et al[1] modeled a novel intracavitary mold applicator used for endorectal cancer treatment in 2006. They used EBT film for verification of radial and anisotropy functions and they found out that experimental results agree with GEANT4 calculations within

measurement uncertainties. The calibration curve used in their RCF measurements was created directly in water using Ir-192 brachytherapy source in an in-house built holder made of Lucite. The dose range in their measurements extends to 18 Gy and they used two different polynomials to fit the calibration curve, which minimized the uncertainty on the fitting procedure: 0.5 – 7 Gy with uncertainty of 1.5% and 7 – 16 Gy with uncertainty of 2.5%. The use of such piecewise models in fitting reduces the uncertainty in fit depending on the goodness of data, at the expense of the increased work complexity.

In 2007, Evans et al[4] introduced an improved quality assurance check for source positioning using radiochromic film instead of traditional radiographic film that has been used by co-registering autoradiographic and diagnostic images of the associated applicator. Such improvement solved a persisting problem of filmless PACS-based clinics that do not have access to radiographic film and wet developers.

Chiu-Tsao et al[52] performed dosimetry of I-125 seed in Solid Water™ phantom using EBT-1 film in 2008. They evaluated the use of radiochromic film in LDR brachytherapy for radial distances of 0.6 mm to 50 mm. The calibration curve that they used was created in I-125 at 5.8 mm from the source and to doses up to 33 Gy. They verified that the anisotropy and radial functions are in agreement with TG-43U1. They reported that dosimetry with EBT GAFCHROMIC™ film is a viable alternative to TLD dosimtery for I-125 seed dose characterization.

Yang and Rivard[53] used EBT-1 GAFCHROMIC™ film and ionization chamber based measurements in polystyrene to compare with Monte Carlo (MCNP5) calculated dose distributions around three different D-shaped applicators that are peripherally applied in Ir-192 breast brachytherapy. They found an agreement within 2% between measurements and MC. They reported 1% discrepancy between MC and film measurements for dose profiles at 30 mm depth. Their calibration curve was obtained from a 6MV linear accelerator

and an energy correction to Ir-192 energy was calculated from MC and applied in order to use the calibration curve in Ir-192 measurements.

Sellakumar et al[54] characterized the dosimetric properties of HDR Ir-192 brachytherapy source using EBT-1 GAFCHROMIC™ film and compared their values to TG-43. They built their calibration curve in Solid Water™ without background correction at 10 mm distance from the source using two film pieces per point (dose). They found agreement with MCNP5 calculated doses within ±2.8% which they argued was due to the fact that the calibration phase of EBT film was done in Solid Water™ while MCNP5 calculations used water as a phantom and the material difference represents the difference in the agreement.

A recent study that came out in March 2010 by Sarfehnia et al[55] compared direct absorbed dose to water measurements from HDR Ir-192 brachytherapy source using four different methods: water calorimetry, ionization chamber, Gafchromic film and TG-43 (well-type ionization chamber with an ADCL traceable $S_K$ calibration coefficient). They built a special holder for the films and 6F comfort catheter with metallic supports that provide rigidity to the catheter during source/dummy insertion and diminish any displacement that might be caused by water. It also helps in reducing the effect of transient time which is the time that the source takes in order to reach the specified position. Their calibration curve was obtained from a 6MV linear accelerator and an energy correction to Ir-192 energy was calculated from MC and applied in order to use the calibration curve in Ir-192 measurements. The overall uncertainty in their RCF measurements was 1.78%. They could reach such uncertainty by reducing the uncertainty in the source-to-detector positioning where they used a traveling microscope that measured the distance before and after measurements with 0.1 mm maximum difference. The source to film distance they used was nominally 50 mm and they compared all measurements to water calorimetry results at 55 mm. They found an agreement

of dose rate normalized to air-kerma strength between water calorimetry and other techniques within 0.83%.

Radiochromic film dosimetry with HD-810 model has been used by Duggan et al[56] in 1999 to measure the dose distribution in a plane parallel to and at a radial distance of 2 mm from the axis of a catheter-based, beta source for intravascular brachytherapy in Solid Water™. This was tested because AAPM Task Group 60 recommends that the dose rate be measured at a reference point located at a radial distance of 2 mm from the center of the catheter axis. AAPM Task Group 60 also recommends that the dose rate along the catheter axis at a radial distance of 2 mm should be uniform to within ±10% in the center two-thirds of the treated length, and the relative dose rate in the plane perpendicular to the catheter axis through the center of the source should be measured at distances from 0.5 mm to $R_{90}$ (the distance from a point source within which 90% of the energy is deposited) at intervals of 0.5 mm. Their average dose rate agreed with the dose rate measured with a well ionization chamber by the replacement method using source trains calibrated with an extrapolation chamber at NIST. All of the dose rates conformed to the specifications of TG-60. The calibration curve that they used was linear and measured in Solid Water™ phantom.

## 1.4 Literature review on radiochromic film dosimetry

Any dosimetry system incorporates not only the radiation detector but also all analytical methods that relate the radiation-induced signal to the absorbed dose at a specific location in a given material.[57] Accordingly, radiochromic film dosimetry system should be understood as an ensemble of the film model, densitometer and measurement protocol.

The signal measured from the transparent film is commonly referred to as an optical density (OD) and it represents a convolution of the densitometer light source emission spectrum, the film absorption spectrum, and the spectral sensitivity of the densitometer's detector.[58] Hence, an accurate knowledge of

the radiochromic film absorption spectrum and its behavior with dose are important for understanding the differences in dosimetric sensitivity when different densitometers are used,[59] and for designing a suitable optical densitometer in order to achieve optimal sensitivity of the film dosimetry system

### 1.4.1 History of radiochromic films

Before reaching the current status of RCF dosimetry, a number of improvement have been made to find the most sensitive, energy independent and stable structure. Pioneers of the radiochromic film industry such as McLaughlin et al[64] and David Lewis (GafChromic™ film manufacturer) have tested the feasibility of introducing this radiation-sensitive detector in high-dose clinical applications since the available version of this film at that time was relatively insensitive for doses less than tens of Gy.

The first film model that was investigated in 1991 by McLaughlin et al[64] was the HD-810 which consisted of 6.5 μm thin active layer coated on a 100 μm thick polyester base. As indicated by Devic et al[60] the relative sensitivity of the film is shown to be dependant mainly on the thickness of the active layer since the GAFCHROMIC™ component (active layer) remained the same for most of the subsequent film models. This was evident in the low sensitivity of HD-810 film where it required around 30 Gy to yield an Optical Density (OD) of 1 when read by laser scanning densitometer at 633 nm.

A newer film model was introduced and used also in clinical applications which was the MD-55-2 where number 2 refers to the double structure that this film has which is successive to the MD-55-1 that had only single 16 μm active layer. The improvements of this film model over the HD-810 included not only higher sensitivity, but also the ability of immersion into water. The dose range quoted for this film model is between 1 – 100 Gy. However, some problems were related to the adhesive layer of the film and its

uniformity and thus an improved model called High Sensitivity (HS) with 38 μm single active layer was introduced without the adhesive layer.

Introduction of external beam radiotherapy (EBT-1) GAFCHROMIC™ film model[61] after HS film model represents a major step in the improvement of both film sensitivity and uniformity that narrated the use of the film as a precision dosimeter. With EBT-1 film model, uncertainties as low as 2% could be achieved which is sufficient for clinical applications.[66,89] EBT-1 has a symmetrical structure around its center and it has a total active layer thickness of 34 μm. The composition of the sensitive layer in GAFCHROMIC™ EBT-1 film model was modified and resulted in 10 times more sensitive detector than previous film models.

Devic et al[60] investigated the difference in sensitivity between all film models in a spectral study of light absorption properties of these film models. This comparison is illustrated in left part of Fig. 1-1 which represents schematically the absorption spectra for various common GAFCHROMIC™ film models exposed to a dose required to achieve a net absorbance of approximately one at the absorption band maximum for a given film model. It has been reported in the literature[62] that the absorption spectra in the range from 400 nm to 800 nm have the same shape for the MD-55 and the HS type radiochromic film. Moreover, by comparing the absorption spectra for the early HD-810,[63, 64] MD-55[62] as well as HS films,[65] Devic et al[60] concluded that all these film models have the same sensitive layer base material and that the increased sensitivity of the GAFCHROMIC™ film models has been achieved mainly by increasing the thickness of the sensitive layer: 6.5 μm for the MD-810, 32 μm for the MD-55, and 38 μm for the HS model. On the other hand, Fig. 1-1 also indicates that the EBT-1 model GAFCHROMIC™ film has a different composition of its sensitive layer and a significantly increased sensitivity. The tenfold increased sensitivity, measured at the maximum absorbance wavelength (673 nm for HS, and 635 nm for EBT-1), was achieved by a modified composition[66] of the sensitive layer resulting, additionally, in a

qualitative shift of the absorption spectrum of the new film toward lower wavelengths.[65] The main characteristic of the film model that directly influences the sensitivity of the radiochromic film dosimetry system is its extinction coefficient at the peak absorbance as well as the efficiency with which radiation produces the polymer.

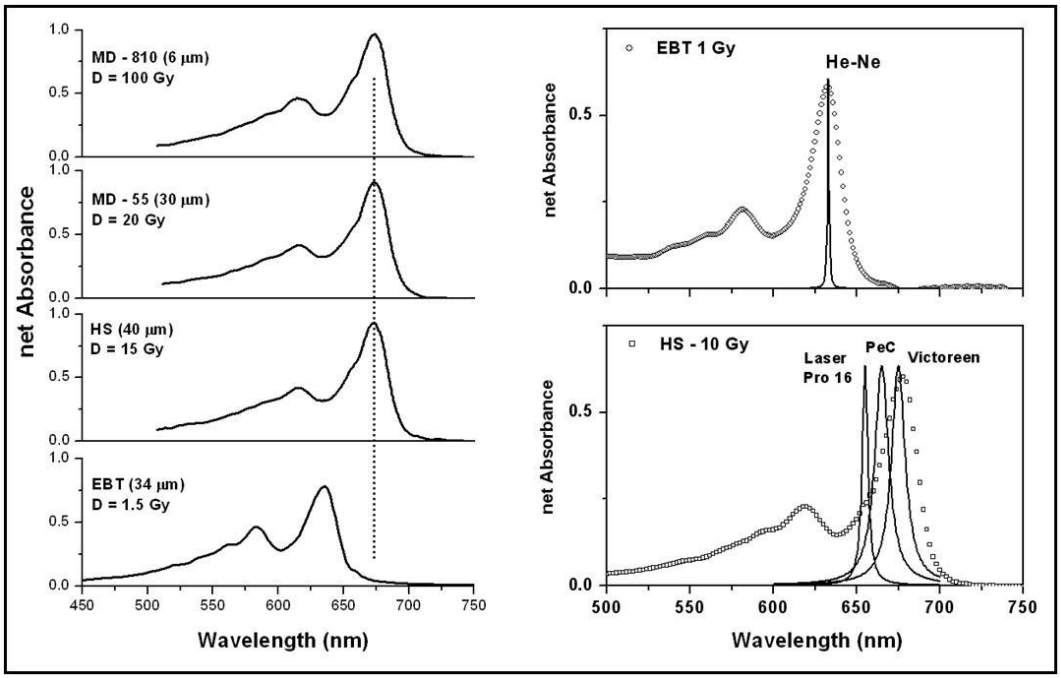


Fig. 1-1. Absorption spectra for different GAFCHROMIC™ film models: the original HD-810, MD-55 and HS models as well as the new EBT-1 model (Left). Absorption spectra (shown with data points) for two GAFCHROMIC™ film models (HS and EBT-1) and the light emission spectra (solid curves) for four different optical densitometers: He-Ne laser of the Molecular Dynamics Personal Densitometer; Laser Pro 16, PeC CMR-604, Nuclear Associates Radiochromic Densitometer, Victoreen Model 37-443

### 1.4.2 Introduction of EBT-2 GAFCHROMIC™ film model

Recent investigations into the limits of the measurement uncertainty with the radiochromic film dosimetry system employing the EBT-1 film model[67] have revealed that a remaining 2% level of the dose measurement uncertainty is mostly attributed to the non-uniformity of the sensitive layer of the film. Despite the fact that this level of non-uniformity with EBT-1 film

model is far much better than what was the case of its predecessors (10-15% for MD-55, and 6-8% for HS) and results in an acceptable uncertainty for clinical applications, manufacturer has decided to further improve the film's response uniformity by adding a yellow dye to the sensitive layer. According to the manufacturer, the principal purpose of this dye, referred to as a marker dye, is to correct for subtle differences in the thickness of the active layer. It is also assumed that the marker dye is uniformly distributed throughout the sensitive layer and that change in the optical density of the film when exposed to radiation is not affected by the presence of this marker dye. This yellow dyed film model is the new EBT-2 which was introduced early in 2009 and succeeded EBT-1 i.e. no more production of EBT-1 is carried out.

#### 1.4.2.1 Structure of EBT-2 GAFCHROMIC™ film model

The structure of the latest EBT-2 GAFCHROMIC™ film model is made by combining a clear polyester over-laminate with the active film coating. The substrate of the active film is clear (175 μm) polyester coated with an active layer film (nominally 30 μm thick) over which a topcoat (nominally 5 μm) is applied. The over-laminate (50 μm) polyester with approximately 25 μm of pressure-sensitive adhesive is bonded to the coated side of the active film. As the latest film model is not symmetric, the bottom surface of the EBT-2 model radiochromic film can be recognized by observing the reflection, which appears to be blurred as compared to the clear reflection when the top surface of the film reflects the fluorescent light from the film surface. The overall atomic composition (including all layers) of the EBT-2 GAFCHROMIC™ film model is H (40.85%), C (42.37%), O (16.59%), N (0.01%), Li (0.1%), K (0.01%), Br (0.01%) and Cl (0.04%)[1] resulting in an overall effective atomic number[2] number of 6.84.

[1] Dave Lewis, ISP, private communications.
[2] $Z_{eff}$ of EBT-2 Lot #F020609 has been calculated according to McCullough and Holmes, Med. Phys., 12:237-242, 1985

### 1.4.2.2 EBT-2 and EBT-1 GAFCHROMIC™ film models comparison

The configuration of EBT-2 GAFCHROMIC™ film model versus EBT-1 is shown in Fig. 1-2. The most obvious difference between EBT-2 and its predecessor is the yellow color of the film, which arises from the presence of the marker dye incorporated in the active layer.

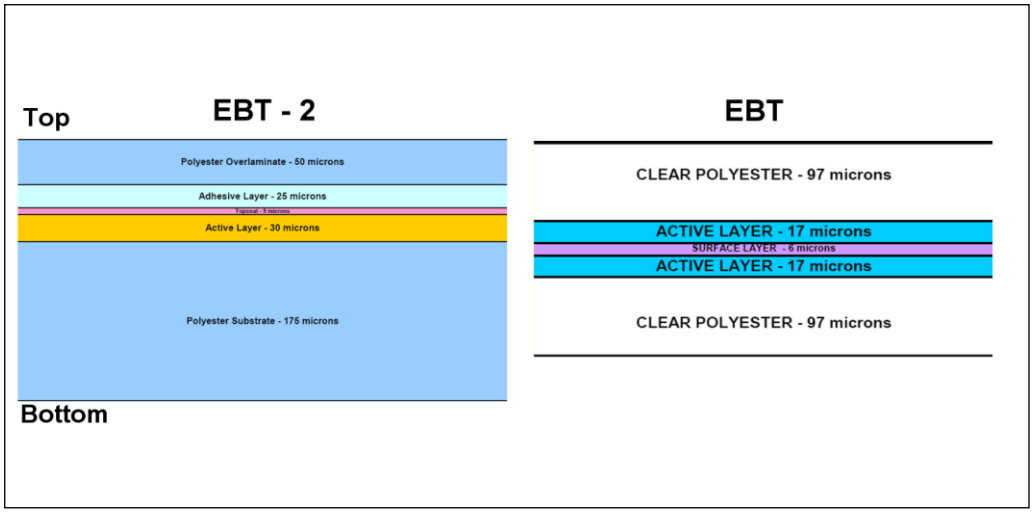


Fig. 1-2. Structure of the latest EBT-2 (left) and previous EBT (right) GAFCHROMIC™ film models.

In a recent study (Devic et al[68]), we have investigated the spectral properties of EBT-2 to complete the family of absorption spectra of radiochromic films started earlier by Devic et al[60]. Changes in the absorption spectra of the EBT-2 GAFCHROMIC™ film irradiated to various doses were determined as follows. Every film piece was scanned prior to radiation exposure to record the $A_{unexp}(\lambda)$ (unexposed absorption spectrum). At the very same time, we measured the $A_{unexp}^{control}(\lambda)$ absorption spectrum of the control film piece which represents a film piece that is not irradiated (or zero dose film piece) and any change in the absorbance for this film piece reflects the film absorbance changes due to environmental conditions, e.g., temperature, visible light, humidity, etc. Both film pieces were scanned after irradiation at a given time post-exposure with the irradiated film piece being scanned the first one

and in such a way $A_{\exp}(\lambda)$ and $A_{\exp}^{control}(\lambda)$ (absorption spectrum of the irradiated and control film piece respectively) have been determined. Final change in the absorption spectrum that comes from the irradiation only has been calculated as:

$$\text{net}\Delta\boldsymbol{A} = (\Delta\boldsymbol{A}) - (\Delta\boldsymbol{A})^{\text{control}} = \left(\boldsymbol{A}_{\text{exp}} - \boldsymbol{A}_{\text{unexp}}\right) - \left(\boldsymbol{A}_{\text{exp}}^{\text{control}} - \boldsymbol{A}_{\text{unexp}}^{\text{control}}\right). \quad (1\text{-}2)$$

In such a way, obtained absorption spectra have been analyzed in terms of their intensity dependence of either post-irradiation time or dose. All spectra obtained in this work were fitted with eight Lorentzian functions:

$$y = \sum_{i=1}^{8} \frac{2 \cdot A_i}{\pi} \cdot \frac{\omega_i}{4 \cdot (x - x_{ci})^2 + \omega_i^2}. \quad (1\text{-}3)$$

where $x_{ci}$ represent centers of a given profile, $A_i$ are the corresponding integrals below the profile and $\omega_i$ stand for the full width at half maximum (FWHM) of the given Lorentzian profile. Lorentzian profiles are commonly used when optical transitions between electron bands are modeled. We used the same Levenberg-Marquardt quasi–Newton minimization method as in our previous work. [60]

Fig. 1-3 represents absorption spectra of the latest EBT-2 and previous EBT GAFCHROMIC™ film models. Top part of Fig. 1-3 illustrates the absorption spectra of the unexposed and exposed to 1 Gy film pieces for the two film models. Absorbance of the latest film model features pronounced absorption band in the blue part of spectrum, which originates from the yellow marker dye added on purpose by the manufacturer to correct for film inhomogeneities when the film is used with flat-bed document scanners.

Bottom part of Fig. 1-3 represents the resultant change in net absorbance for the two film models, determined using Eq. (1-2). It is apparent from the bottom of Fig. 1-3 that two film models experience the very same dose change in net absorbance. This result confirms the manufacturer's hypothesis

that the addition of the yellow marker dye is not affecting the dosimetric properties of the latest film model. However, sensitivity of the latest EBT-2 model GAFCHROMIC™ film appears to be slightly lower than its predecessor. This is not surprising as the sensitive layer of the new film model is slightly thinner than for the old one, 30 μm vs. 34 μm respectively, as indicated in Fig. 1-2.

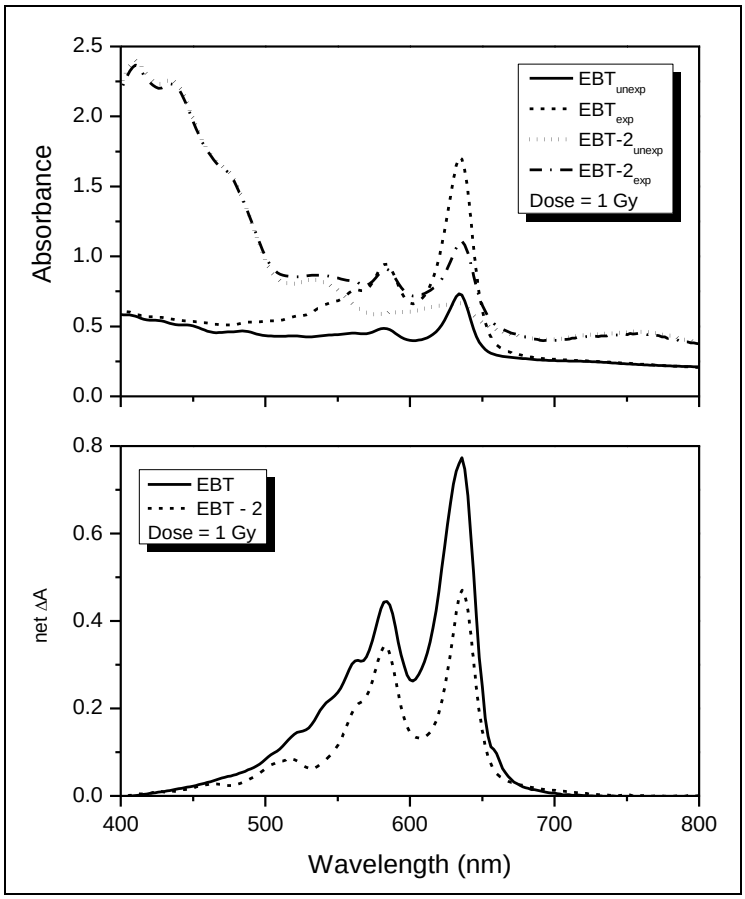


Fig. 1-3. Absorption spectra of the latest EBT-2 and previous EBT GAFCHROMIC™ film models: absorbance spectra of unexposed and exposed to a dose of 1 Gy film pieces (top); resultant net absorbance changes for the two film models (bottom).

Results of our fitting procedures have revealed the same behavior of the absorption peaks as compared to the previous, EBT-1 model GAFCHROMIC™ film. Center of the first absorption band varies from 430 nm at low doses to 480 nm at higher doses. Most probable reason for this relatively large shift is fairly low intensity of this absorption band at low doses in the blue

part of the absorption spectrum. As we have shown in our previous work [92], blue part of the absorption spectrum should be used when the film is irradiated to doses larger than 50 Gy. The highest energy absorption band also changes its position with dose from 639.5 to 644.5 nm. All the other absorption bands do not change their position with dose delivered to the film. Similarity between peak positions is additional confirmation that there is no change in terms of films dose response between two film models.

#### 1.4.2.3 Response of EBT-2 GAFCHROMIC™ film models

In the same study, we have measured the absorption spectra dependence on both dose and time. Top part of Fig. 1-4 represents resultant change in net absorbance of the EBT-2 GAFCHROMIC™ film model as a function of dose in a dose range from 25 cGy to 600 cGy scanned 24 hours post-irradiation. Bottom part of Fig. 1-4 shows the change of the net absorbance as a function of post-irradiation time ranging from 3 minutes to 120 hours (5 days) for a single piece of film irradiated to a dose of 1 Gy. Both figures indicate that positions of absorption bands do not change by either dose or time post exposure.

Butson et al[69] has also published a similar study of EBT-2 response to different doses where they have acquired absorption spectra of EBT-2 and compared it to EBT-1. They found that late production EBT-1 (2009) varies in net optical density by 10 % to 15 % from the new production EBT-2 film.

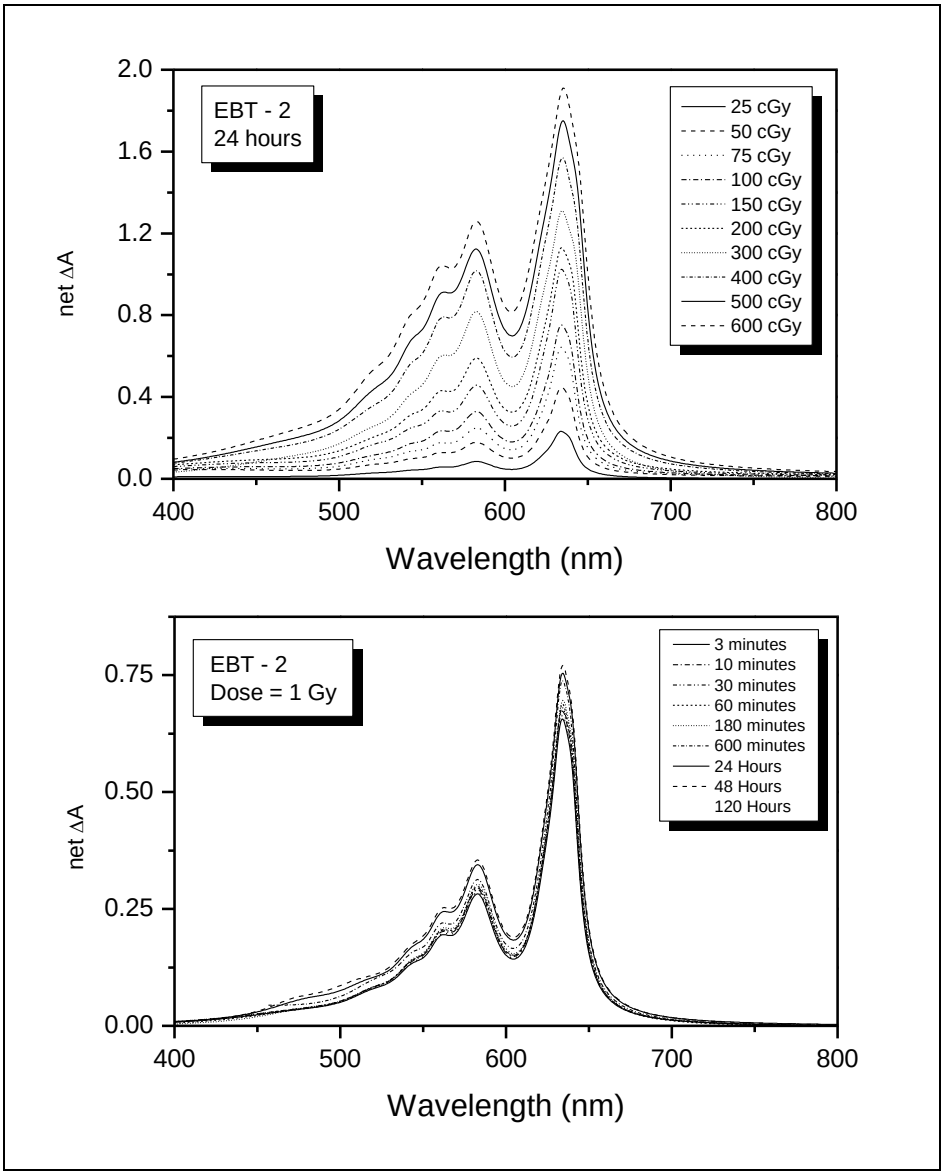


Fig. 1-4. Resultant change in net absorbance of the EBT-2 GAFCHROMIC$^{TM}$ film model as a function of dose scanned after 24 hours (top), and as a function of time for a single film piece irradiated to dose of 1 Gy (bottom).

### 1.4.2.4 Energy dependence of radiochromic film

Perturbation of radiation field is not a significant issue in new radiochromic films EBT-1 and EBT-2 because their physical density and effective atomic number is close to that of water as indicated earlier. However, manufacturer added a small amount of Chlorine which would reduce energy dependence limitations since it has atomic number slightly larger than that of water. EBT-2

is expected to have more dependence on energy (compared to EBT-1) because of the addition of Bromine and Potassium. Recently in 2010, Sutherland et al reported that in the photon energy range of 100 keV to 18 MeV the absorbed-dose energy dependence of EBT-1 and EBT-2 was found to be energy independent within ±0.6%.

**a. Energy dependence of EBT-1 film model**

Many studies have investigated the energy independence in EBT-1 film model. Chiu-Tsao et al[70] has reported energy independence for I-125, I-192, Pd-103 and 6 MV energies. Butson et al[71] reported similar finding but for larger energy range that extends between 50 kV to 10 MV with maximum variation of 10% indicating the improvement of 30% variation in HS film model. Ebert et al[72] (2009) reported significant energy dependence within the measurement uncertainty for 50 kV and therefore did not recommend the use of EBT film for low energy x-rays.

The best comparison of previous studies and Monte Carlo simulation results was done recently by Sutherland et al[73] (2010) and they indicated that below 100 keV, the absorbed-dose energy dependence of EBT varies by approximately 10% due to changes in mass energy absorption coefficient ratios of water to film materials, as well as an increase in the number of electrons being created and scattered in the central surface layer of the film. Their results are found to disagree with previous experimental studies suggesting the possibility of intrinsic energy dependence at lower photon energies. Fig. 1-5 summarizes the comparison of their work with previous ones.

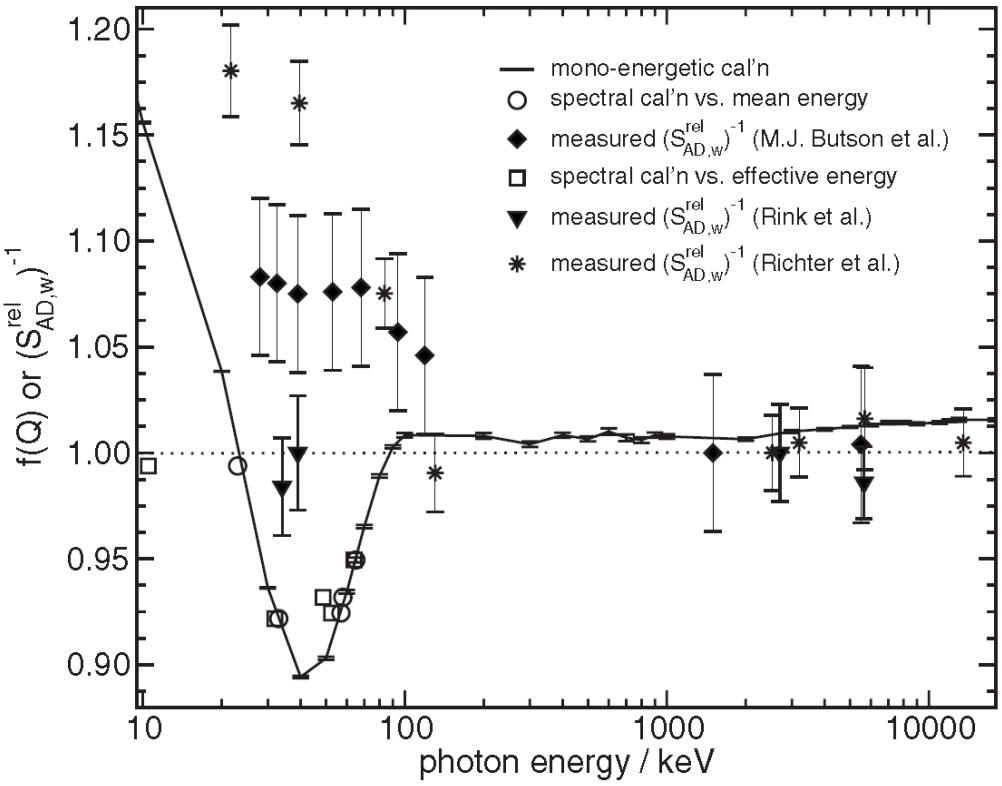


Fig. 1-5. Energy response of EBT-1 film in terms of absorbed dose from different studies (used with permission from Justin Sutherland)

**b. Energy dependence of EBT-2 film model**

Butson et al[69] reported that EBT-2 film has been shown to have a very low energy dependence with a 6.5% ±1% variation in optical density to absorbed dose response for x-ray beam irradiations with energy from 50 kVp up to 10 MV. These results are slightly better than EBT-1 which had a 7.7% ±2% variation over the same energy range.

Sutherland et al reported 50% or 10% variations in the absorbed-dose energy dependence at low photon energies, depending on the manufacturing lot due to changes in the ratio of mass energy absorption coefficients of the active emulsion layers of EBT-2 to water (See Fig. 1-6). They reported that caution is recommended when using GAFCHROMIC™ EBT-1/EBT-2 films at photon energies below 100 keV.

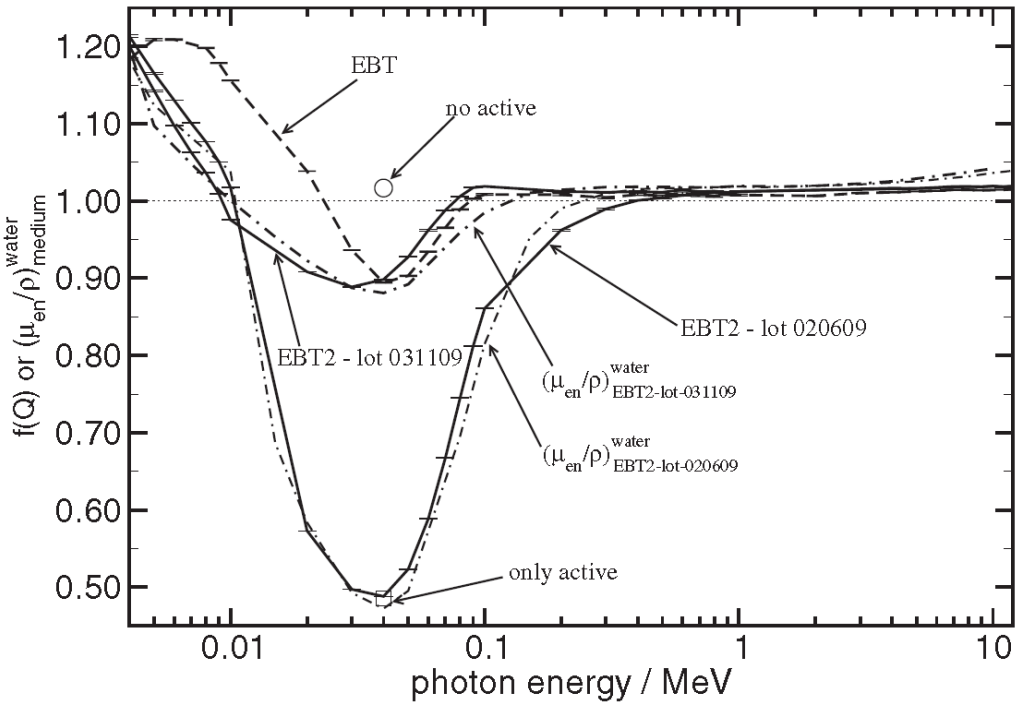


Fig. 1-6. Energy response of EBT-2 film compared to EBT-1 in terms of absorbed dose (used with permission from Justin Sutherland). It is shown that EBT-2 is strongly dependent on the manufacturing batch number.

### 1.4.3 Introduction to readout system (scanner)

The choice of the readout system that will measure the magnitude of film darkening (color change due to radiation, presumably) from a background is very important since it can affect the sensitivity one can get from the radiochromic film. Scanners available for radiochromic film fall within two categories: single wavelength or multi-wavelength (white light) scanners. General guideline for maximum sensitivity is that light source spectrum should peak at the same wavelength range of the maximum absorption of the measurement sample's spectrum.

#### a. Single wavelength scanners

The single wavelength scanners utilize technologies such as He-Ne laser diodes and Light Emitting Diodes (LED) arrays. These can provide high spatial resolution at a given wavelength. For example, LaserPro 16 (eRadLink Inc.)

uses solid state laser with emission spectrum centered at 658 nm, Molecular Dynamics Personal Densitometer (Molecular Dynamics, Sunnyvale, CA) and UltroScan XL (LKB Pharmacia) use He-Ne laser from a PMT (Photo Multiplier Tube) with wavelengths centered around 633 nm. LED diodes scanner examples are Victoreen Model 37-443 (Nuclear Associates Radiochromic Densitometer, Carle Place, NY) and CMR-604 (Photoelectron Corp) which has wavelength centered at 671 nm (11 nm FWHM) and 665 nm (20 nm FWHM) respectively. Right part of Fig. 1-1 represents the absorption spectra for two GAFCHROMIC™ film models, the EBT-1 model and the HS model, together with the emission spectra of the light sources of four commonly used optical densitometers.[59] The He-Ne laser based optical densitometer with peak emission centered at 633 nm would not adequately match the absorption maximum for the original GAFCHROMIC™ film models, whereas for the EBT-1 film appears to be a perfect match. On the other hand, all previous optical densitometers, tailored to the absorption maximum of the original radiochromic films would experience a decreased sensitivity when used in combination with the latest GAFCHROMIC™ EBT-1 film model.

However, the use of He-Ne laser based optical densitometer is not recommended for two-dimensional radiochromic film dosimetry, because it provides coherent and polarized light; two properties of laser light that can lead to serious problems when using laser-based optical densitometers for radiochromic film dosimetry. Dempsey et al[74] demonstrated that laser light coherence can create interference patterns. Radiochromic films have been shown to suffer from variation in optical density when the light source is linearly polarized and the film is rotated.[75] If the light source and the detector are both linearly polarized, variations in the measured optical density can amount to 15% for the HS model GAFCHROMIC™ film[76] when the film is rotated through 360$^{o}$.

**b. Multiple wavelengths scanners**

This kind of scanners utilizes white light from a fluorescent lamp which emits light with all wavelengths. Useful absorption range of radiochromic films are seen from 400 nm to 800 nm (Devic et al[60] (2006)) especially at the red color wavelengths which extends between 600 nm to 700 nm approximately. Green color wavelength extends approximately between 500 nm to 600 nm and blue color wavelengths lies between 400 nm to 500 nm. Split of a color image into these three color channels can be achieved with either RGB photographic scanners or spectrophotometers with chopper assembly that enables wavelength selection. RGB scanners examples include AGFA Arcus II with maximum spatial resolution of 1200 dpi (dots per inch) and Vidar VXR 16 with maximum spatial resolution of 285 dpi, Expression 1680 Pro (Epson) with optical spatial resolution of 1600 dpi, Expression 10000XL (Epson) with optical resolution of 2400 dpi. Both Epson scanners' resolutions can be extended to 12800 dpi by built-in software interpolation. All these RGB scanners use linear CCD array system for detection of light

Spectrophotometer example is Perkin Elmer Lambda 650 double-beam, double-monochromator, ratio recording UV/Vis spectrophotometer. Optical system uses holographic grating monochromator with 1440 lines/mm UV/Vis blazed at 240 nm. With a tungsten-halogen and deuterium lamp as light sources the spectrophotometer can perform scans between wavelengths of 190 nm and 820 nm with accuracy of ±0.15 nm. As a detector Lambda 650 spectrophotometer uses an R955 photomultiplier tube. In our study[68] we used spectral resolution of 2 nm and the acquisition time per wavelength set to 0.52 sec. A Perkin Elmer Solid Sample Holder (Part. No. B0080822) was modified to assure that film pieces are always positioned perpendicular to the direction of the light beam.

#### 1.4.3.1 Choice of a scanning system

Some issues need to be identified before choosing a specific scanner for radiochromic film dosimetry. One has first to decide which quantity he/she wants to relate to dose. There are two current trends in establishing calibration curves in film dosimetry: absorbance and optical density. Although they represent the same thing (a measure of light intensity) physicists refer to absorbance as the absorption spectrum of radiochromic films versus wavelength and then they manually select wavelength windows that correspond to a certain color range (Devic et al[68]) and report the integration over the wavelength of these windows against dose which results in non linear relationships. For optical density (OD), it is more likely to use RGB scanners where signal is already split into three color components while scanning using color filters of the CCD arrays in document scanners. Such scanners provide Pixel Values (PV) where one can acquire transmittance of light from these values and transform them into optical densities which are more conveniently plotted against dose in a non linear relationship.

Issues related to the choice of scanner and/or scanning radiochromic films are presented in the following sections.

**a. Scanning resolution**

This includes maximum spatial resolution of the scanner expressed in dpi (dots per inch) or µm/pixel where 1 µm/pixel correspond to 25400 dpi and color depth which is more referred to as bit-map and available as 24 bit or 48 bit where each color channel uses 8 bit and 16 bit respectively that correspond to $2^8$ and $2^{16}$ color depths; respectively. These issues were discussed by Ferreira et al[77] in 2009 and found not to have significant change when plotting the calibration curve regardless of the fact that larger color depths explore more of the higher spatial resolution provided by the grain size of the GAFCHROMIC structure, which would be useful in high dose gradients.

**b. Scanner warm-up, fluctuation and lamp darkening**

Warm up effect refers to the time that the scanner lamp and electronics need to reach stable temperature while fluctuation refers to scan-to-scan difference in signal for the same setup and measurement. Lamp darkening originally was thought to be an effect coming from the scanner's light source and that it causes extra darkening on the film. It was shown by Paelinck et al[78] that for successive scans, optical density increases. However, it was proven by Lynch et al[79] for the same type of the scanner (1680 Pro) that this increase was due to the increase in temperature of the scanning bed which he showed to be constant after certain level in more than 1000 scanning repetitions.

Extensive research of warm up effect was done by various authors such as Devic et al[59] for AGFA Arcus II, Paelinck et al[78] and Battum et al[89] for Epson Expression 1680 Pro, Ferreira et al[77] and Martisikova et al[80] using the Epson Expression 10000 XL and they found that performing three scans for scanners AGFA and 1680 Pro before any measurements diminishes the effect, while performing a preview with the Epson Expression 10000XL is sufficient.

Epson Expression 10000 XL acquires a background calibration signal before every transmission scan and uses it as a basis signal (zero line). Once the scanner is turned on, it is important to perform a preview scan in transmission mode in order to warm-up the electronic elements in the scanner to reach optimum thermal state as specified by the manufacturer. It has been shown in the literature[80] that the net change in OD (ΔnetOD) fluctuation decreases to less than 0.5% after performing a preview scan.

We have checked the energy deposition into the film whether from scanning lamp or temperature change in scanner bed in our work (Devic et al[68]) and we found out that the fluctuation of scanning the same piece of film 16 consecutive times is less than 0.11% which is expected because Epson Expression 10000XL scanner uses a cold cathode lamp and it acquires a

calibration signal prior any scan (see Fig.1-7). Fuss et al[81] reported 0.03% fluctuation in few minutes scanning and 0.7% in day to day fluctuation.

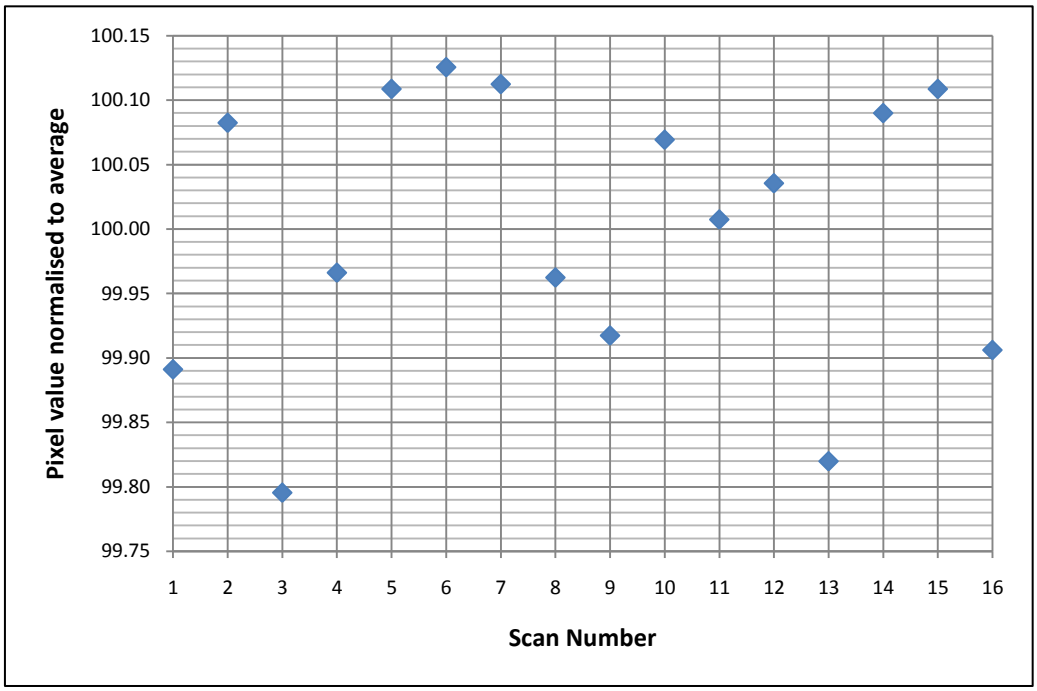


Fig. 1-7. Energy deposition into a single 4" × 2.5" piece of EBT-2 film from scanner light source and temperature of the scanning bed in 16 consecutive scannongs. Scanner type is Epson 10000XL.

**c. Scanner noise**

The problem of scanner noise is dependent on inherent noise of the scanner detection electronics (CCD arrays) and this might affect the analog to digital conversion process in the acquisition of pixel value (PV). Averaging images from multiple scans is a recommended way that tackles this problem where five scans of unexposed film pieces are performed in this procedure. Another effective way to remove the scanner noise is to utilize a 2D Weiner filter during image processing of the film piece and avoid multiple scans.[59] So, only one scan is taken for every film piece instead of five consecutive scans of the same film piece to correct for scanner noise. Devic et al[60] have found that in the case of a uniformly irradiated film, the 2D Weiner filter (applied over 7 × 7 pixels in size) is sufficient for the scanner noise reduction and that the averaging over five scans would not further improve signal to noise ratio of the

scanned image. This, however, does not necessarily apply for the case of large dose gradient fields, in which case more local, 3 × 3 pixels, 2D Weiner filter in combination with multiple scans may be a better solution for scanner noise removal and preservation of the actual local signal gradients at the same time. The 2D Weiner filter, which uses a local estimate of the noise power spectrum has an advantage is preserving systematic variations in film's optical density and it was also used by Ferreira et al[77].

On the other hand one also needs to correct for any deformities in the scanning bed (spikes), defined as pixels in the image that differ in intensity from the blank (un-attenuated) signal, which is equal to $2^{16}$. Once the five images of the unexposed film pieces have been acquired, blank scans are taken (again five times) over the same scanning region as the previously acquired images with film pieces.

**d. Scanner uniformity (light scattering effect)**

The effect of scanner non-uniformity is a convolution of decreased scattering of light along the lamp axis toward the edges and CCD arrays sensitivity. Fig. 1-8 illustrates the scanner uniformity of Epson Expression 10000XL and it shows that the scanner has a good uniformity (minimal drop in sensitivity) in the horizontal axis which is expected but a significant change on the vertical axes. This test was performed on five regions as one can conclude from the same figure. It is expected that we see this non uniformity in the vertical axis where it has been indicated in the literature for other flatbed scanners[77, 79, 82, 89] but it can be accounted for by mathematical descriptions of each dose line with respect to distance from central axis where the uniformity is normalized as done by Devic et al[60] and Battum et al[89]. Lynch et al[79] exposed film strips to sunlight in step-wedge way and used them to create correction curves for the drop of sensitivity in the vertical axis of the scanner. Menegotti et al[83] did a similar approach but using radiation instead of the sunlight. However, keeping films in the same location and selecting regions of interest close to the center of the film is shown effective in diminishing the effect of light scattering.

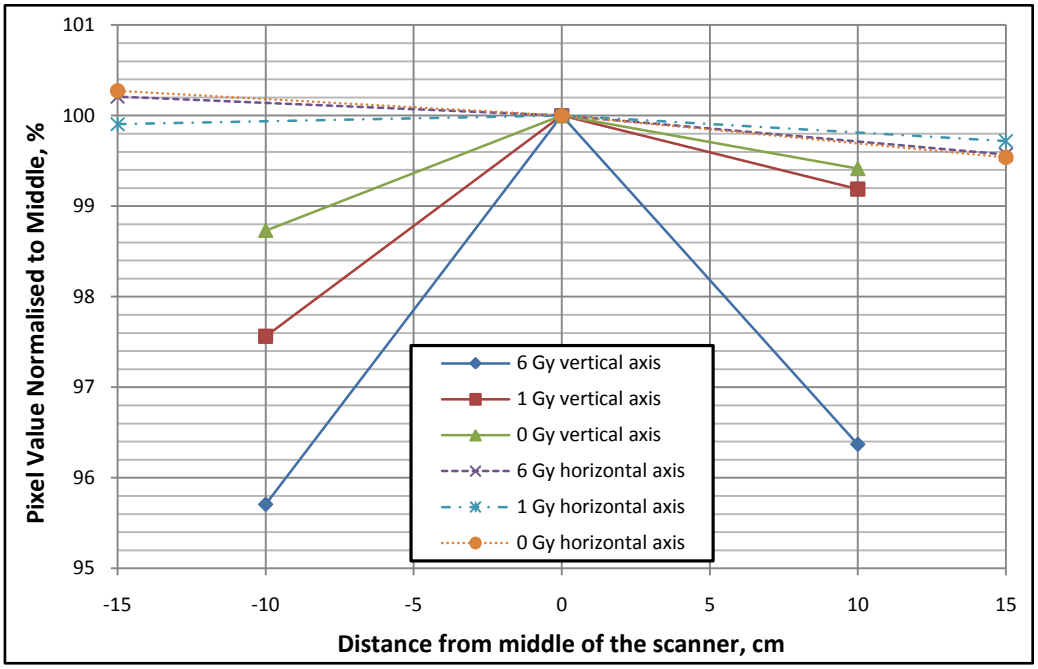


Fig. 1-8. Light scattering effect from EBT-2 film scanned in an Epson 10000XL scanner. Uniformity is shown to drop significantly in the vertical axis along the scanner lamp (perpendicular to scanning direction).

### e. Scanning dependence on orientation

GAFCHROMIC™ film models have experienced polarization dependences in measured transmission in the past.[75] This is governed by the difference in polarization direction between light source and the needle-like structure (Rink et al[84]) of EBT film models. We have tested the optimum film position of the latest film model (EBT-2) with respect to the scanning bed of an Epson Expression XL10000 flat-bed document scanner that would provide highest sensitivity for our measurements in a recently accepted study[85] for publication. We used a 4" × 2.5" film piece for this test where the shorter edge of this film piece was on the longer side of the 8" × 10" film sheet and we have found that despite the fact that film is not symmetric, flipping the film on the scanner bed does not introduce any significant change in measured transmission signal through the film (Fig. 1-9). However, rotation of the film pieces on the scanner bed still leads to an error of almost 10% if care is not taken about rotational position of the film pieces during scanning procedure. Also, we have found that

a “portrait” film orientation with respect to the scanning bed (long edge of the 8” × 10” film sheet is aligned with the long edge of the scanning bed) gives a higher measured signal (Fig. 1-9). Accordingly, we have decided to use the “landscape” film piece orientation that translates into the “portrait” orientation on original film sheet in all of our measurements presented in this work when document scanner is used. The film’s batch number of the GAFCHROMIC$^{TM}$ EBT-2 film model used in this work was F06110901.

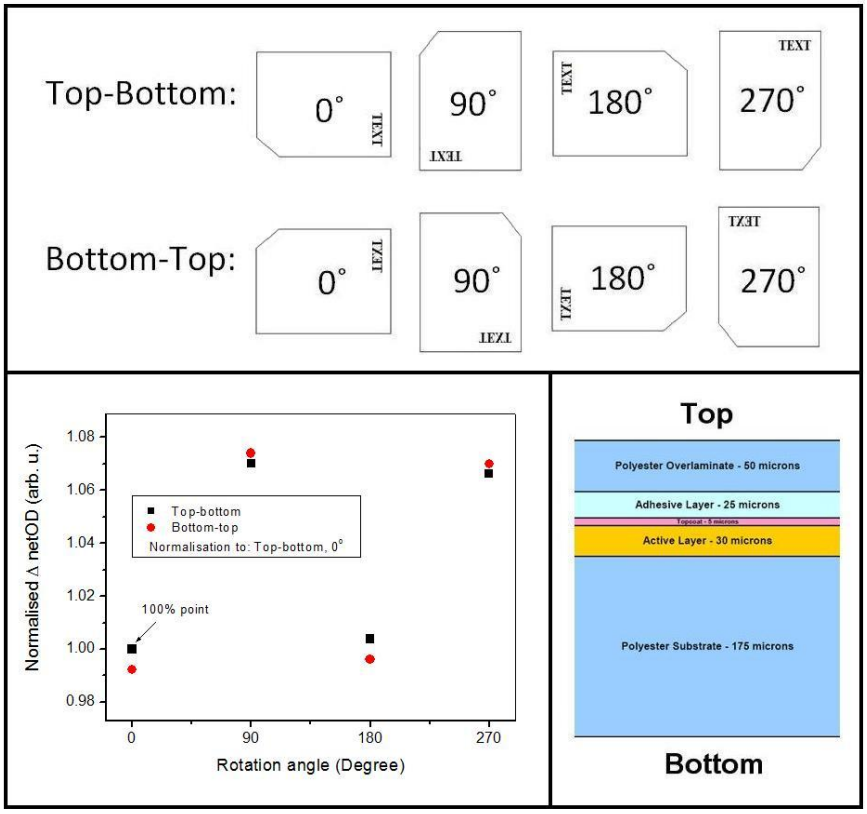


Fig. 1-9: A top view of different 4” × 2.5” EBT-2 GAFCHROMICTM film orientations (top) used to determine the optimum net change in optical density and the angular dependence of intensity of this signal (left). Top and bottom layers of the film are defined as shown (right). Film orientations were handled separately in the center of the scanner.

Other studies by Buttum et al[89] and Lynch et al[79] agree with our polarizational and orientational findings but the percentage difference in optical density was higher for other scanner types.

**f. Scanner cost**

One has to keep in mind the price difference between scanning systems. Transmission RGB scanners provided revolutionary step into radiochromic film dosimetry as the signal they provided was proven to be within the film's homogeneity level and they are much cheaper than other types mentioned before. Some studies in the literature also compared reflection mode scanners to transmission ones (Kalef-Ezra et al[86] for MD-55-2, Richely et al[87] for EBT-2) and they found that reflection mode is superior to transmission mode in sensitivity which is expected because the light is absorbed twice in the reflection mode. However, Richely et al[87]commented that reflection mode is not a superior alternative to transmission mode because they found 1.2% difference in signal between film piece scanned alone and similar piece scanned with surrounding film which suggest mistreatment of signal uniformity. Reflection scanners were studied because they are much cheaper than transmission scanners and more investigation is needed to confirm if they are a valid alternative to trusted transmission scanners.

### 1.4.4 Scanning protocol

As mentioned earlier, RCF dosimetry system is an ensemble of (a) a radiochromic film type, (b) scanning densitometer, and (c) a scanning protocol that relates the film and the densitometer together by describing how to achieve correct dose measurements. Scanning protocol has the highest impact on the accuracy and precision of measurements and thus we have to define exactly all scanning procedures and maintain the same protocol in scanning all film pieces. This importance is seen easily from the number of papers in the literature that had discussed different issues that might introduce unacceptable errors in dose measurements. According to the extensive data available in the literature, the most important ones are: orientation of the film piece, location of the film piece on scanning bed (light scattering effect or scanner uniformity), size of film piece, size of scanning window, size of region of interest on the film piece image, difference in optical properties (polarization for instance) between film

piece and scanner light source, sensitivity of CCD arrays in the scanner, scanner warm-up, energy deposition into the film piece from multiple scanning, scanner fluctuation and noise, post irradiation time, humidity effect, dark signal correction, background correction, thermal and temporal history of the film pieces and film non-uniformity.

#### 1.4.4.1 Radiochromic film measurements in water (humidity effect)

Several studies have been reported so far on the impact of radiochromic film immersion in water. Butson et al[88] reported on the effect of water diffusion on an older MD-55 model GAFCHROMIC™ film. They showed that only a small penetration rate was seen from water into the film affecting the outer areas of the film, with penetration being less than 0.5 mm per hour. They also reported that if the optical density of the film is measured 7-10 days after the films were permanently removed from water, the optical density of the film at the centre remained unchanged within experimental errors while a slight change of 3%–5% was observed up to approximately 2 mm inside the visible edge of the water penetration mark. Battum et al[89] tested the achievable limits of the EBT-1 model GAFCHROMIC™ radiochromic film dosimetry system in water. They found that after 15 minutes of immersion in water a slight light blue fog of about 2 mm width along the film edges was visible due to water penetration. After drying the film at room temperature for 1 hour no such water trace was detectible even if the film is scanned. Since they were scanning films more than 6 hours post-irradiation, i.e., immersion in water, they have suggested no additional precautions for this effect. Rink et al[90] have studied the impact of temperature and hydration effects on absorbance spectra and radiation sensitivity of the EBT model GAFCHROMIC™ radiochromic film. They found that sensitivity of EBT film model to ionizing radiation is also a function of the hydration of the sensitive layer. They concluded that water influences the three-dimensional structure of the monomer crystals and desiccating the samples shifted both the absorbance peak to a higher wavelength and decreased sensitivity.

#### 1.4.4.2 Impact of post irradiation time

One of the major drawbacks of the current radiochromic film dosimetry protocols is the post-irradiation waiting time. Most of the current radiochromic film dosimetry protocols suggest that films should be scanned at least 8 hours post-irradiation,[61, 66] which is the time assumed to be necessary for the film darkening to saturate. Martisikova et al[80] showed that the polymerization does not stop after 24 hours and that it stabilizes in 7 days

In a recent study, Devic et al,[68] we have studied the evolution of absorption spectra of the EBT-2 film model with respect to time and dose. We showed the evolution of absorption spectrum of radiochromic EBT-2 GAFCHROMIC™ film model with scanning times ranging from 3 minutes up to 5 days post-irradiation and in a dose range from 0 Gy to 6 Gy. We also described a method that can establish time error constraints on the post-irradiation scanning time that will still provide an acceptable dose error for clinical applications if the protocol employing shorter post-irradiation scanning time is implemented in the clinic which will be discussed in more details later.

#### 1.4.4.3 Scanning protocols in the literature

Most of the scanning protocols that have been reviewed provide collective studies that fall within the following:

(1) Mathematical description the relationship between film darkening intensity and dose i.e. the so called calibration curve.

(2) Description of film darkening intensity: Absorbance, optical density and pixel values.

(3) Corrections needed for different effects mentioned in this literature review that are related to the film, scanner or both.

(4) Preservation of the same scanning technique between calibration phase and dose measurement phase.

(5) Selection of scanning color channel that is more suitable for dose measurements.

(6) Assessment of uncertainty analysis on dose measurements.

One also has to bear in mind that the source of both uncertainty on measured OD and uncertainty on dose determination in RCF dosimetry will greatly depend on the design of the protocol used. The uncertainty analysis fro various radiochromic film dosimetry systems are available in the literature.[53, 55, 66, 87, 89] The most comprehensive characterization of these sources is presented in the study performed by Bouchard et al.[91] We have adopted a complementary approach where we tried to accommodate common sources of uncertainty found in these studies into our own protocol.

## 1.5 Aim of the project

Purpose of this project was to compare the calibration curve from EBT-2 GAFCHROMIC$^{TM}$ film irradiated from Ir-192 in water to the same calibration curve created by irradiating film pieces in Solid Water$^{TM}$ for the following doses: 0, 0.25, 0.5, 1, 1.5, 2, 2.5, 3, 3.5, 4, 5, 6, 8, 10, 20, 30 and 50 Gy. This is advantageous because it allows us to carry on dosimetry measurements in the more convenient Solid Water$^{TM}$ medium which is less cumbersome experimentally. We want to study/achieve the following:

1) Establish radiochromic film dosimetry protocol for HDR Ir-192 source

2) Investigate absorption spectra of EBT-2 GAFCHROMIC film.

3) Investigate the impact of post-irradiation time waiting in EBT-2.

4) Find an optimal mathematical model that relates dose and optical density in EBT-2.

5) Assess which color channel provides accepted balance between sensitivity, accuracy and precision.

6) Assess the performance of EBT-2 film in water medium

7) Establishing a dose conversion factor that converts *dose to water* to *dose to Solid Water$^{TM}$*

# Chapter.2: Investigation of EBT-2 film performance

## 2.1 Study of post-irradiation time impact on EBT-2 GAFCHROMIC™ film dosimetry

In this section we investigate the impact of the post-irradiation time on our measurements of the change in optical density. The reason for this investigation is twofold: It explores the inaccuracy associated with small variations in scanning times, and it also enables us to scan the films after shorter times post-irradiation, which is very convenient especially in the source alignment phase as will be emphasized later. The method explained here provides means by which one is able to estimate the polymerization rate and as long as time is monitored, film pieces can be scanned in very short times as low as 30 minutes post-irradiation with careful handling of the film.

### 2.1.1 Irradiation and scanning procedures

To investigate the time evolution of the absorption spectra of the EBT-2 film model, one film piece, exposed to a dose of 1 Gy, was scanned together with a control[68,92] (unexposed) film piece at various times (3, 10, 30, 60, 180, 600 minutes, and 24, 48 and 120 hours) post-irradiation. On the other hand, to assess the dose error that may arise due to the time discrepancy for the established radiochromic film dosimetry protocol we have also scanned set of films exposed to various doses after 30 minutes and 24 hours. Irradiations were performed by exposing EBT-2 film pieces (4” × 2.5” in size) with a Cobalt-60 photon beam from a Theraton 780 teletherapy unit (Atomic Energy of Canada Limited, Canada).

The post-irradiation time has been analyzed using absorption spectra of film samples measured with a Perkin Elmer Lambda 650 double-beam, double-monochromator.

### 2.1.2 Estimation of post-irradiation time impact on measured dose

Top portion of Fig. 2-1 represents the two wavelength band areas centered around 633 nm and 583 nm, over which absorbance was integrated to study film response behavior as a function of dose and post-irradiation time. The two bands corresponds to the red (Band 1) and green (Band 2) color channels from the RGB transmission scans obtained on the flat-bed color scanners. Middle section of Fig. 2-1 represents the integral intensity of the two band areas as a function of time for the same film piece irradiated to a dose of 1 Gy. By applying the log-log scale it appears that polymerization process that contributes to the darkening of the film (or increase in absorbance) persists even after 5 days, but at much smaller rate than within the first 24 hours. Bottom part of Fig. 2-1 illustrates the two band areas intensities as a function of dose for film pieces scanned 30 minutes and 24 hours post exposure. Integration over the whole wavelength range would correspond to optical densitometers working in a gray-scale mode, and it was shown previously that such devices do not provide the optimal sensitivity for the radiochromic film dosimetry system when compared to the extraction of the red channel from the 48-bit RGB mode (16 bits per color) scanned film images on a flat-bed document scanners.[59] One should also bear in mind that sensitivity curves depicted in the bottom part of Fig. 2-1 represent the best achievable sensitivity curves as they have been obtained using the spectrophotometer. Once the absorption spectrum is convolved with the emission spectrum of the light source and sensitivity spectrum of detector (linear CCD array, in the case of flat-bed document scanners) the obtained *netOD* vs. *Dose* calibration curve will have lower sensitivity compared to the one shown at the bottom section of Fig. 2-1.

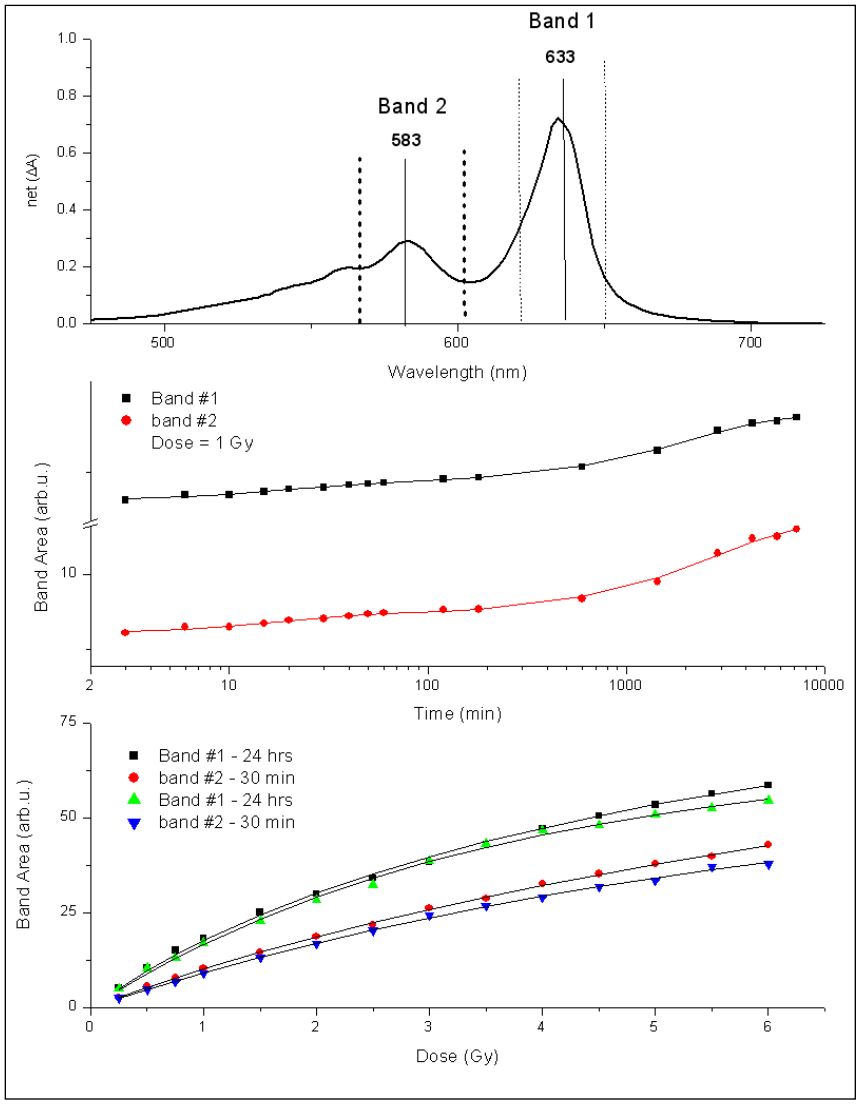


Fig. 2-1. Two wavelength band areas centered around 633 nm and 583 nm, over which absorbance was integrated (top); integral intensity of the two band areas as a function of time for the film piece irradiated to dose of 1 Gy (middle); two band areas intensities vs. dose for film pieces scanned 30 minutes and 24 hours post exposure (bottom).

Fig. 2-2 shows results of the method used to estimate dose error due to post-exposure scanning time window for piece of film irradiated to a dose of 1 Gy and scanned after 30 minutes. Top portion of Fig. 2-2 represents change of net absorbance around 30 minutes time evolution curve with net absorbance values sampled within ± 5 minutes time window. Bottom part of Fig. 2-2 represents results of applying the sampled changes of absorbance on time evolution curve to the net absorbance dose response curve around 1Gy for the

same film piece. Tracing back the change in net absorbance to the dose axis, we determined that dose error at the level of 1 Gy ranges from -0.4% to 0.3%. We have applied the same method to assess dose error using both red and green color bands at 30 minutes and 24 hours post-exposure scanning time protocols. The time window investigated was ± 5 minutes for 30 minutes protocol and 2 hours for 24 hours post-irradiation scanning time protocols. Results of our analysis are summarized in Table 2-1, which reveals that with specified time windows around scanning times for a particular protocol expected dose errors are within 1% from the exact dose value.

Table 2-1: Dose error due to post-exposure scanning time window

| **Dose Error at 1 Gy** | **30 ± 5 minutes** | **24 ± 2 hours** |
|---|---|---|
| **Band 1 (Red)** | ±0.4 % | ±0.6 % |
| **Band 2 (Green)** | ±0.4 % | ±0.6 % |

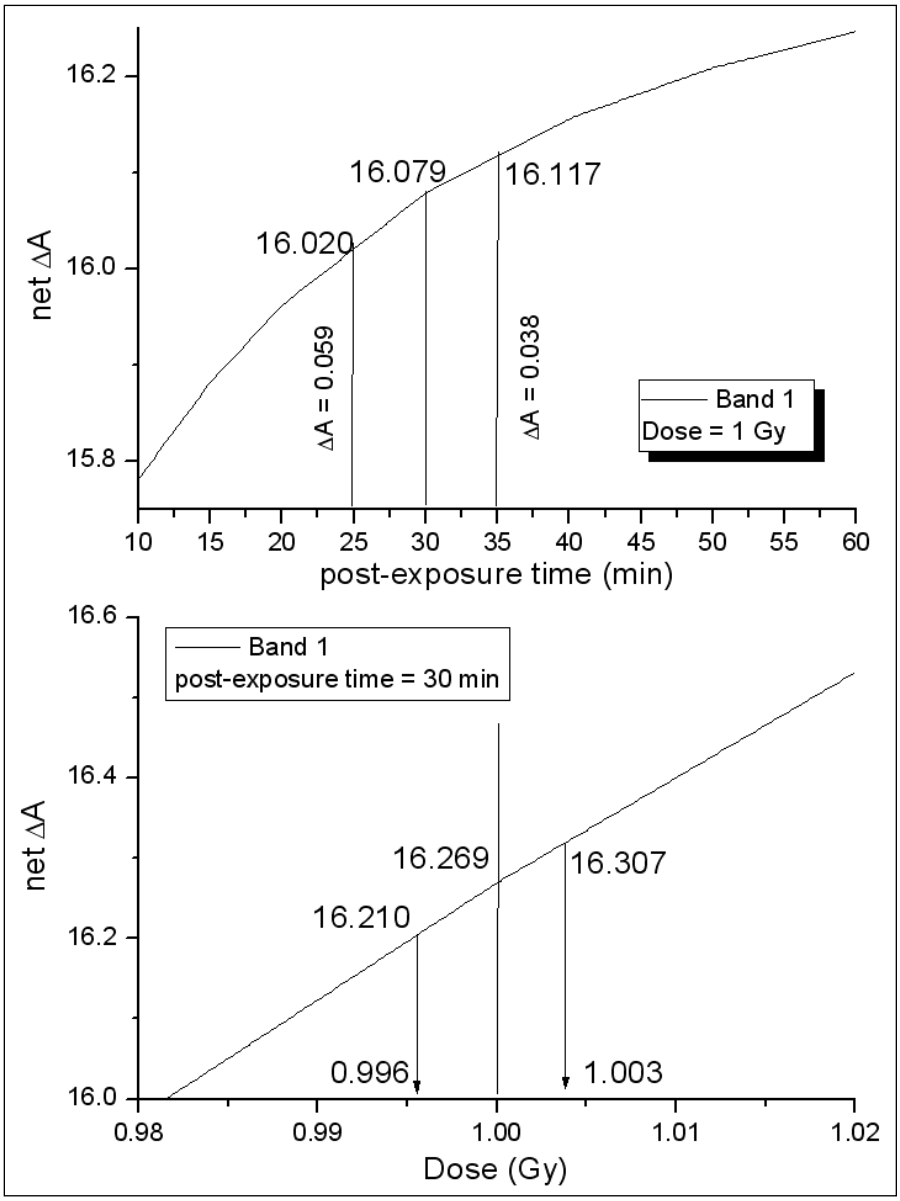


Fig. 2-2. Dose error due to post-exposure scanning time window: change of absorbance around 30 minutes time evolution curve for the piece of film irradiated to dose of 1 Gy (top); change of absorbance around 1Gy dose response curve for the piece of film scanned 30 minutes post-irradiation (bottom).

### 2.1.3 Clinical test case for the post-irradiation time impact

To test the feasibility of using radiochromic film dosimetry protocol by scanning irradiated film pieces earlier than currently recommended 8 hours, we created two calibration curves by scanning films irradiated to various doses and scanned using Epson Expression XL10000 flat-bed document scanner after 6

minutes and 24 hours. Calibration curves were created following the modified radiochromic film dosimetry protocol described earlier.[92] One intensity modulated radiotherapy (IMRT) plan was delivered to a piece of the EBT-2 GAFCHROMIC™ film and scanned 6 minutes and 24 hours post-irradiation. Using the red color channel of the 48-bit RGB mode (16 bits per color) scanned images two dose images of the very same IMRT plan were obtained that correspond to radiochromic film dosimetry protocols that are scanning irradiated film pieces 6 minutes and 24 hours post-irradiation. Two dose images, expected to be identical, were imported into FilmQA verification software (International Specialty Products, Wayne, NJ) and compared in terms of dose-difference, distance to agreement and gamma function.

Fig. 2-3 represents results of dose maps comparison for the IMRT plan with dose maps reconstructed using 6 minutes and 24 hours post-irradiation scanning protocols. Calibration curves that are used to convert *netOD* of the irradiated film to dose are shown on the top-left section of Fig. 2-3. Top-right section of the same figure represents the gamma function comparison for the two dose maps using 0.5%, 0.5 mm criterion while distance-to-agreement (DTA) with 0.5 mm criterion and dose-difference (DD) with 0.5% difference have been shown on the bottom-left and bottom-right part of Fig. 2-3 respectively.

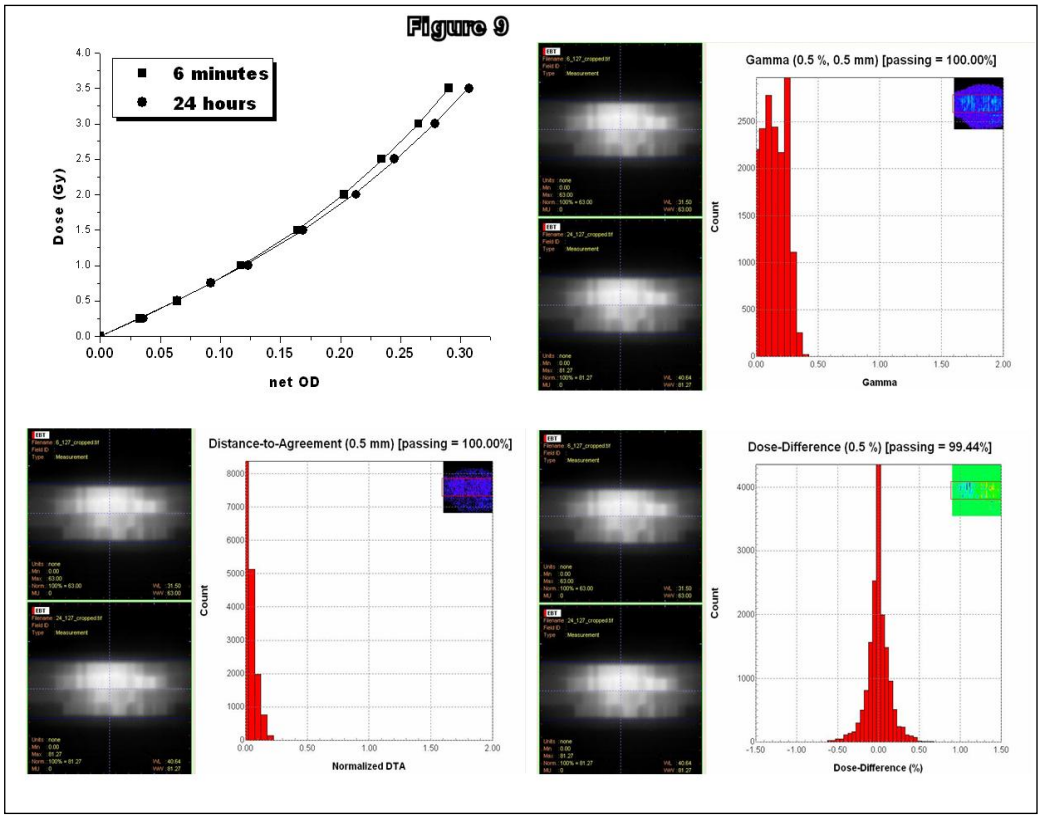


Fig. 2-3. Results of dose maps comparison for an IMRT plan; dose maps are reconstructed using 6 minutes and 24 hours post-irradiation scanning protocols: netOD to dose calibration curve (top-left); gamma function with 0.5%, 0.5 mm criterion (top-right); distance-to-agreement with 0.5 mm criterion (bottom-left); and dose-difference with 0.5% difference (bottom-right).

Scanning windows for two post-irradiation time protocols were 2 seconds for 6 minutes and 1 hour for 24 hours film scanning procedure. Results presented in Fig. 2-3 suggest that two dose distributions for a given IMRT dose maps are virtually indistinguishable in terms of three two-dimensional image metrics: Gamma-function, DTA, and DD. However, one has to be careful in the implementation of different post-exposure scanning time protocols and acceptable time widows around chosen scanning time. The time and dose dependent changes in absorbance or optical density should be created for a chosen scanning time, similar to the two graphs (middle and bottom) given in Fig. 2-1. By inspecting the corresponding changes in absorbance or optical density within reasonable broad scanning time windows, expected dose error should be estimated using the method outlined in Fig. 2-2 and if dose error is

acceptable the allowed scanning time window for a given post-irradiation scanning time protocol can be adopted.

## 2.2 Evaluation of EBT-2 Model GAFCHROMIC™ Film Performance in Water

While it appears that water immersion may not have a significant impact on the transmission properties of the radiochromic films, at least if the film pieces are not kept in water for a long time, there is an obvious change in the optical density of the film, which depends on the time film was immersed in water and location on the film piece where this change is observed. Although the contemporary use of radiochromic film may not require a long time immersion of film pieces in water, certain emerging radiochromic film dosimetry applications (e.g. reference dosimetry for brachytherapy sources) may impose submerging film pieces in water for hours.

In this section, we summarize our recent work, Aldelaijan et al[85], which was accepted for publication in Medical Physics Journal. In this work we reported on the results from our systematic investigation of the EBT-2 model GAFCHROMIC™ film immersion in water for a range of various parameters: time the film spent in water, time the film was left to dry out after being removed from water, size of the film pieces, impact of the initial optical density of the film piece, and certainly measurement position on the film piece where the water influenced change in optical density. To further investigate the nature of water's impact on the radiochromic film transparency, absorption spectra of the film pieces were recorded prior and after water immersion. Finally, we reported on the magnitude of dose errors that one may encounter if the appropriate correction procedure recommended in this study is not applied.

### 2.2.1 Irradiation, scanning and water control procedures

Pieces of the EBT-2 model GAFCHROMIC™ film of different sizes (2" × 2", 4" × 4" and 8" × 8") and initial optical densities (0 and 3 Gy from a T-780 Cobalt-60 teletherapy unit) were immersed in water for times ranging from

30 minutes to 24 hours. Pieces of film were immersed in a water tank as depicted in Fig. 2-4. Film pieces were residing in water at a depth of 125 mm supported from the bottom by small (19 mm in diameter) Teflon rods. Change of the *netOD* was sampled in the middle of the film piece over a region of interest (ROI) being half the size and centered with respect to the film.

To perform a systematic study on the effect of immersion time (T) on film pieces, immersion times ranged from 30 minutes to 24 hours. Since data reported in literature suggests that water diffusing into the film during immersion eventually evaporates once the film is permanently removed from water, we also studied the impact of the scanning time ($\Delta t$) that ranged from 0 hours (films scanned right after removal from water) to 72 hours post-immersion.

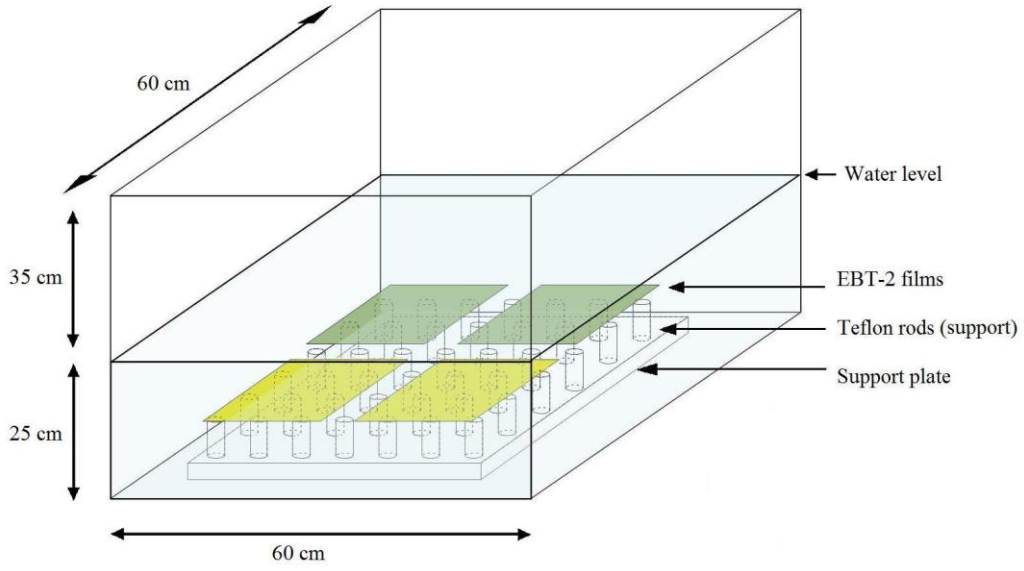


Fig. 2-4: Diagram of the experimental setup showing four pieces of EBT-2 GAFCHROMIC$^{TM}$ film immersed into water. Teflon rods are used to keep the films at the same level during the whole immersion period. Difference in color of the films refers to different initial optical densities (doses).

Two film pieces of the same size (4" × 4") and different optical densities (0 and 3 Gy) were used to measure the net absorbance change spectrum of the older EBT-1 film model. Two film pieces were scanned prior to and 24 hours after immersion in water.

To test the measured two-dimensional change in optical density of the film pieces immersed in water, we used Epson Expression XL10000 flat-bed document scanner. The films were scanned with the methods described in Chapter 4, and changes in optical density were determined following the very same protocol described there. To quantify the change in optical density due to the effect of water only, a control piece of film was always used, concept of which is described in detail in section 4.1.4. Final change in optical density *(*Δ*netOD*) was calculated by subtracting the optical density change of the control film piece from the optical density change of the measurement film piece immersed in water. Once the resulting image was obtained, profiles have been taken through the center of the film along the two orthogonal directions by averaging 10 lines, corresponding to 2 mm wide band on the Δ*netOD* image with a scanning resolution of 127 dpi.

To further investigate pathways of water penetration into the film, we used two 8" × 8" in size film pieces (0 and 3 Gy) with the edges sealed with three layers of duct tape prior to immersion in water. Sealed film pieces were left in water for 24 hours and once removed from water sealing tape was removed. Films were scanned right after removal from water ($\Delta t = 0$ hrs) and three days later ($\Delta t = 72$ hrs). At the very same time, another two pieces of film (0 and 3 Gy) with unsealed edges were treated in the very same manner. The *netOD* from the unsealed pieces of film will be compared with the *netOD* from the sealed pieces of film in order to determine the intensity of water penetration through the protective polyester layer of the film and diffusion into the film edges where we assume that the sealed films represents penetration effect and subtracting the *netOD* of it from the *netOD* of unsealed pieces of film should yield some information about the diffusion of water through film edges.

To assess the anticipated dose error that would result from the change of *netOD* due to water immersion (and not irradiation) we have calculated the corresponding dose values using the appropriate dose calibration curve we use for our radiochromic film reference dosimetry protocol.

### 2.2.2 Absorption spectra change with water presence

Fig. 2-5 represents absorption spectra of two 4" × 4" EBT-2 GAFCHROMIC$^{TM}$ film pieces before (dotted, black) and 24 hours after immersion in water (dashed, red), as well as the resultant net absorbance change (solid, green). The left part is for a non irradiated piece of film, and right part is for a 3 Gy piece of film. The resultant net absorption change represents the absorbance incurred from water only. It is apparent that this change is more dominant around the main absorption peaks, centered around 583 nm and 634 nm. This result suggests that there might be an optical density change which has to be accounted for if accurate dose measurements are to be performed with pieces of the EBT-2 model radiochromic film immersed in water. However, this does not appear necessary for the case of the blue channel (400 – 500 nm) where the change is shown to be uniform and independent of dose. Difference in the magnitude of the resultant reflectance between 0 Gy and 3 Gy film piece also suggests that we may expect difference in the correction we have to apply.

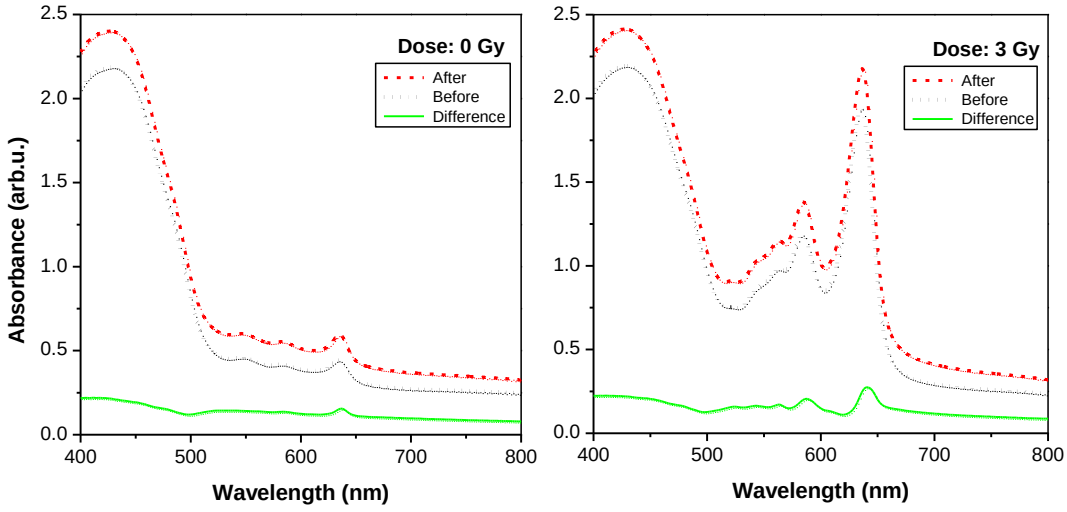


Fig. 2-5: Absorption spectra of two 4" × 4" EBT-2 GAFCHROMICTM pieces of film before (dotted, black) and after (dashed, red) 24 hours immersion in water and resultant net absorbance change (solid, green): a zero dose piece of film (left), and a 3 Gy piece of film (right).

### 2.2.3 Estimation of water impact on EBT-2 GAFCHROMIC™ film dosimetry system

Fig. 2-6a shows an example of the horizontal Δ*netOD* profiles across an 8" × 8" piece of EBT-2 film immersed in water for different immersion times between 30 minutes and 24 hours and also it illustrates the penetration depth of a 2" × 2" film piece that was kept for 24 hours in water. Fig. 2-6b magnifies the left edge of the film pieces (shown in Fig. 2-6a) and clearly indicates two effects due to the film immersion in water dependent on the immersion time period: (a) an increase in Δ*netOD* throughout the film and (b) an increase in water penetration depth through the edges of the film. This penetration reaches 6 mm if the film was left for 24 hours in water and scanned right after removing the film piece from water but if the film piece is scanned 24 hours after removing from water the penetration reaches 9 mm (Fig. 2-6c). This finding is similar to previously published data for MD-55 GAFCHROMIC™ film model.[93] However, it is apparent that Δ*netOD* stabilizes after penetration distances and no pronounced changes in the texture of the film are noticed,

which allowed us to use sampling region of 150 mm for the specified film size in Fig. 2-6a. For smaller film sizes, sampling of Δ*netOD* was performed over 75% of the film piece width (38 mm). Result shown in Fig. 2-6c further suggests that the process of water penetration and evaporation from the film pieces could be governed by different processes. Nevertheless, one can assume that if film pieces are immersed in water, a certain region around the edges should be avoided for dose measurements if the film was kept in water for a long time. Finally, Fig. 2-6d suggests that the increase in Δ*netOD* is transient and if the film pieces are left in air after removing from water for a longer period of time, most of the water absorbed by the film will eventually disappear.

Table 2-2 summarizes the impact of in-water immersion on film pieces of the EBT-2 model GAFCHROMIC$^{TM}$ film for various immersion times (T), two film sizes (2" × 2", and 8" × 8 ") and two post-immersion scanning times (Δ*t*= 0 and 24 hours). Values of edge penetration and the Δ*netOD* were sampled on the corresponding profiles shown in Fig. 2-6 for various film pieces used in this study. Edge penetration values were sampled on all four edges of the film and averaged values as well as their corresponding standard deviations are reported in the table. Depth of edge penetration does not depend on the initial optical density of the film, but it increases with immersion time in water. It is also of note that post-immersion waiting time lead to a slight increase in the penetration depth. As we will demonstrate later, this effect is due to two different mechanisms of water transport through the layered structure of the film.

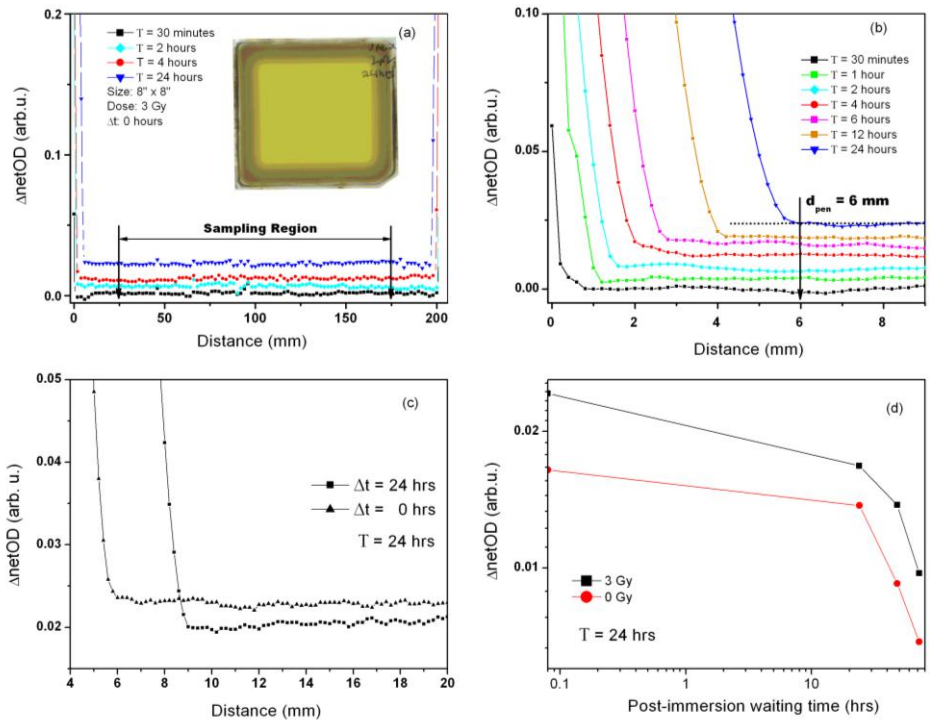


Fig. 2-6: Results of net optical density profiles changes: (a) across an irradiated 8" × 8" piece of EBT-2 GAFCHROMIC™ film immersed in water for times between 30 minutes and 24 hours and scanned directly after immersion time elapsed. Inset represents a scanned image of the immersed zero dose film piece in water for 24 hours; (b) enlarged section of the top image close to the film edge showing that water penetration through edges of the film and net change in optical density both increase with immersion time (b); (c) impact of the post-immersion waiting time on the penetration depth; (d) impact of the post-immersion waiting time on Δ*netOD* in the central portion of the film piece.

Last four columns in Table 2-2 summarize the sampled changes in Δ*netOD* as well as the anticipated dose errors one may incur from the presence of water, which was estimated from the calibration curve established for the batch of films we are using. Values of Δ*netOD* as well as their corresponding standard deviations were sampled over a region of 38 mm and 150 mm for the 2" × 2" and 8" × 8" film pieces respectively. For the short immersion times (30 minutes) measured Δ*netOD* is of the order of the estimated standard deviation, the anticipated dose errors can be neglected. However, if longer immersion times are anticipated, dose errors as large as 7% might be expected if no corrective actions are performed. It is also of note that the magnitude of the

effect is more pronounced for smaller film pieces, and slightly higher for the film piece exposed to 3 Gy.

Table 2-2: Impact of water presence on EBT-2 GAFCHROMIC$^{TM}$ film

| Scanning Time (hrs) | Size, (inch) | Immersion Time (hrs) | Edge Penetration | | 0 Gy (zero dose) | | 3 Gy | |
|---|---|---|---|---|---|---|---|---|
| | | | 0 Gy (mm) | 3 Gy (mm) | Δ(netOD) $\times 10^{-2}$ | Anticipated dose error (cGy) | Δ(netOD) $\times 10^{-2}$ | Anticipated dose error (cGy) |
| Δt = 0 | 2" × 2" | 0.5 | 1.6 ± 0.3 | 1.2 ± 0.3 | -0.09 ± 0.06 | -0.7 | -0.76 ± 0.07 | -5.9 |
| | | 4 | 2.8 ± 0.0 | 2.5 ± 0.2 | 0.76 ± 0.05 | 5.9 | 1.08 ± 0.07 | 8.3 |
| | | 6 | 3.5 ± 0.2 | 3.0 ± 0.3 | 1.19 ± 0.05 | 9.2 | 1.73 ± 0.06 | 13.4 |
| | | 24 | 6.5 ± 0.2 | 6.2 ± 0.3 | 2.61 ± 0.07 | 20.3 | 2.86 ± 0.04 | 22.2 |
| | 8" × 8" | 0.5 | 1.2 ± 0.6 | 1.5 ± 0.1 | -0.1 ± 0.1 | -0.7 | 0.2 ± 0.1 | 1.5 |
| | | 4 | 2.6 ± 0.6 | 2.8 ± 0.4 | 0.5 ± 0.1 | 4.1 | 1.0 ± 0.2 | 7.5 |
| | | 6 | 3.9 ± 0.9 | 4.1 ± 0.3 | 0.8 ± 0.1 | 6.3 | 1.3 ± 0.2 | 9.8 |
| | | 24 | 6.1 ± 0.2 | 6.3 ± 0.7 | 1.8 ± 0.1 | 13.9 | 2.3 ± 0.1 | 17.7 |
| Δt = 24 | 2" × 2" | 0.5 | 1.1 ± 0.5 | 0.9 ± 0.5 | -0.0 ± 0.1 | -0.3 | 0.08 ± 0.06 | 0.6 |
| | | 4 | 3.6 ± 0.3 | 3.1 ± 0.3 | 0.71 ± 0.06 | 5.5 | 1.09 ± 0.06 | 8.5 |
| | | 6 | 5.4 ± 0.9 | 4.4 ± 0.3 | 1.11 ± 0.06 | 8.6 | 1.44 ± 0.05 | 11.1 |
| | | 24 | 9.0 ± 0.0 | 8.7 ± 0.5 | 2.32 ± 0.06 | 18.0 | 2.65 ± 0.05 | 20.6 |
| | 8" × 8" | 0.5 | 2.7 ± 0.9 | 1.7 ± 0.5 | -0.1 ± 0.1 | -0.7 | 0.0 ± 0.1 | 0.2 |
| | | 4 | 3.8 ± 0.6 | 4.9 ± 0.5 | 0.5 ± 0.1 | 3.9 | 0.9 ± 0.2 | 6.8 |
| | | 6 | 5.3 ± 0.2 | 5.9 ± 0.2 | 0.8 ± 0.2 | 6.2 | 1.2 ± 0.2 | 9.2 |
| | | 24 | 8.9 ± 0.2 | 8.9 ± 0.5 | 1.5 ± 0.2 | 11.3 | 2.1 ± 0.1 | 16.0 |

Table 2-3 summarizes the impact of different pathways used by water to penetrate into radiochromic film pieces. Values of Δ*netOD* were sampled in the very same way as data presented in Table 2-2. In the case of a sealed film piece, there is still presence of water in the central portion of the film indicating that water does not diffuse through the edges of the film (from now on we will call this process a Diffusion effect) but it also enters into the film through the protective polyester layers, the process which we will refer to as penetration effect.

It should be noted that the Δ*netOD* results of diffusion effect are obtained by subtracting the penetration effect (Δ*netOD* results of sealed film) from unsealed film Δ*netOD* results. Looking at change of Δ*netOD* for both sealed and unsealed film pieces during the first 72 hours it is shown that it drops by 0.01 independently of the initial optical densities (doses), which support the idea of water evaporation. We also noticed that most of the water

appearing in the center of the film comes through penetration process, unlike the intuitively anticipated diffusion effect through the edges of the film. If we compare change in Δ*netOD* for sealed and unsealed film pieces as much as 60% of the water for zero dose film and 50% of water for the irradiated film come from penetration effect (through the polyester layer).

Table 2-3: Penetration and diffusion of water during 24 hours into the center of sealed and unsealed 8" × 8" pieces of EBT-2 GAFCHROMIC$^{TM}$ film

| **Film status** | **Scanning Time, Δt (hours)** | **0 Gy (zero dose)** | | **3 Gy** | |
|---|---|---|---|---|---|
| | | **Δ(netOD)×10$^{-2}$** | **Anticipated dose error (cGy)** | **Δ(netOD)×10$^{-2}$** | **Anticipated dose error (cGy)** |
| | | **0 Gy (zero dose)** | **3 Gy** | **0 Gy (zero dose)** | **3 Gy** |
| **Unsealed film** | 0 | 1.9 ± 0.1 | 14.7 | 2.3 ± 0.1 | 17.7 |
| | 72 | 0.6 ± 0.1 | 4.6 | 1.1 ± 0.1 | 8.8 |
| **Sealed film** | 0 | 1.1 ± 0.1 | 8.9 | 1.2 ± 0.1 | 9.6 |
| | 72 | 0.1 ± 0.1 | 0.9 | 0.2 ± 0.1 | 1.5 |
| **Difference** | 0 | 0.7 ± 0.2 | 5.4 | 1.0 ± 0.2 | 8.1 |
| | 72 | 0.5 ± 0.2 | 3.8 | 1.0 ± 0.2 | 7.4 |

To further confirm our finding of water pathways, we have immersed another 8” × 8” film piece in water for 48 hours, but we now placed two Teflon rods on top of each other with an applied pressure on the top one to assure a firm contact. Result of this experiment is illustrated in Fig. 2-7, which clearly indicates that water can not penetrate from top and bottom parts into the film due to Teflon rods. The film image on the top left part represents the red component only with contrast enhancement to show the effect.

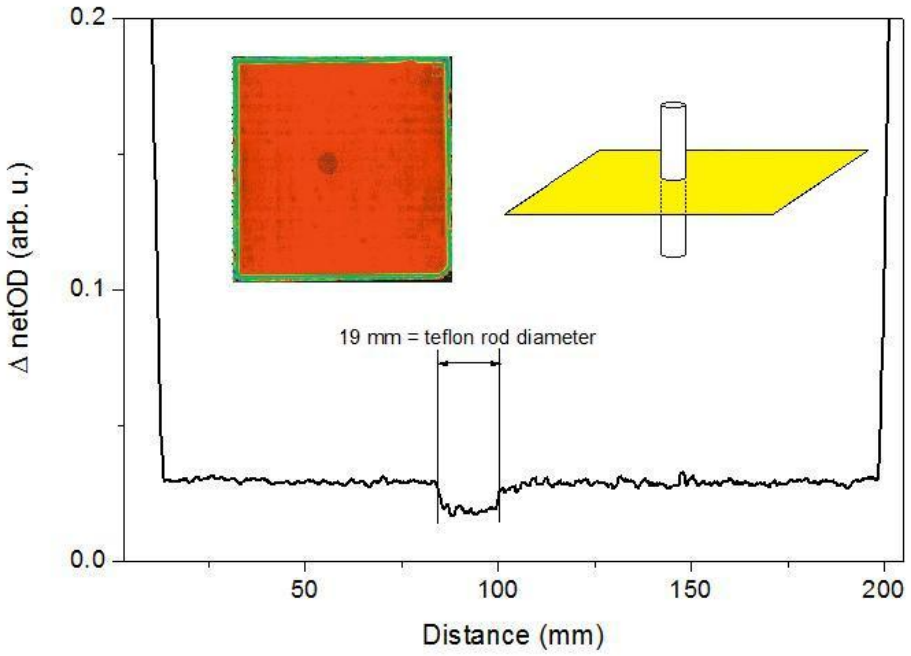


Fig. 2-7: A profile across an 8" × 8" piece of EBT-2 GAFCHROMIC$^{TM}$ film immersed in water for 48 hours with a 19 mm piece of Teflon rod standing on top of it and scanned directly post-immersion.

### 2.2.4 Correction protocol summary

As we have shown in previous sections, there is an undoubtful impact of radiochromic film immersion in water on the measured change in optical density that may lead to systematic errors if the film is kept in water for longer periods of time. As we have shown, the magnitude of the impact depends on many parameters: size of the film piece, initial optical density, post-immersion waiting time prior to scanning (defined by the current radiochromic film dosimetry protocol in place), and the time film was kept in water.

There are some potential aspects that could help reduce the effects of water and decrease this extra Δ*netOD* impelled on the film that was kept in water during dose measurements with radiochromic films. It is important to understand all the steps involved in acquiring the Δ*netOD* for films immersed in water, which must be incorporated into the current film dosimetry protocol. Keeping this in mind, we suggest using the following corrective techniques:

(i) Intuitively, it is recommended to wait enough time before scanning the films which would decrease the change in optical density incurred from water by more than 40% if the post-immersion scanning time was in the range of 72 hours and more.

(ii) Since the magnitude of the water diffusion through the edges appears to be more intense (it reaches penetration depth of almost 10 mm for 24 hours immersion time) we recommend that in such experiments, region of up to 10 mm from the edges of the film should be discarded for dose analysis.

(iii) The use of control film piece will prove useful in correcting for the possible dose measurement errors in the central part of the film piece, (a control film is a piece of the same or similar optical density of measurement film piece in this case). Control film piece should be immersed in water for the same time as the measuring film piece (piece to be irradiated). The resultant change in optical density of the control film piece should be subtracted from the measuring one.

(iv) Another method which helps in reducing the uncertainties on measured doses is establishing a calibration curve in water directly in a specific irradiation modality (beam quality). However, one has to bear in mind that the period of time that films are going to spend in water depends on the dose rate of the radiation beam used. For radioactive sources, this is a function of source activity while it is not in linear accelerators.

# Chapter.3: Experimental Setups and Irradiation Procedures

## 3.1 Introduction

For various experimental purposes, there are different approaches in which one can perform dose measurements in water and Solid Water™ using radiochromic films (RCF). Whatever is the approach, all the elements in the experimental setup have to be identified and good understanding of the contribution of each step to the dose measurement process is necessary.

Generally, we can define our RCF dosimetry-based experimental setup by identifying four elements: (a) the radiation source, (b) irradiation geometry, (c) the primary radiation receiver (the film) and (d) reading device (the densitometer). The radiation source to be used is the Iridium-192 which has an energy spectrum with effective energy of 370 keV or 400 keV if the energy absorbed in source and encapsulation was included.[25] Such a source is used in High Dose Rate (HDR) brachytherapy units, and the one we use is in this work is the V3 Digital (Nucletron, Veenedaal, The Netherlands) HDR remote afterloader. The primary radiation receiver is the latest radiochromic film model, EBT-2 GafChromic™ (International Specialty Products, Wayne, NJ) and all films used in this work were from batch number F06110901. The reading device is comprised of a flatbed Epson Expression 10000XL flat bed document scanner (Epson, Nagano, Japan) that provides 48-bits RGB images, and software which reads those images and split them into Red, Green and Blue components, which enables the conversion of pixel values into optical densities. The software we used was MatLab 7.7.0.471 (MathWorks, Natick, MA).

To establish calibration curve for Ir-192 using EBT-2 radiochromic films, we are interested in a region of interest that will define the dose delivered from the radioactive source. The dose homogeneity of this region is very important and one has to set limits to what is deemed homogeneous. For our

procedure we are interested in a ± 0.5% homogeneity in nominal dose delivered, which translate to an area between 99.5% and 100.5% of the delivered dose and our aim is to maximize the size of this region, but we also should keep in mind other important factors such as: (a) Source-to-film distance, (b) Time of irradiation, and (c) Total uncertainty on the delivered dose. These factors must be optimized altogether because they are dependent on each other; the larger is the source-to-film distance, the longer treatment times we would specify for the same dose but the lower uncertainties we would accumulate on the dose measurements. Elongated treatment times that exceed two hours can lead to errors on reported doses in the case of water geometry as indicated previously, and such errors can be accounted for with the methods proposed back then, but minimizing the immersion times as short as possible is always the best option.

The first intuitive approach would be designing a holder that consist of a film insert and a catheter holder that has a fitting dimension that accommodates the catheter used for the treatment, which is 4F[3] in our case. The main issues associated with this approach are the size of homogenous region of interest and the trade-off relation mentioned before between signal strength (smaller source-film distances provide higher signal and thus shorter irradiation times) and uncertainty on the measured dose (smaller source-film distances yield higher uncertainties on the measured doses). So, we have to be as close as possible to the source in order to minimize treatment times with an acceptable level of uncertainties which can be devised as 2% for clinical applications.

The signal strength versus uncertainty trade-off problem is inevitable and thus we try to increase size of the region of interest as much as possible. The geometry that we adopted in this work is an AP-PA approach (Antero-Posterior – Postero-Anterior) which was used by Reynaert et al[42]. This method provides a larger region of dose homogeneity if positional accuracy of both

[3] French scale most correctly abbreviated as Fr, but also often abbreviated as FR or F is commonly used to measure the catheter size (circumference) is in millimeters, in which 1 F = 0.33 mm in diameter or 1 mm = 3 F

sources can be achieved. We have investigated the treatment times needed in AP-PA geometry for different source-to-film distances and corresponding ±0.5% dose confidence region using Oncentra treatment planning system (Nucletron, Veenedaal, The Netherlands). Results are summarized in Table 3-1 for a fresh source (Apparent activity of 9.617 Ci). Fig. 3-1 illustrate the dose homogeneity region for source-to-film distance of 30 mm.

Table 3-1: sizes of different region of interest for different source-to-film distances and corresponding treatment times.

| Source-to-film distance (mm) | Total 50 Gy Treatment time (s) | ±0.5% dose confidence region (mm) |
|---|---|---|
| 30 | 4000 | 4 × 4 |
| 40 | 7000 | 6 × 6 |
| 50 | 11000 | 7 × 7 |

## 3.2 Holder design for water setup

In order to justify which confidence region would be chosen as our setup, we have to fully understand the dynamics involved in the setup. Mobile parts are: film piece, catheters and source positions. These displacements are caused by either presence of water or source mobility, or maybe both. However, it is desired to fix the positions of the film piece and catheters during the irradiation period and to limit the source position to ±1 mm as quoted by the manufacturer, which is the position reproducibility of the afterloader motor.

A setup similar to the one used by Sarfehia et al[55] was used. In one hand, to fix the position of the film piece in the water geometry, we decided to build the film piece holder with an insert that exactly accommodates a 2” wide film piece where the film does not move in the direction parallel to the film width and the film movement will be only limited in the insertion direction (see

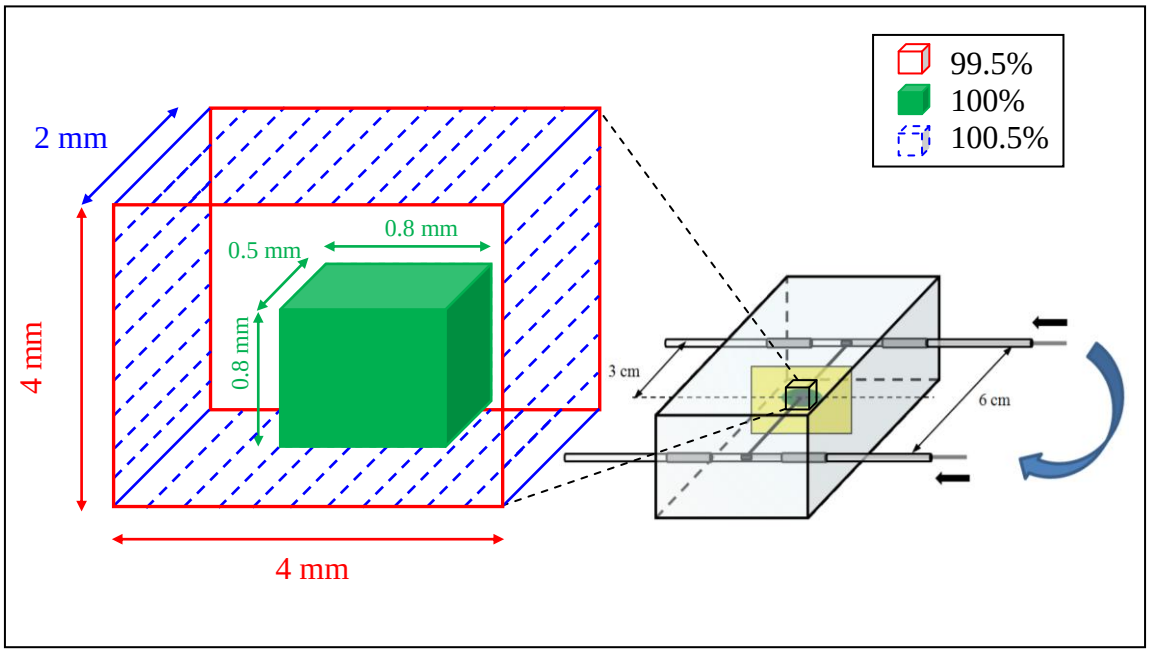


Fig. 3-1: Illustration of the AP-PA irradiation approach with dose homogeneity regions for a source-to-film distance of 30 mm.

Fig. 3-2a). On the other hand, to fix the position of the catheters we used plastic buttons and plastic slotted hex nuts that provide firm support and tension on the catheter once set properly (see Fig. 3-2b). Also, we limited the movement of the catheter in the presence of water by applying metallic catheters that support the plastic comfort catheter and also minimize the effect of transient time which is the time that the source spends to get to the prescribed position. By these measures, we believe that the catheter movement is negligible and we only have to care about the film movement in the insertion direction and the source positioning from both channels.

The material that we used in building the holder for water setup is plastic which is considered a water equivalent and according to Meli et al[27], this should not influence the scattering environment by much. See Fig. 3-2a and Fig. 3-2d for the film holder layout.

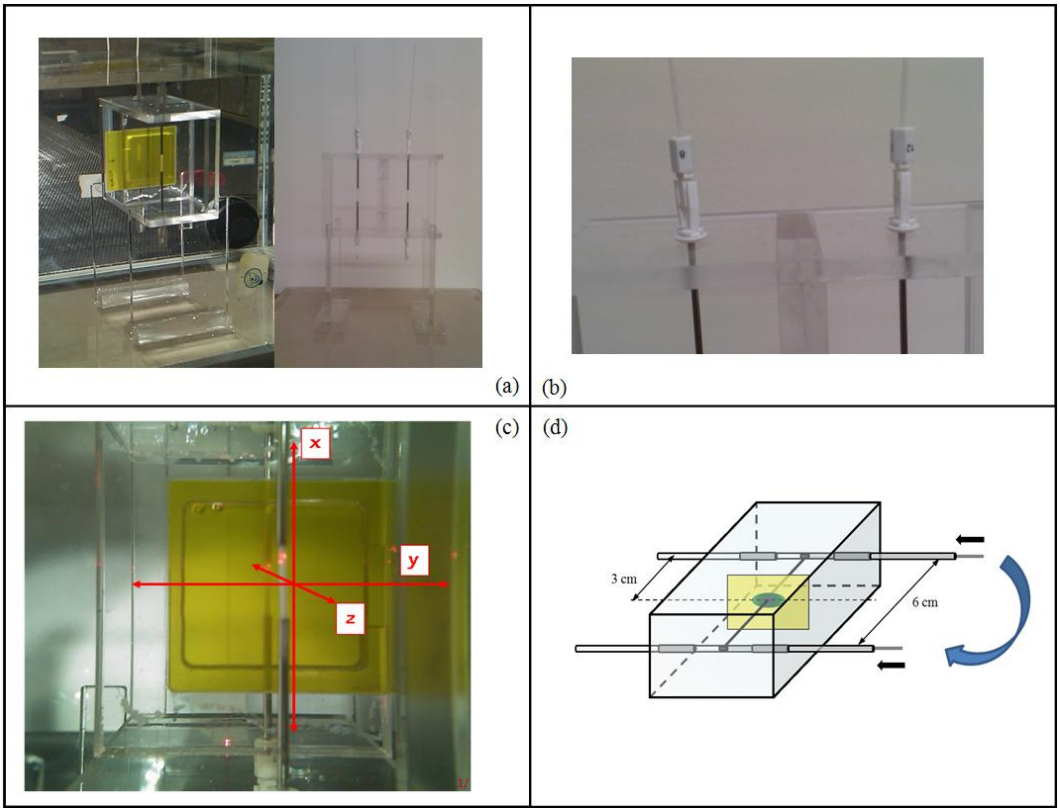


Fig. 3-2: (a) photographic picture of the film holder in water setup. (b) button and hex-nut affixing system used to support the comfort catheters. (c) Our definition of movement axes in our setup. (d) Illustration of the AP-PA irradiation scheme.

## 3.3 Holder design for Solid Water™ setup:

The dynamics in the Solid Water™ setup are more limited than the water setup. However, we were limited to the Solid Water™ pieces available in our clinic and it is noticed that the sheer force in the center of the Solid Water™ pieces might cause some movement around the central vertical axis which made it necessary to limit this movement, so we built a holder that accommodates exactly these pieces as seen in Fig. 3-3a. Thicknesses of the four sides of each solid water piece were measured using a digital calipper with ±2 mm uncertainty, and they were positioned in order to give a nominal source-to-source separation of 60 mm and then all pieces were labeled to keep the same arrangement each time we use the phantom (see Fig. 3-3b for Solid Water™

thicknesses). A 50 mm thick piece of Solid Water™ was used to give sufficient backscatter for each channel.

To limit the catheter positions, we drilled straight pathways through two 30 × 30 × 1 $cm^3$ pieces of solid water that accommodate exactly the diameter of the catheters as shown in Fig. 3-3b. We also hammered the end of each catheter inside the solid water and thus made sure that the catheters do not move at all (see Fig. 3-3c). For the film movement, we have used fixed film sizes and drawn a region that defines the film bed as shown in Fig. 3-3d were the film pieces will be taped, and we made sure to keep track of the film piece orientation by marking one of the corners on the film bed which corresponds to a labeled corner on the film piece.

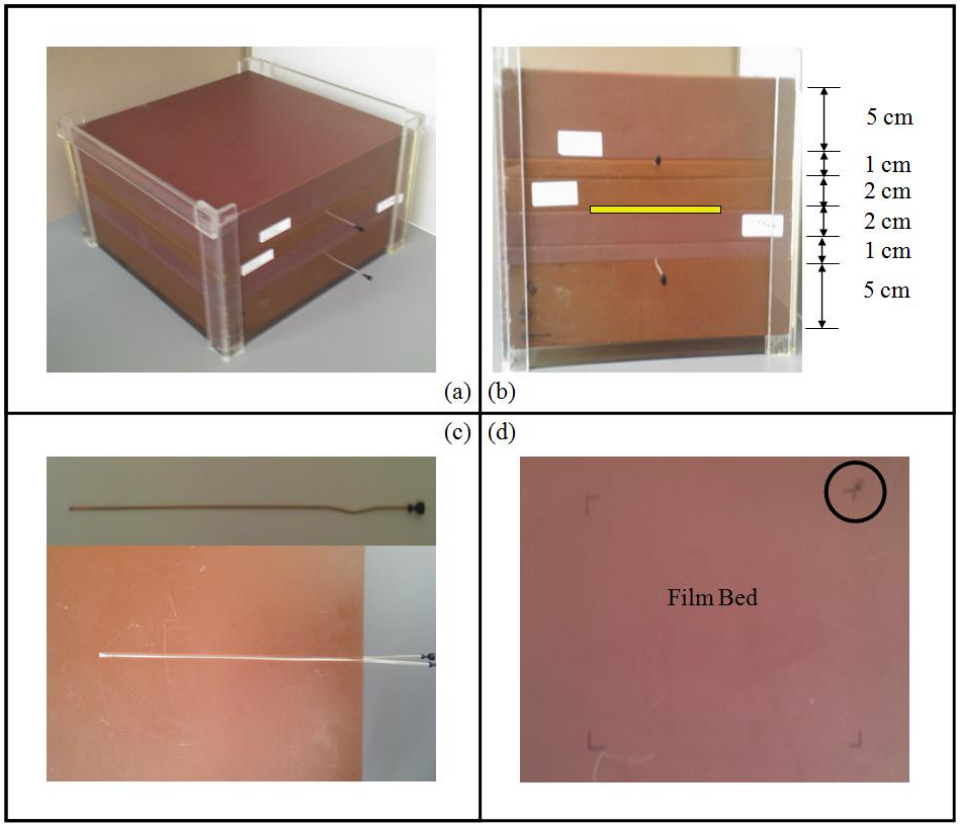


Fig. 3-3: (a) photographic picture of Solid Water™ setup showing the supporting base. (b) catheters and film layers with nominal thicknesses of Solid Water™ pieces. (c) catheter insertion on the bottom and x-ray marker used to monitor the catheter in CT scans on top. (d) Illustration of the film bed area and how we kept fixes orientations during the setup.

## 3.4 Reproducibility in positioning

We defined directions of movement for each item in both water and Solid Water$^{TM}$ setups in the previous section. Now, we will define geometrical axes of each direction in order to explain how we achieve a reproducible source position from each channel. With the aid of Fig. 3-2c, we define the axes as the following:

x-axis: the movement of the source and the film piece.

y-axis: the movement of the film piece.

z-axis: the distance between the two channels and corresponding film piece position in-between them.

To ensure that the source-to-source distance is 60 mm, we scanned both setups in an AcQSim CT simulator (Philips, Netherlands) with a voxel size of 1 × 1 × 3 $mm^3$ and we measured the source-to-source distance and it was 60.1 mm and 58 mm for water setup and solid water setup respectively (see Fig. 3-5 and Fig. 3-6). Accordingly, we have adjusted the new plans for both setups in order to revisit the dimensions of confidence region (dose homogeneity), but the difference was negligible.

Our goal is to achieve positional accuracy in all geometrical axes. As explained earlier in the previous section, we will neglect the movement of the film in x and y axes and thus we will only consider source position along the x-axis and film position in the z-axis. As mentioned before, the afterloader motor provides reproducibility in positioning within ±1 mm in any channel. It is of great importance to achieve position reproducibility in the x-axis on the film piece and not in the catheter (see Fig. 3-4).

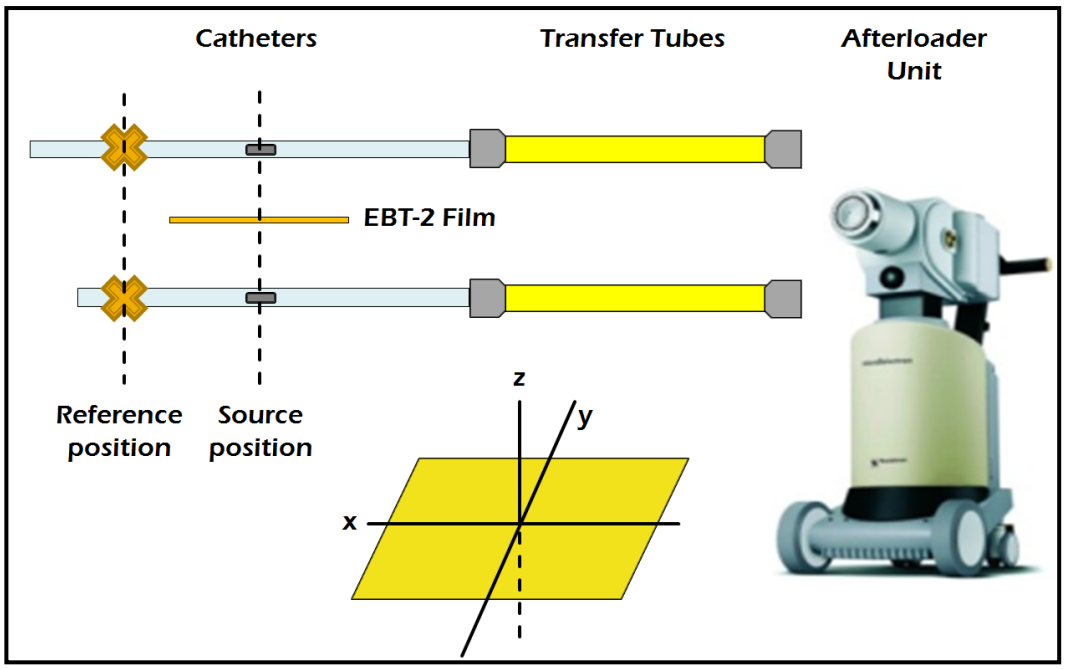


Fig. 3-4: Illustration of the source position with respect to the catheters. It illustrates the method of achieving correct source position from a preset reference position which was determined during commissioning.

In order to achieve this reproducibility, we have started with an initial position that we calculated by measuring the distance between the end position that the afterloader motor can provide which we call “reference position”, and the center of a dummy source (see Fig. 3-5 and Fig. 3-6). The reference position was measured during the commissioning of the brachytherapy unit and it is at 1238 mm. By subtracting the source-to-reference distance from the reference position we get the initial position which was found to be 1169 mm for channel 1 which corresponds to a source-to-reference distance of 69 mm and 1173 mm for channel 2 which corresponds to a source-to-reference distance of 65 mm.

It is important to note that for each channel we use a different piece of film of the same size. We put the first piece of film and then send the source through channel 1 to the specified position, and then we interrupt the treatment after the delivery is complete in channel 1 and we put the other piece of film and complete the treatment which will register the source position in channel 2. This procedure is repeated for three sets of films in total and the time elapsed

between each film piece in a set is monitored so we can scan the film pieces after irradiation at any convenient time and we do not have to wait 24 hours before scanning the film as long as we scanned the pieces at the right times. [68] After scanning the film pieces with a resolution of 127 dpi, and acquiring the netOD images, we decided to take vertical (y) and horizontal (x) profiles across a 100 × 100 pixels region of interest around the dose distribution and we fitted a Gaussian per 10 pixels in both x and y axes which corresponds to 100 points in the region of interest. Each combination of x and y Gaussians will return a position as a maximum point in the distribution and the average position from both x and y axes will be taken as the maximum. Next step is to check if the position of this maximum point in channel 2 matches with the one from channel 1 and achieving the same point from both channels is the goal of this alignment exercise. We had to do this for three times until we achieved reproducibility in x-axis of ±5 pixels which corresponds to ±1 mm on the film piece and thus we decided to use a 2 × 2 $mm^2$ region of interest which is well within dose homogeneity region and its reproducibility. Table 3-2 summarizes the results of the source position matching experiments.

Table 3-2: Matching of source positioning from both channels in the setup. Positions here refer to the maximum value gotten form Gaussian fits in both x and y axes. Δ*t* refers to the time monitored between signals recorded from Channel 1 and Channel 2.

| ***Film sets*** | ***Channel*** | ***Source position (mm)*** | ***x-position (pixel)*** | ***y-position (pixel)*** | **Δ*t* *(min)*** |
|---|---|---|---|---|---|
| *1, 2, 3* | *1* | 1169 | 145 ± 2 | 113 ± 2 | 03:43 |
| | *2* | 1173 | 121 ± 2 | 121 ± 2 | |
| *4, 5 ,6* | *1* | 1172 | 137 ± 2 | 114 ± 2 | 03:49 |
| | *2* | 1171 | 129 ± 2 | 125 ± 2 | |
| *7, 8, 9* | *1* | 1173 | 202 ± 2 | 139 ± 1 | 03:39 |
| | *2* | 1170 | 200 ± 2 | 137 ± 2 | |

A similar exercise was performed for the Solid Water$^{TM}$ setup and reproducibility in x-axis was achieved at ±1 mm on the film piece.

Next is to check signal reproducibility in z-axis, and this is to make sure that the film is within the 2 mm range of what we have specified to provide deemed dose homogeneity. In other words, we are looking at the signal intensity in the z-axis after we achieved correct positioning of the maximum point in the distribution. Any difference in signal intensity between the two channels will be nullified by treatment time weighting until we get reproducibility close to 50% contribution from each channel. It is worth mentioning that we have 2 mm confidence line across the film, so a difference as large as 5% is still acceptable.

In order to check the signal intensity (which is a function of the distance between sources in z direction) we have performed a similar exercise as for source positioning alignment test along x-axis. We used a set of two film pieces of the same size per channel. Subsequently, we fitted the horizontal and vertical Gaussians to find the position of the maximum and then we took a 2 × 2 mm region of interest around the maximum and found the average pixel value and corresponding standard deviation. We have repeated this exercise three times for each time setting and have found a difference of around 4%. Thus, we decided to weight the times 100:96 for (channel 1: channel 2) but we found a difference of almost 12% so we knew that we reversed the weights and thus we came up to differences in the order of 2% after correcting, but it was not consistent, so we thought it might be attributed to the fact that the pieces we used had different background and we decided to select sets of film with similar backgrounds. By doing this we reached signal difference of less than 1% in water setup and 2% in Solid Water$^{TM}$. Table 3-3 summarizes the signal weighting exercise.

Table 3-3: Signal weighting due to difference in signal from each channel. Weighting is done by time and it is done in order to be at the center of dose homogeneity region.

| *Applied weight* | *Film sets* | *Channel* | *PV (unexp)* | *PV (exp)* | *Net OD* | *% ΔNet OD* | *Δt (min)* |
|---|---|---|---|---|---|---|---|
| *100:100* | *1* | *1* | *52835* | *37049* | 0.1541 | 3.3% | 04:58 |
| | | *2* | *52163* | *36996* | 0.1492 | | |
| | *2* | *1* | *53389* | *37185* | 0.1571 | 5.6% | 04:09 |
| | | *2* | *53549* | *38015* | 0.1488 | | |
| | *3* | *1* | *52955* | *37003* | 0.1557 | 3.8% | 04:03 |
| | | *2* | *53506* | *37882* | 0.1500 | | |
| *100:96* | *4* | *1* | *53260* | *36690* | 0.1619 | 12.5% | 03:55 |
| | | *2* | *52668* | *37818* | 0.1438 | | |
| | *5* | *1* | *53072* | *36774* | 0.1593 | 12.3% | 03:31 |
| | | *2* | *52749* | *38053* | 0.1418 | | |
| | *6* | *1* | *53212* | *37094* | 0.1567 | 10.7% | 03:46 |
| | | *2* | *52915* | *38195* | 0.1416 | | |
| *96.5:100* | *7* | *1* | *51819* | *36670* | 0.1502 | 0.8% | 06:03 |
| | | *2* | *52867* | *37519* | 0.1489 | | |
| | *8* | *1* | *52751* | *37184* | 0.1519 | 2.8% | 03:48 |
| | | *2* | *53286* | *37924* | 0.1477 | | |
| | *9* | *1* | *52591* | *36861* | 0.1543 | 5.7% | 03:39 |
| | | *2* | *52780* | *37705* | 0.1461 | | |
| *98:102* | *10* | *1* | *52317* | *36839* | 0.1523 | 3.3% | 03:49 |
| | | *2* | *52364* | *37283* | 0.1475 | | |
| | *11* | *1* | *52619* | *37145* | 0.1512 | 0.7% | 04:03 |
| | | *2* | *51963* | *36766* | 0.1502 | | |
| | *12* | *1* | *52674* | *36784* | 0.1559 | 2.9% | 03:49 |
| | | *2* | *52610* | *37107* | 0.1516 | | |
| *96.8:103.3* | *13* | *1* | *53745* | *37413* | 0.1573 | 0.6% | 03:59 |
| | | *2* | *53784* | *37526* | 0.1563 | | |
| | *14* | *1* | *52974* | *36984* | 0.1560 | 0.3% | 03:42 |
| | | *2* | *52813* | *36905* | 0.1557 | | |
| | *15* | *1* | *52749* | *37270* | 0.1509 | 0.3% | 03:52 |
| | | *2* | *52785* | *37335* | 0.1504 | | |

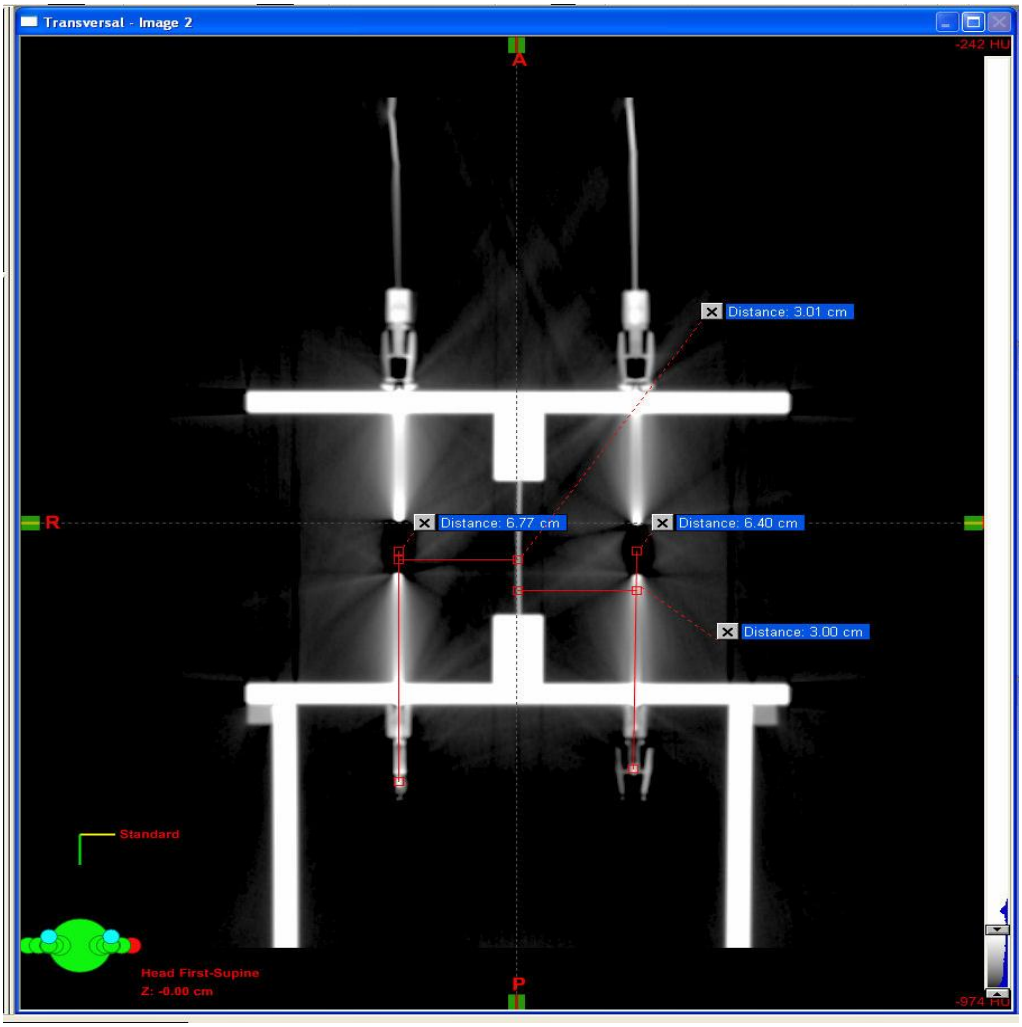


Fig. 3-5: CT scan of water setup where we can see the source-to-film distance that we have to subtract from the reference position to reach correct source position.

We have selected a source-to-film distance of 30 mm because it provides a homogenous dose distribution within 2 mm region along z axis at the center between the two source positions, while providing the shortest immersion times possible with acceptable uncertainty in Pixel Values within region of interest on scanned images. We also found in the literature as indicated in Thomason et al[36] and Williamson et al[37] that at 30 mm the dose gradient is almost uniformly circular. The final setup is shown in Fig. 3-7 for water setup. Our dose points are 0, 0.25, 0.5, 1, 1.5, 2, 2.5, 3, 3.5, 4, 5, 6, 8, 10, 20, 30 and 50 Gy.

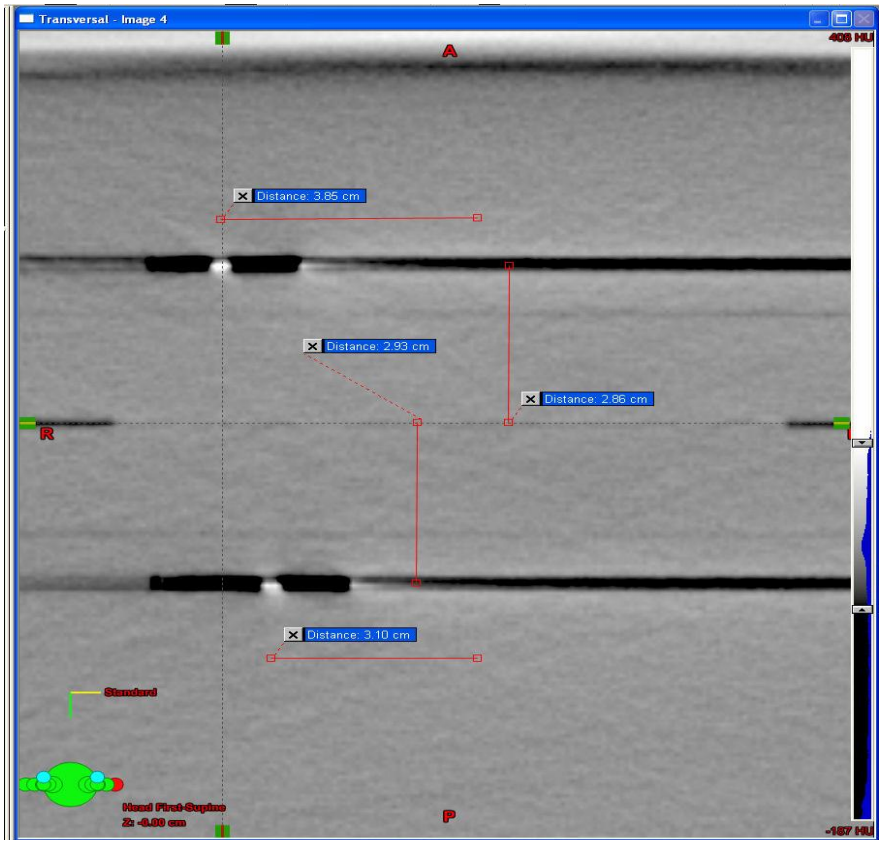


Fig. 3-6: CT scan of Solid Water™ setup where we can see the source-to-film distance that we have to subtract from the reference position to reach correct source position.

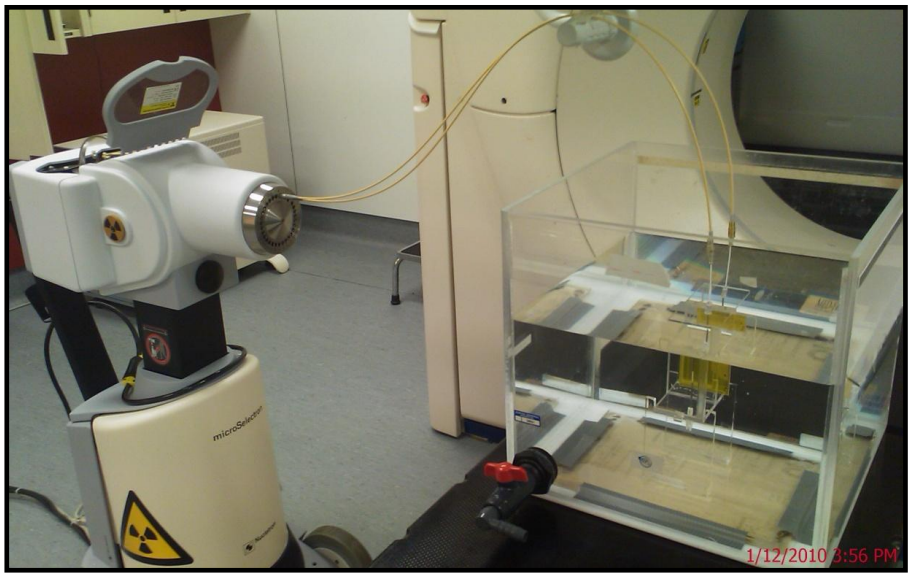


Fig. 3-7: A photograph of the in-water irradiation from Ir-192 source.

# Chapter.4: Dose measurements analysis

## 4.1 Measurement of Optical Density

This section focuses on scanning procedures and steps involved in acquiring net change in optical densities ($\Delta netOD$) in this work. In order to establish our scanning protocol we investigated many issues that may affect the accuracy and precision in obtaining OD values. These issues are related to the (1) film, (2) scanner, and (3) software used to acquire Pixel Values (*PV*).

Effects that we have studied include orientation of the film piece, size of film piece, location of the film piece on scanning bed (light scattering effect or scanner uniformity), size of the scanning window, size of the region of interest on the film piece image, difference in optical properties (polarization for instance) between film piece and scanner light source, sensitivity of CCD arrays in the scanner, scanner warm-up, energy deposition into the film piece from multiple scanning, scanner fluctuation and noise, post irradiation time, humidity effect, dark signal correction, background correction, thermal and temporal history of the film pieces and film non-uniformity. Most of these issues were discussed in the literature review Section 1.3.

There are also important aspects that have to be identified in the protocol that include the choice of color channel that provides higher signal with acceptable uncertainties on reported doses, non-linear mathematical model that is used to describe the behavior of the film and finally dose range which affects parameterization and selection of the equation used in the mathematical model. Devic et al[92] explained how to optimize the use of all color channels in order to cover broad dynamic range of doses and they provided recommendations on selection of color channels for each dose range. They also showed improvements on the scanning protocol they presented in their earlier work. In this work, we adopted the same procedures explained in that protocol and we will mention these procedures for completion of the work.

### 4.1.1 Improving Accuracy of Measurements (Control film concept)

Beside of all the issues and corrections mentioned above, the principle of zero-dose or control piece of film was one of the major improvements in the accuracy of RCF dosimetry.[92] The role of zero-dose film piece is to correct the optical density change of an irradiated film piece for the environmental effects (temperature, humidity, exposure to the scanner light, etc.) that could lead to the measurable changes in the optical density of the radiochromic films. It is also important to emphasize that the size of the zero-dose film piece must be the same as the film pieces to be irradiated and that the zero-dose film piece must be from the very same box as the film pieces used for calibrations or measurements. It is assumed that all the changes due to the mentioned factors will be recorded by this control film piece and final net change in optical density ($\Delta netOD$) is calculated by subtracting the optical density change of the control film piece from the optical density change of the measurement film. This unexposed control film piece principle works well in solid water irradiations. However, we had to revisit this principle in our in-water measurements because as shown in section 2.2, the impact of water on EBT2 film has some dependence on initial optical density. An extra measure had to be taken to control the dose, which is to use a control piece of film of the same (or very similar) initial optical density and immerse it in water for the same time as the measurement film piece, as explained in the correction protocol in section 2.2. It is also important to note that we will refer to this principle by "control film piece" instead of "zero-dose film piece" where it lost its meaning.

### 4.1.2 Scanning procedure

As mentioned before, we have used an Epson Expression 10000XL flatbed scanner to scan all of our film pieces. All technical characteristics and details of this scanner are described in a comprehensive HTML reference guide available at the manufacturer's website[4].

[4] http://www.epson.com/

Film pieces are scanned using EPSON SCAN 3.01A software, with maximum OD range and all filters and image enhancement options turned off. The film pieces were scanned in the 48-bit RGB mode (16 bits per color) and saved as tagged image file format (TIFF) image files. All images were scanned with an image resolution of 127 dpi which translates into 0.2 mm/pixel. Accordingly, the 2 mm × 2 mm ROIs over which the net optical densities (*netOD*) were determined consisted of 10 × 10 pixels.

The film pieces were then irradiated in accordance with the procedure described in Chapter.3. Once irradiated, the films were left for a period of 24 hours to self-develop, and then they were scanned again in the same way as before and with the same orientation as the un-irradiated scans. This allowed film-to-film co-registration, and avoidance of image rotation as much as possible, which can introduce unnecessary averaging of adjacent pixels. In general, scanned images with irradiated films will have a scanning region different from that of the un-irradiated film pieces. Therefore, for the removal of defective pixels (resulted from scanning bed deformities) in scanned film images, five blank scans are made again of the film scanning region.

The filtered single scan (2D Weiner filter) was adopted as the scanning protocol which shows an advantage mainly time-wise because we decided to scan film pieces individually in the middle of the scanner to avoid systematic errors due to scanner non-uniformity in the vertical axis of the scanning bed. Another important issue to keep in mind is that all filtrations should happen after co-registering unexposed film piece (background signal) from irradiated film piece and before splitting color channels so we preserve original information. This will be explained in details later in section 4.1.3.

Last step in the scanning procedure is to determine the zero-light transmitted pixel value ($PV_{bckg}$), which characterizes the background signal of the scanner, as well as its corresponding standard deviation ($\sigma_{bckg}$), over the same ROI. This is done by scanning five times some thick flat opaque black sheets that cover the scanning bed completely with their thickness comparable

to the film thickness, and then take the average of this image for each color channel individually. This is reported in the literature as the dark signal[59] where it sets the coarse procedure to a finer level in terms of determining the accuracy of OD measurements.

It was mentioned previously that OD represents a convolution of: (1) scanning lamp emission spectrum, (2) absorption spectrum of the film, and (3) sensitivity of CCD arrays. However, measured PV also incorporates optical properties of parts that are in the light's path making the OD a complex relative convoluted dimensionless signal

### 4.1.3 Image Processing

For each dose point in the calibration curve, there is a set of seven scanned images used to calculate radiation induced change in optical density of the corresponding film piece. These images are of the same scanning parameters and they are: (1) measurement piece before irradiation, (2) measurement piece after irradiation, (3) control film piece before irradiation, (4) control film piece after irradiation, (5) average blank image before irradiation, (6) average blank image at the time of scanning irradiated images, and (7) dark signal image. It is important to emphasize that images (1), (3) and (5) are scanned consecutively with minimal time in-between, and similarly for images (2), (4) and (6) while image (7) is acquired only once. Once all the images are obtained, they were imported to an in-house image manipulation routine written with MatLab 7.7.0.471 (Math Works, Natick, MA) used to determine change in optical density using raw Pixel Values (PV) from each set of images.

The first step in processing the images was the identification of defective pixels. Having two glass plates in the optical pathway, the system can exhibit many imperfections. These were defined as pixels whose PV differ by more than 5% than the average of the blank image pixels. These can be recognized as deviation from the theoretical value of $2^{16}$ for certain points within the scanning region of the empty bed caused by specs or dust on the light

pathway from the lamp to the CCD detector. We found that the percentage of faulty pixels was smaller than 0.4%. This step is important because our ROI lies within a 10 × 10 pixels and these faulty pixels can significantly skew both the 2D mean PV and its standard deviation of this ROI. This image can be used by setting faulty pixels to a negative value (-1) and all other pixels that passed the criteria to a positive value (1) and thus it is simply applied by multiplication to the measurements' images and a simple routine will exclude any negative pixels from calculations.

After the defective pixels were identified, both the average blank image and measurements images (before and after irradiation) are read and cropped to the film piece dimensions. It is important to keep the same cropping procedure i.e. size in all measurement images and the average blank image where they both had the same scanning settings in the first place. Also, cropping procedure should preserve all RGB data and do not select only RED channel, as this is a common practice in the contemporary radiochromic film dosimetry protocols.

Next step was to register the two measurement image: before and after irradiation. This is done in two steps: (1) minimal image rotation, and (2) selecting same ROI in both images. Image rotation was preferably avoided by trying to align film piece horizontally as much as possible with an L-shape plastic tool. However, when the scanner bed is closed some shift might occur because of sudden air-pressure change and further rotation analyses were necessary. The rotation works by selecting two points on the top horizontal edge of the film piece and it calculates the angle between the line that connects the two points and a horizontal line taken from the lower point. Knowing this angle, the film piece was rotated respectively. After that, the code asks the user to choose a point in the top-left corner with zooming options allowed in order to select the optimum point which will act as a reference point in the following context: the measurement image after irradiation is analyzed first and reference point will be selected. Then a point that will be the center of ROI will be selected by the user semi-automatically and sequentially the background image

(un-irradiated) will be analyzed by selecting the top-left corner manually while the code will select the same ROI location as irradiated film piece image automatically because it was already given the $x$ and $y$ coordinates of the measurement point.

The semi-automatic selection of ROI from the irradiated film piece is done in two steps. First, the user is asked to select the point where he thinks that it represents the maximum point in the distribution. After that the code will establish a 100 × 100 pixel$^2$ region around this point from a single layer (RED component) and it will select 100 points inside this region and for every point it will fit a Gaussian in the $x$-axis and another in the $y$-axis where the location of the maximum point in the Gaussian will represent the predicted location of our sought measurement point. This will result in a total of 20 Gaussians in 10 sets where each set has an $x$ and $y$ components, and then an average of each set of ten will be assumed is the location of the maximum point in the distribution. This is a fair argument as long as we have large number of ensembles (pixel values) in each line (100 points) and also Gaussian fits has a good $R^2$ value and are accepted as a distribution pattern for Ir-192.

Once the coordinates of the central measurement point were identified, the code returns to the original rotated image and splits the tri-layered image to three single-layered images where each represent a color channel and corrects for scanner noise and imperfections respectively. The code then mimics the 10 × 10 pixels ROI on all RGB images and finds the 2D mean and its standard deviation. It is important to understand that fitting the Gaussians was used only to determine the location of the central measurement point. This whole procedure is repeated five times and arrays of 2D means ($PV_{unexp}$ or $PV_{exp}$) and standard deviation ($\sigma_{unexp}$ or $\sigma_{exp}$) in PV are established for irradiated and un-irradiated images separately where mean PV will be subtracted correspondingly and corrected for dark signal effect thereafter using a spreadsheet software.

### 4.1.4 Dose Response

Film dose response is usually expressed by measured *netOD* as a function of dose delivered to the film. However, to use the film for the measurement of an unknown dose, dose is more conveniently plotted as a function of measured *netOD* and the data can be fitted with an appropriate function using a least square method. It is of great importance to notice that this dosimetry system is dependent on the batch number of the film All films used in this work were from batch number F06110901. Once the calibration curve is created, the next step in radiochromic film dosimetry protocol is to establish uncertainties that are coming from both experimental and fitting procedures. The first experimental part of uncertainty is mainly caused by contribution from *netOD* measurement reproducibility and other factors that were discussed in the introduction of this section. We will denote this uncertainty as the "experimental" uncertainty on dose. The second source of uncertainty is caused by the fit process and its parameters determined during the film calibration and will be referred to as the "fit" uncertainty on dose.

Up to this point, we have acquired *meanPV* of both irradiated ($PV_{exp}$) and un-irradiated ($PV_{unexp}$) film pieces and standard deviations on both. It is assumed that *PV* is a measure of light's intensity and the ration $PV_{exp}/PV_{unexp}$ is independent of $PV_0$, the light's intensity before hitting the film. This is subject to the assumption that $PV_0$ is always the same regardless of the object being scanned. *NetOD* independence of $PV_0$ can be recognized after applying the Beer-Lambert law which is a measure of absorbance of light in a given material. Whereas absorbance resembles *OD*, one can define *netOD* by the difference in absorbance between irradiated and un-irradiated film pieces or $OD_{exp}$ and $OD_{unexp}$. Derivation of *netOD* is reproduced from Devic et al[60] in equation (4-1).

$$netOD^i(D_j) = OD^i_{exp}(D_j) - OD^i_{unexp}(D_j)$$

$$= -log_{10}\left(T^i_{unexp}(D_j)\right) + log_{10}\left(T^i_{exp}(D_j)\right)$$

$$= log_{10}\left(\frac{PV_0}{PV^i_{exp}(D_j) - PV_{bckg}}\right) - log_{10}\left(\frac{PV_0}{PV^i_{unexp}(D_j) - PV_{bckg}}\right)$$

$$= log_{10}\left(\frac{PV_0}{PV^i_{exp}(D_j) - PV_{bckg}} \cdot \frac{PV^i_{unexp}(D_j) - PV_{bckg}}{PV_0}\right)$$

$$= log_{10}\left(\frac{PV^i_{unexp}(D_j) - PV_{bckg}}{PV^i_{exp}(D_j) - PV_{bckg}}\right) \quad (4\text{-}1)$$

Where both $PV_{unexp}$ and $PV_{exp}$ are corrected for dark signal ($PV_{bckg}$), $i$ refers to the $i$-th ROI chosen for the same $j$-th dose, $T^i_{unexp}$ and $T^i_{exp}$ refers to the transmittance before and after irradiation.

However, this is not our final expression of *OD* as we have not yet included the control film piece. The total net change in optical density ($\Delta netOD$) is calculated as:

$$\Delta netOD^i(D_j) = log_{10}\left(\frac{PV^i_{unexp}(D_j) - PV_{bckg}}{PV^i_{exp}(D_j) - PV_{bckg}}\right) - log_{10}\left(\frac{PV^i_{cb}(D_j) - PV_{bckg}}{PV^i_{ca}(D_j) - PV_{bckg}}\right) \quad (4\text{-}2)$$

where $PV^i_{cb}(D_j)$ and $PV^i_{ca}(D_j)$ refers to Pixel Values from control film piece before and after sought effect respectively.

Using error propagation expression and ignoring cross correlations, the uncertainty on measured $\Delta netOD$ can be written as:

$$\sigma^i_{\Delta netOD}(D_j) =$$

$$\frac{1}{ln10}\sqrt{\begin{aligned}&\frac{\left(\sigma^i_{PV_{unexp}}(D_j)\right)^2}{\left(PV^i_{unexp}(D_j) - PV_{bckg}\right)^2} + \frac{\left(\sigma^i_{PV_{exp}}(D_j)\right)^2}{\left(PV^i_{exp}(D_j) - PV_{bckg}\right)^2} + \frac{\left(\sigma^i_{PV_{cb}}(D_j)\right)^2}{\left(PV^i_{cb}(D_j) - PV_{bckg}\right)^2} + \frac{\left(\sigma^i_{PV_{ac}}(D_j)\right)^2}{\left(PV^i_{ac}(D_j) - PV_{bckg}\right)^2} \\ &+ \left(\frac{\sigma_{bckg}}{\left(PV^i_{exp}(D_j) - PV_{bckg}\right)^2} - \frac{\sigma_{bckg}}{\left(PV^i_{unexp}(D_j) - PV_{bckg}\right)^2} + \frac{\sigma_{bckg}}{\left(PV^i_{cb}(D_j) - PV_{bckg}\right)^2} - \frac{\sigma_{bckg}}{\left(PV^i_{ca}(D_j) - PV_{bckg}\right)^2}\right)^2\end{aligned}}$$

(4-3)

The final $\Delta netOD(D_j)$ was determined as a weighted mean:

$$\Delta netOD(D_j) = \frac{\sum_{i=1}^{N}\left(\Delta netOD^{i}(D_j)/\left(\sigma^{i}_{\Delta netOD}(D_j)\right)^{2}\right)}{\sum_{i=1}^{N}\left(1/\left(\sigma^{i}_{\Delta netOD}(D_j)\right)^{2}\right)}, \quad (4\text{-}4)$$

Where $N=5$ and corresponds to the number of ROIs sampled over the central part of the film piece, and the corresponding uncertainties were calculated as:

$$\sigma_{\Delta netOD}(D_j) = \frac{1}{\sum_{i=1}^{N}\left(1/\left(\sigma^{i}_{\Delta netOD}(D_j)\right)^{2}\right)}, \quad (4\text{-}5)$$

It has to be clear that the control for in-water measurements is a piece of the same initial optical density (dose) which aims to separate water impact from all other OD contributors, while the control for in-solid water measurement is an un-irradiated piece of film (zero dose film piece). For our in-water measurements, we used pieces already irradiated in Cobalt-60 photon beam to the same doses as controls where they share similar thermal history because all our measurement film pieces are kept in the same storage room. Control film pieces were irradiated in cobalt beam more than two weeks before used as control and we assume that their optical density was stable at the time of immersion in water.

## 4.2 Dose Measurements and Uncertainty Analysis

While discussing dose measurements and how good our RCF dosimetry system is, we have to investigate both its accuracy and precision. In our case, accuracy refers to reproducibility of the mean value of dose measured from a number of points that has received the same dose, while precision tells us how close this reproducible signal to the actual value and it indicates the uncertainty in our measurements. The end goal of any dose measurement technique is to optimize accuracy and precision altogether.

Three aspects have been considered that affect the uncertainty analysis of reported doses beside accuracy and precision of *netOD* measurements. These aspects are: (1) Mathematical description (equation) used to describe the

relation between *netOD* and *D*, (2) color channel used for analysis, and (3) dose range used.

### 4.2.1 Mathematical description of netOD-D relationship

In the previous section, we have shown the conversion of pixel values into optical densities and it was indicated that the dose (*D*) is plotted more conveniently as function of *netOD* in order to be used for future dose measurements. The relation between *D* and *netOD* is non linear and the most reported mathematical model of this relation is based on empirical basis and does not describe any chemical behavior in the active layer of the film. With optimization of precision in mind, polynomials of the second order or higher were shown to provide acceptable balance between reported error on dose values and the uncertainties associated with fitted doses. This model uses fitting of the analytical form:

$$D_{fit} = b \cdot netOD + c \cdot netOD^{n} \tag{4-6}$$

where the constant term was assumed to be zero because there's no clear physical potential that the active layer of the film would have any thresholds with dose. This was tested and the constant is always very close to zero with the empirical fitting and thus was ignored.

In fitting this model, parameters have been found using the "Levenberg-Marquardt" quasi – Newton minimization method, weighted using the following distribution:

$$w_i = \frac{1}{\left(\sigma_{netOD_i}\right)^2} \cdot \frac{1}{\sum_i \frac{1}{\left(\sigma_{netOD_i}\right)^2}} \tag{4-7}$$

In order to predict the uncertainty in the measurement of an unknown dose while using the calibration curve for each dosimetry system, we have used the expression for error propagation:[94]

$$\sigma_y^2 = \sum_i \left( \frac{\partial y}{\partial x_i} \right)^2 \cdot \sigma_{x_i}^2 \tag{4-8}$$

assuming absence of cross-correlation terms. In the above equation, $\partial y/\partial x_i$ is a derivative of a given calibration function over the parameter $x_i$. From Equation (4.6), we considered *netOD*, *b* and *c* to be variable parameters; a was always forced to be 0 and n was considered to be a constant.

However, this mathematical model was meant to be used with EBT-1 film model and we needed to optimize a model that will be used for EBT-2 film model considering that the structure of the film has changed. We have considered different groups of mathematical models: (1) Physical or Chemical –based models reported in the literature, (2) Empirical models reported in the literature, and (3) Best empirical models provided by different fitting software. Here, we will only show the equation used and corresponding uncertainty analysis according to the rules of error propagation.

***(1) Physically based models:***

These models are based mainly on the adoption of single-hit/single-target theory developed by Silberstein[95] and Valentine for radiographic films in 1965. However, these models were edited and optimized with different features that describe the physical behavior of radiochromic films as much as possible. Among those, we tested the single hit model in some reported forms as in equation (4-9) and (4-10)

1) Raw single hit model, (del Moral et al[96], Zhu et al[97], Battum et al[89], Menegotti et al[83]):

$$\mathrm{OD} = \mathrm{a_1} - \mathrm{a_2} \cdot \mathrm{e}^{-\mathrm{a_3} \cdot \mathrm{D}} \tag{4-9}$$

2) Gamma single hit model, (del Moral et al[96]):

$$\mathrm{OD} = \mathrm{a_1} - \frac{\mathrm{a_2}}{(\mathrm{a_3}+\mathrm{D})^{\mathrm{a_4}}} \tag{4-10}$$

We have rewritten these models to describe dose from a given optical density where uncertainties on measured optical density were taken as in the expression shown in equation 4-5. The corresponding models are:

$$OD = a_1 - a_2 \cdot e^{-a_3 \cdot D} \quad \rightarrow \quad D = \ln\left(\frac{a_1 - OD}{a_2}\right)^{-\frac{1}{a_3}} \tag{4-11a}$$

$$OD = a_1 - \frac{a_2}{(a_3 + D)^{a_4}} \quad \rightarrow \quad D = \left(\frac{a_2}{a_1 - OD}\right)^{\frac{1}{a_4}} - a_3 \tag{4-12a}$$

Total uncertainties on dose for these models are (respectively):

$$\sigma_D = \sqrt{\left(\frac{\sigma_{a_1}}{a_3 \cdot (a_1 - OD)}\right)^2 + \left(\frac{\sigma_{a_2}}{a_2 \cdot a_3}\right)^2 + \left(\frac{\sigma_{a_3} \cdot \ln\left(\frac{a_1 - OD}{a_2}\right)}{{a_3}^2}\right)^2 + \left(\frac{\sigma_{OD}}{a_3 \cdot (a_1 - OD)}\right)^2} \tag{4-11b}$$

$$\sigma_D = \sqrt{\begin{array}{l}\left(\frac{\left(\frac{a_2}{a_1 - OD}\right)^{\frac{1}{a_4}}}{a_4 - OD}\right)^2 \cdot (\sigma_{a_1})^2 + \left(\frac{\left(\frac{a_2}{a_1 - OD}\right)^{\frac{1}{a_4}}}{a_2 \cdot a_4}\right)^2 \cdot (\sigma_{a_2})^2 + (\sigma_{a_3})^2 + \\ \left(\frac{\left(\frac{a_2}{a_1 - OD}\right)^{\frac{1}{a_4}} \cdot \ln\left(\frac{a_2}{a_1 - OD}\right)}{{a_4}^2}\right)^2 \cdot (\sigma_{a_4})^2 + \left(\frac{\left(\frac{a_2}{a_1 - OD}\right)^{\frac{1}{a_4}}}{a_4 - OD}\right)^2 \cdot (\sigma_{OD})^2\end{array}} \tag{4-12b}$$

where the cross correlation between fitting parameters was ignored.

***(2) Empirical models:***

The most reported models that describe the relationship between *netOD* and *D* are the previously mentioned non linear polynomials of 2nd order or higher. Devic et al[59] used polynomials of 2nd order to fit *D* as function of *netOD* and they showed extensive uncertainty analysis that was adopted by Martisikova et al[80], Fiandra et al[98] and Ferriera et al[77]. Crop et al[99] showed that a 3rd order polynomial would be sufficient to get significant *p*-values (≤1%) for

calibration fit. Here we'll test the model reported by Devic et al[60] and its corresponding uncertainty:

$$D = a + b \cdot netOD + c \cdot netOD^{n} \tag{4-13a}$$

$$\sigma_{D_{tot}}(\%) = \frac{\sqrt{netOD^2 \cdot \sigma_b^2 + netOD^{2n} \cdot \sigma_c^2 + (b + n \cdot c \cdot netOD^{n-1})^2 \cdot \sigma_{netOD}^2}}{D_{fit}} \cdot 100 \tag{4-13b}$$

***(3) Software-optimized empirical models:***

Most of the tested mathematical models were selected from two fitting software: TableCurve™ and Origin™ software respectively. The equation selection criteria was based on the satisfaction of certain statistical, parametrical and mathematical conditions: (1) $R^2$ value of more than 0.99, (2) least standard error on fit parameters, (3) lowest number of parameters (between 2 and 4 parameters), (4) the fit function has to be monotonically increasing, and (5) the fit function has to go through zero. The equation that satisfies these conditions and provides minimum relative uncertainty for the fitting parameters will be selected. We have investigated the following mathematical models (with corresponding uncertainties):

$$D = a_1 + a_2 \cdot e^{-\frac{netOD}{a_3}} \tag{4-14a}$$

$$\sigma_D = \sqrt{(\sigma_{a_1})^2 + \left(\sigma_{a_2} \cdot e^{-\frac{netOD}{a_3}}\right)^2 + \left(\frac{\sigma_{a_3} \cdot a_2 \cdot netOD \cdot e^{-\frac{netOD}{a_3}}}{a_3^2}\right)^2 + \left(\frac{-\sigma_{netOD} \cdot a_2 \cdot netOD \cdot e^{-\frac{netOD}{a_3}}}{a_3}\right)^2} \tag{4-14b}$$

$$D = (a_1 + a_2 \cdot netOD + a_3 \cdot netOD^2 + a_4 \cdot netOD^3)^2 \tag{4-15a}$$

$$\sigma_D = \sqrt{\begin{matrix}(2 \cdot \sqrt{D} \cdot \sigma_{a_1})^2 + (2 \cdot netOD \cdot \sqrt{D} \cdot \sigma_{a_2})^2 + (2 \cdot netOD^2 \cdot \sqrt{D} \cdot \sigma_{a_3})^2 + \\ (2 \cdot netOD^3 \cdot \sqrt{D} \cdot \sigma_{a_3})^2 + (2 \cdot (a_2 + 2 \cdot a_3 \cdot netOD + 3 \cdot a_4 \cdot netOD^2) \cdot \sqrt{D} \cdot \sigma_{netOD})^2\end{matrix}} \tag{4-15b}$$

$$D = \frac{a_1 + a_3 \cdot netOD}{1 + a_2 \cdot netOD} \tag{4-16a}$$

$$\sigma_D = \sqrt{\left(\frac{\sigma_{a_1}}{1 + a_2 \cdot \text{netOD}}\right)^2 + \left(\frac{\text{netOD} \cdot D \cdot \sigma_{a_2}}{1 + a_2 \cdot \text{netOD}}\right)^2 + \left(\frac{\text{netOD} \cdot \sigma_{a_3}}{a_1 + a_2 \cdot \text{netOD}}\right)^2 + \left(\frac{(a_3 - a_2 \cdot a_1) \cdot \sigma_{\text{netOD}}}{(a_1 + a_2 \cdot \text{netOD})^2}\right)^2}$$

(4-16b)

$$D = \frac{a_1 + a_3 \cdot netOD}{1 + a_2 \cdot netOD + a_4 \cdot netOD^2} \quad (4\text{-}17a)$$

$$\sigma_D = \sqrt{\left(\frac{D \cdot \sigma_{a_1}}{a_1 + a_3 \cdot \text{netOD}}\right)^2 + \left(\frac{\text{netOD} \cdot D^2 \cdot \sigma_{a_2}}{a_1 + a_3 \cdot \text{netOD}}\right)^2 + \left(\frac{D \cdot \text{netOD} \cdot \sigma_{a_3}}{a_1 + a_3 \cdot \text{netOD}}\right)^2 + \left(\frac{\text{netOD}^2 \cdot D^2 \cdot \sigma_{a_4}}{a_1 + a_3 \cdot \text{netOD}}\right)^2 + \left(\frac{D \cdot (a_3 - a_2 + 2 \cdot a_4 \cdot \text{netOD}) \cdot \sigma_{\text{netOD}}}{a_1 + a_3 \cdot \text{netOD}}\right)^2} \quad (4\text{-}17b)$$

### 4.2.2 Selection of best color channel for uncertainty analysis

***(1) Single color channel analysis***

Red channel has been shown to provide higher sensitivity to irradiation than Green and Blue channels and thus it was widely used in current RCF dosimetry protocols.[66, 89] Early studies suggested the use of all three color channels independently for optimized dosimetry system[92, 100, 101] and it was shown by Devic et al[92] that this system was based on optimization of both signal sensitivity and dose uncertainty analysis. However, from our first study[68] we have recognized that the Green channel is a collection of wide absorption peaks that are comparable to the Red channel regarding the area they cover which suggests that Green channel should have improved sensitivity in the dose range lower than 8 Gy.

Not too much of an optimism is held towards utilizing Blue channel for dosimetry because of the strong absorption that happens in that part of the spectrum (400 – 500 nm). This was also seen in our previous work[68] (Fig. 1-3). Thus, only Red and Green channels are to be tested for optimal efficiency in different dose ranges.

***(2) Multiple color channels analysis***

The idea of optimizing all RGB data for dose range independently has encouraged another direction of optimization: utilizing all RGB data with a weighted average approach for the same dose range, which will decrease the uncertainty depending on how much are these color channels correlated. Different color channel combinations can be made with this approach but we have restricted our search to RGB altogether and RG; in addition to single channel analysis.

In physics, different variables are usually described independently or assuming no cross-correlation. However, in our case the correlation between different channels must be determined by the inter-connection of the densitometer's definition of RGB data. We have tested the correlation between different color channels using statistical model as in (4-18) which describes generally the correlation between two variables *X* and *Y*:

$$Cov_{XY} = \frac{\sum XY - \frac{\sum X \cdot \sum Y}{N}}{N-1} \tag{4-18}$$

However, the correlations were found to be very minimal in the whole dose range and thus were ignored. Weighted average signal and associated uncertainty were calculated as:

$$\overline{D}(R,G) = \frac{\partial D}{\partial D_R} D_R + \frac{\partial D}{\partial D_G} D_G \tag{4-19a}$$

$$\sigma^2{}_{\overline{D}} = \left(\frac{\partial D}{\partial D_R}\right)^2 \sigma^2{}_R + \left(\frac{\partial D}{\partial D_G}\right)^2 \sigma^2{}_G + 2 \cdot \frac{\partial D}{\partial D_R} \cdot \frac{\partial D}{\partial D_G} \cdot Cov_{RG} \tag{4-19b}$$

where, $\frac{\partial D}{\partial D_R} = \frac{\frac{1}{\sigma^2{}_R}}{\frac{1}{\sigma^2{}_R}+\frac{1}{\sigma^2{}_G}}$, $\frac{\partial D}{\partial D_G} = \frac{\frac{1}{\sigma^2{}_G}}{\frac{1}{\sigma^2{}_R}+\frac{1}{\sigma^2{}_G}}$, $Cov_{RG} = 0$, *R* refers to Red signal and *G* refers to Green signal.

### 4.2.3 Dose range effect on uncertainty analysis

As the sensitivity of each color channel differs with dose range, the uncertainty analysis of our high doses (10 – 50 Gy) must be affected by this fact

and the utilization of a single channel – Red for instance – might fail because of signal saturation at high doses. In order to complete the recommendations in this protocol, we decided to test three different dose ranges for the selected mathematical model. These ranges are: (1) 0 – 4 Gy, (2) 0 – 8 Gy, and (3) 0 – 50 Gy; where the goal is to find a single equation for the whole dose range and try to avoid piecewise functions because they increase the complexity of work.

### 4.2.4 Total uncertainty on reported doses

By applying various corrections throughout the protocol we have managed to minimize some potential sources of uncertainty in dose measurements. This includes scanning film pieces in the center of the scanner, gentle cleaning of the scanning bed and film pieces to be scanned, controlling thermal history of film pieces and other precautions that were mentioned in Section 4.1.1.

All sources of uncertainty are initially estimated for measured *netOD*, and they are then incorporated into the fitting process for the calibration curve using mathematical models explained earlier. The sources of uncertainty on *netOD* that we have considered are: (1) Source-to-film positioning (signal reproducibility), (2) Scanner homogeneity, (3) Scanner reproducibility, and (4) *netOD* measurements reproducibility. A fifth element is added to the measurement done in solid water which is the uncertainty in determining $(D_{SW}/D_W)^{Ir\text{-}192}$ from Monte Carlo calculations.

# Chapter.5: Results and Discussion

## 5.1 Mathematical model

Various mathematical models were suggested in section 4.2.1 with either physical or empirical basis. The results of testing these models are shown in Fig. 5-1a and Fig. 5-1b for green channel data. Fig. 5-1a shows the total percent uncertainty on measured doses that extends from 0 to 8 Gy, and it shows that physically-based models fail in providing sufficient precision in dose measurement. It also shows that empirical models better describe dose response curve of the EBT-2 film model. On the other hand, in order to justify the uncertainty analysis, shown in Fig. 5-1a, the error between the delivered dose and the calculated dose is presented as percentage in Fig. 5-1b. The two figures test and confirm the results of the uncertainty analysis where one cannot have errors larger than the total uncertainty on the measured dose. In one sigma uncertainty analysis and, it is shown that the physically-based model (equation 4-11a) has a total uncertainty of 11.8% for doses above 1.5 Gy, while all empirical models has total uncertainties of less than 4% above the 1.5 Gy dose line. It is also seen that while most of the empirical models predict the dose within one percent, the uncertainties associated with them are relatively high. The most common model (given by equation 4.6) developed by Devic et al[60] shows the best balance between precision and accuracy with uncertainty of 1.6% on doses larger than 0.25 Gy and 1% on doses larger than 0.5 Gy and 0.3% on doses larger than 2 Gy, and thus was selected the mathematical model in our analysis. The use of Fig. 5.1 can serve as a verification tool of the established radiochromic film dosimetry system because the properties of radiochromic films may change with changes of the environmental conditions, length of post-irradiation waiting period and batch number. By plotting the graph described in Fig. 5-1b can verify that calibration curve and its corresponding uncertainty limits (given in Fig. 5.1a) are still valid.

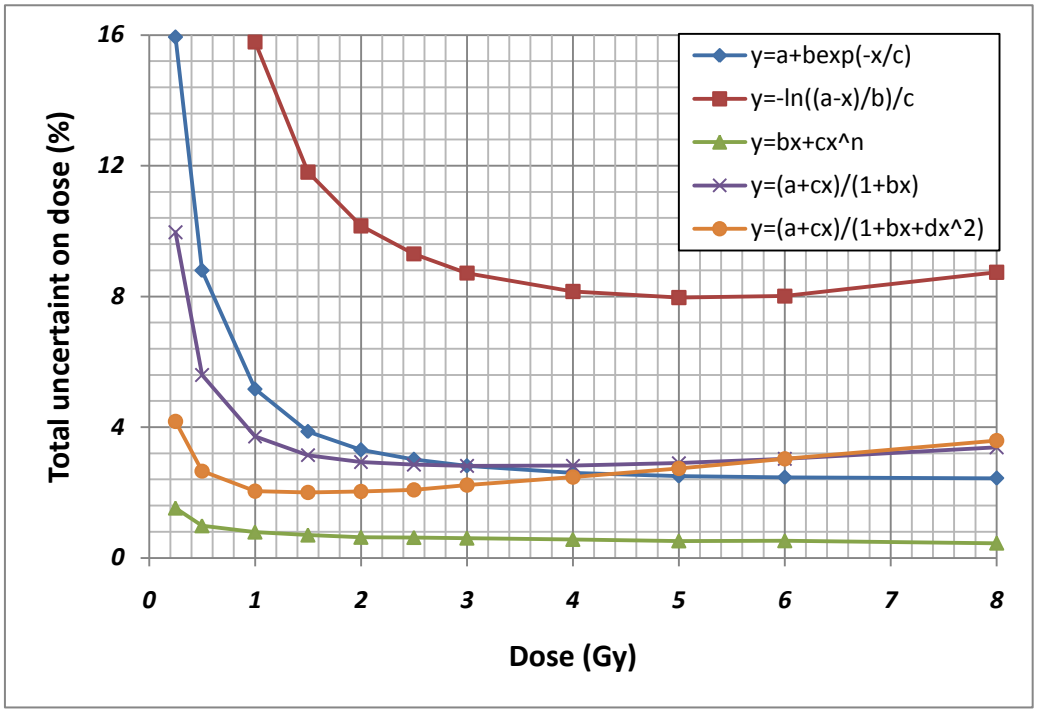


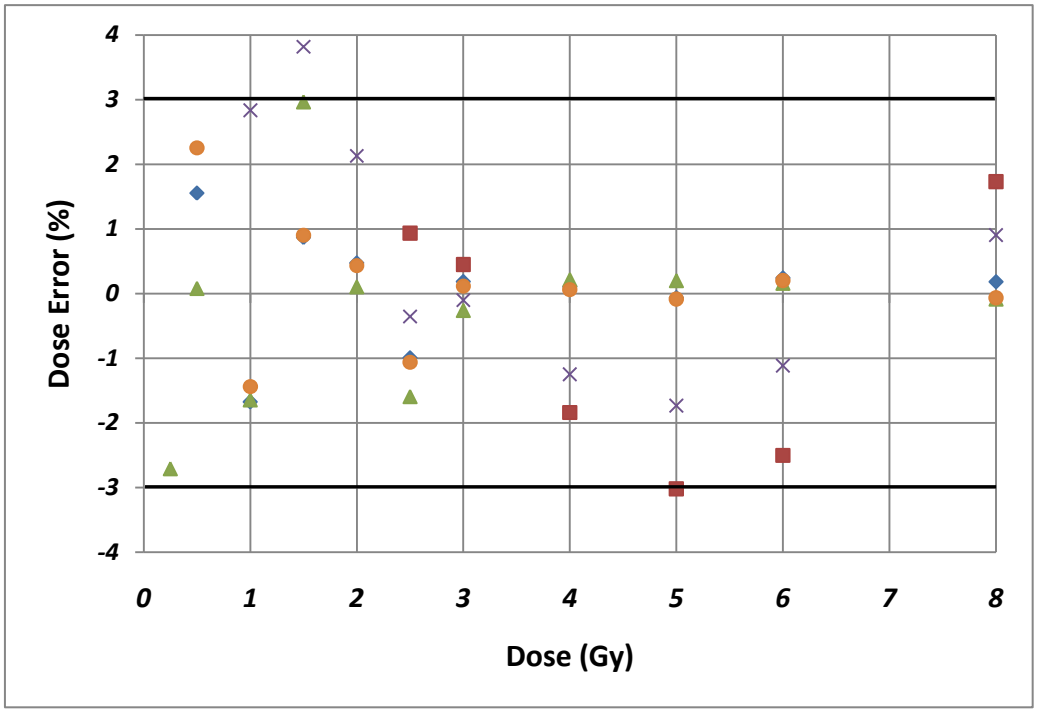


Fig. 5-1: (a) Uncertainty estimates of five different mathematical models for EBT-2 film irradiated by Ir-192 in the Solid Water setup for a dose range of 0 to 8 Gy , while (b) shows the justification of the uncertainty estimation analysis: relative percent error in dose calculated using those models with respect to dose delivered to the film pieces.

## 5.2 Color channel and dose range effect on uncertainty analysis

Fig. 5-2a and Fig. 5-2b shows the uncertainties on measured doses and the percentage error between delivered and calculated doses respectively for green, red channel data and a weighted average between the two channels, in a dose range that extends between 0 and 8 Gy. It is shown that our hypothesis about green channel being suitable for dosimetry is true where the uncertainty on measured dose is comparable with the red channel. Also, the idea of having a weighted average between the red and green channel data shows significant reduction on the uncertainty analysis (as expected) where the covariance term was neglected and no correlation was assumed between the two channels since it was shown to be very minimal. It also shows better performance in estimating the doses as seen in Fig. 5-2b.

However, in terms of sensitivity, red channel provides higher sensitivity than green channel for doses up to 8 Gy approximately where green channel starts to have higher sensitivity and this is demonstrated in Fig. 5-3b which shows the rate of change (first derivative) of each color channel plotted as function of dose from Fig. 5-3a.

Our favor of green channel is moreover justified when we plotted the uncertainties for larger dose range up to 50 Gy where the green channel is shown to dominate in the total uncertainty reported on measured doses (See Fig. 5-4a), and the weighted average method has less significance since it is skewed by the red channel data. This is expected because in the 0-8 Gy dose range, there was a cross over between the uncertainties from each channel while for the 50 Gy dose range the signal is saturated in the red map and uncertainties do not cross, which shows failure in estimating doses as demonstrated in Fig. 5-4b.

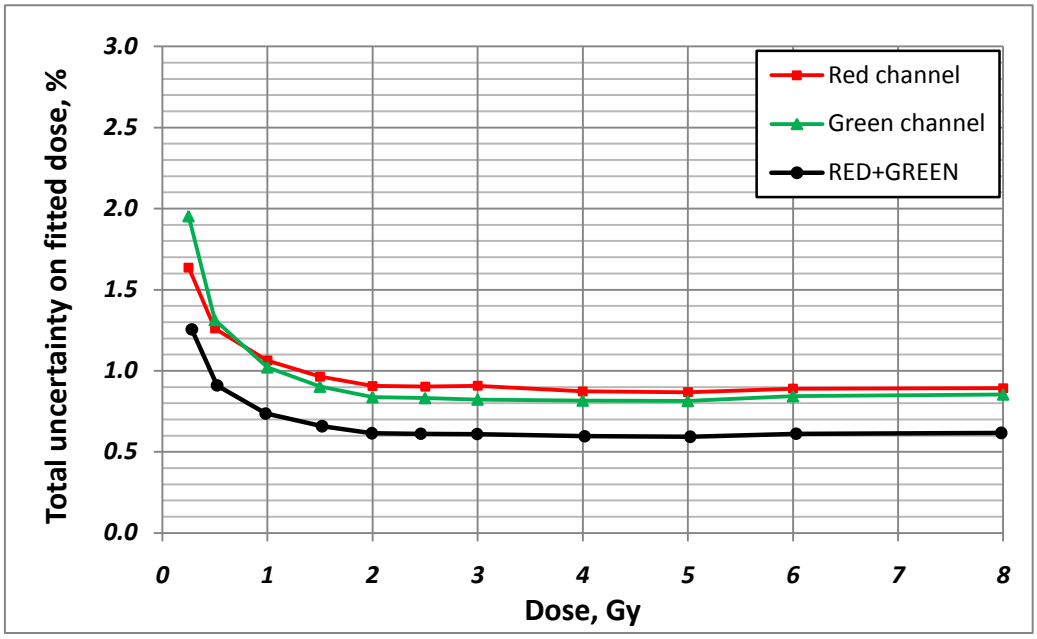


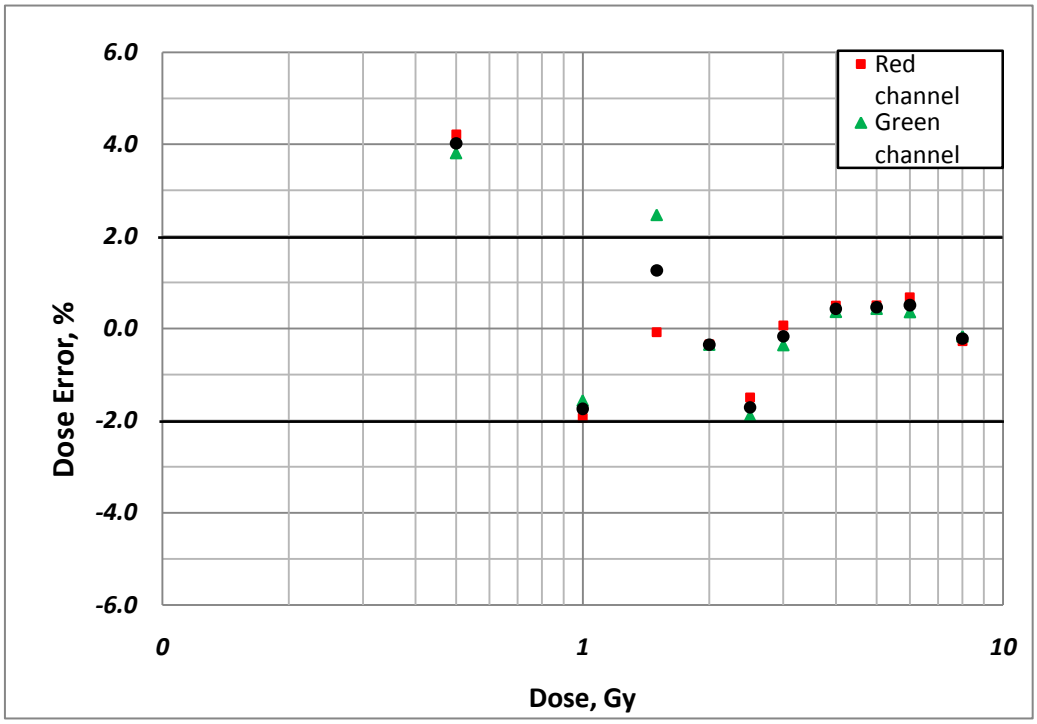


Fig. 5-2: (a) Uncertainty estimates of green, red channel data and a weighted average between them for EBT-2 film irradiated by Ir-192 in the Solid Water setup for a dose range of 0 to 8 Gy, while (b) shows the justification of the uncertainty estimation analysis: relative percent error in dose calculated using those models with respect to dose delivered to the film pieces.

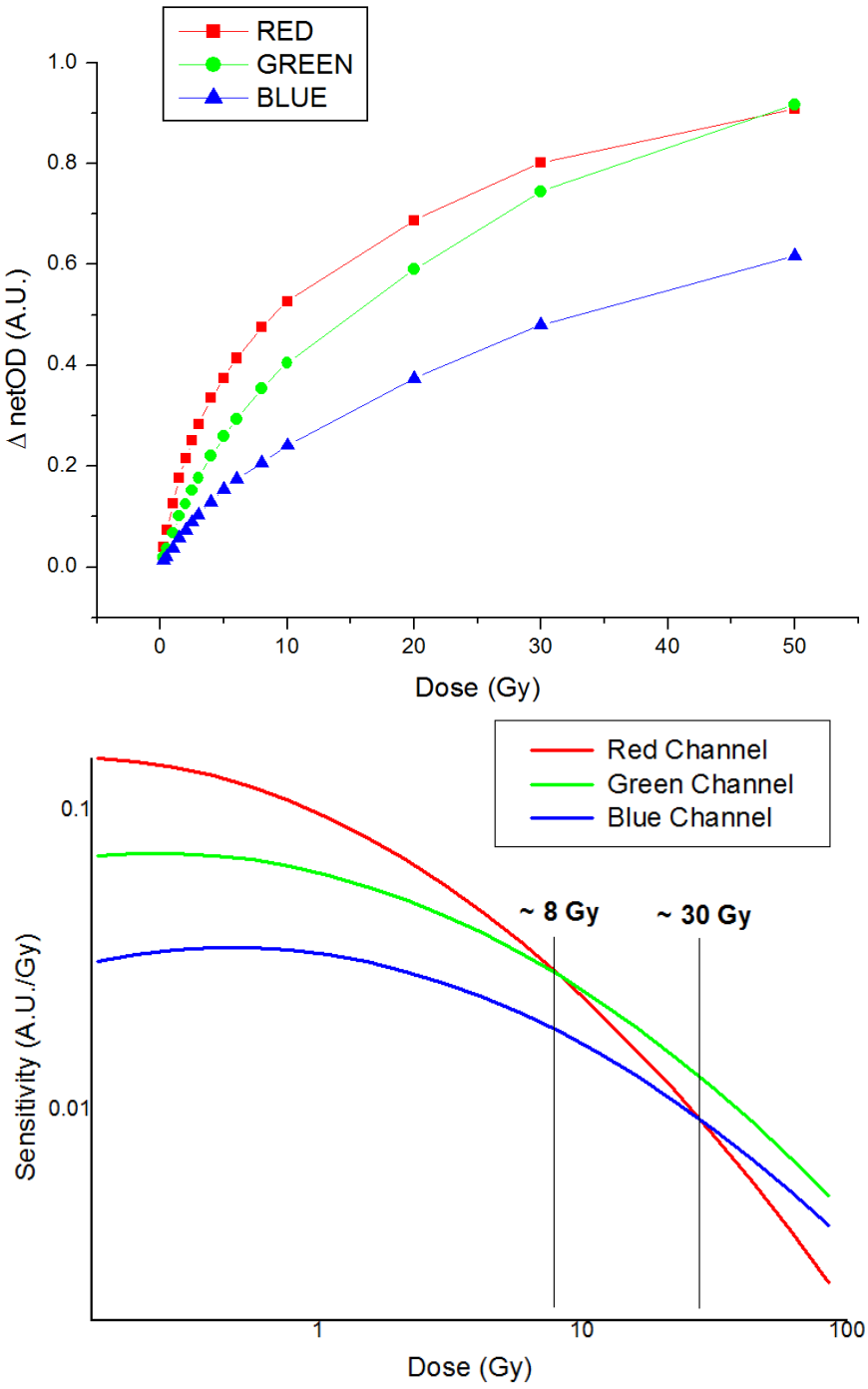


Fig. 5-3: (a) Dose response curves (a), and sensitivity curves fits (b) for the three color channels. lines on the bottom figure indicate the cross-over doses between the highest sensitivities for the three color channels. Data are acquired from EBT-2 films irradiated by Ir-192 in the Solid Water setup for a dose range of 0 to 50 Gy.

We have also tested the use of all RGB channels in a dose range between 8 and 50 Gy where we have seen that blue channel has the lowest uncertainties with all the measured doses falling to less than 2.5% (See Fig. 5-5a and Fig. 5-5b). The effect of dose range in the fitting process is also shown where the tails of both green and red channels differ than those for the 50 Gy dose range. This is expected because the film does not respond linearly with dose and having more or less data available for fitting does not correspond to an increase or decrease in the uncertainty estimation since goodness of fit also depends on reproducibility of the data signal saturation in higher doses.

## 5.3 Final uncertainty analysis for dose measurements

Under the basis of justified investigation of both mathematical model and color map that are more suitable for our dosimetry range, we have selected the widely accepted mathematical model expressed in equation 4-6 with utilization of green channel data only for the whole dose range which is found to be advantageous for EBT-2 model GAFCHROMIC$^{TM}$ film over its predecessors.

That being said, we now have to specify the uncertainties in water setup and Solid Water$^{TM}$ setup separately since water has an impact on the uncertainty in the water setup while it does not in solid water setup. However, solid water setup has a Monte Carlo calculated conversion factor which affects the uncertainty on measured dose.

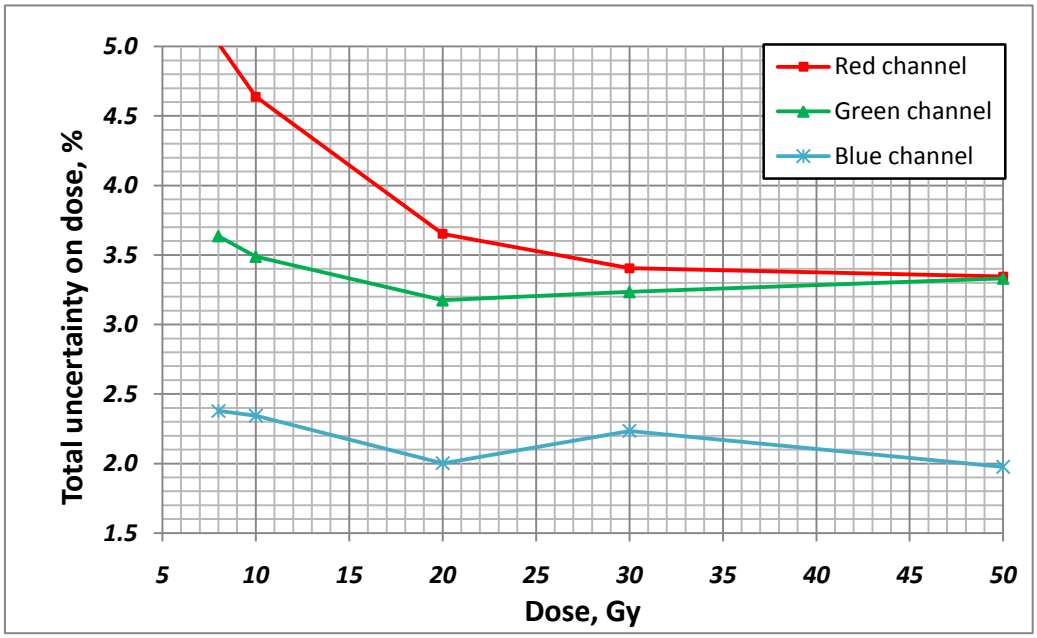


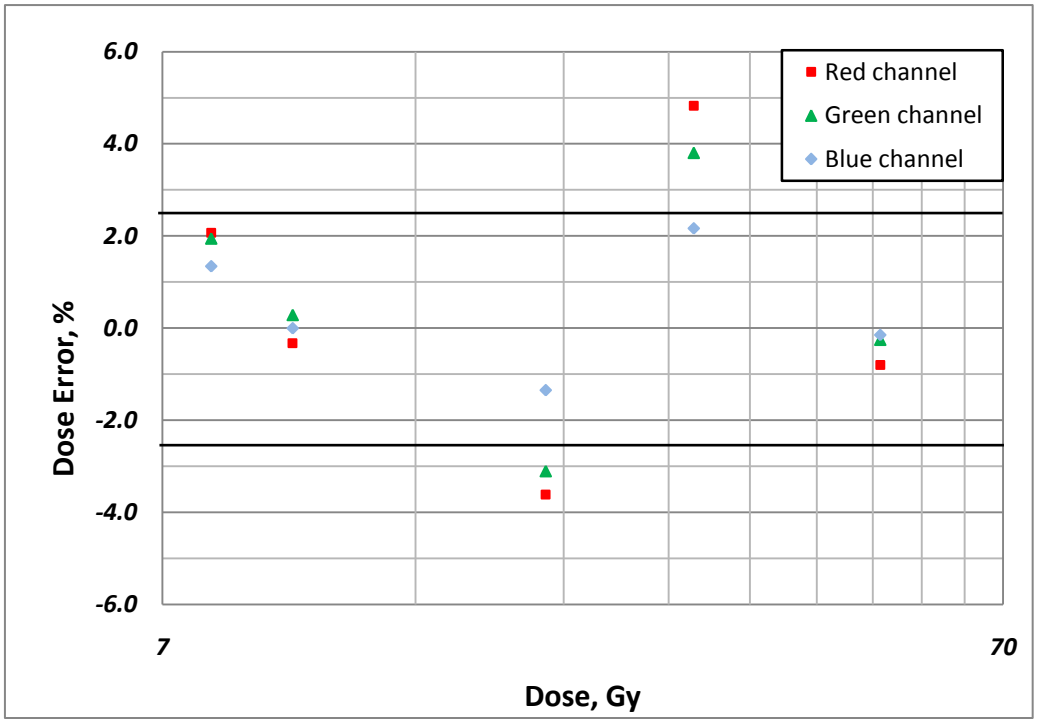


Fig. 5-5: (a) Uncertainty estimates of green, red and blue channels data for EBT-2 film irradiated by Ir-192 in the Solid Water setup for a dose range of 8 to 50 Gy , while (b) shows the justification of the uncertainty estimation analysis where blue channel is shown to provide total uncertainty of less than the 2.5% lines indicated by bold solid black.

### 5.3.1 Uncertainty analysis for in-water measurements

The final uncertainty analysis achieved for in-water measurements of doses larger than 0.25 Gy using EBT-2 GAFCHROMIC$^{TM}$ film is summarized in Table 5-1 and explicitly shown in Fig. 5-6a and Fig. 5-6b (Green Channel). These results show an estimate of uncertainties one will get assuming that precise nominal doses were delivered in the calibration phase and that uncertainty in position was overcame by dose homogeneity region where the uncertainty of our distance measurement tool (CT image) falls within the dose homogeneity region; a fact that was shown in the reproducibility of signal within the ±0.5% line. (See Table 3-1)

Table 5-1: Total uncertainty analysis for in-water dose measurements using EBT-2 model GAFCHROMIC$^{TM}$ film measurements in Ir-192 brachytherapy source. Data represents green channel for doses larger than 0.25 Gy. Type A uncertainties refers to uncertainties that were measured by statistical means while type B uncertainties are uncertainties that were measured by no-statistical means.

| ***Source of uncertainty*** | ***Type*** | |
|---|---|---|
| | ***A*** | ***B*** |
| *Scanner homogeneity* | | *0.20%* |
| *Scanner reproducibility* | *0.11%* | |
| *Calibration curve fit* | | *0.77%* |
| *NOD measurement reproducibility* | *0.99%* | |
| *Water correction (dose control)* | | *1.0%* |
| **Total Uncertainty** | **1.62%** | |

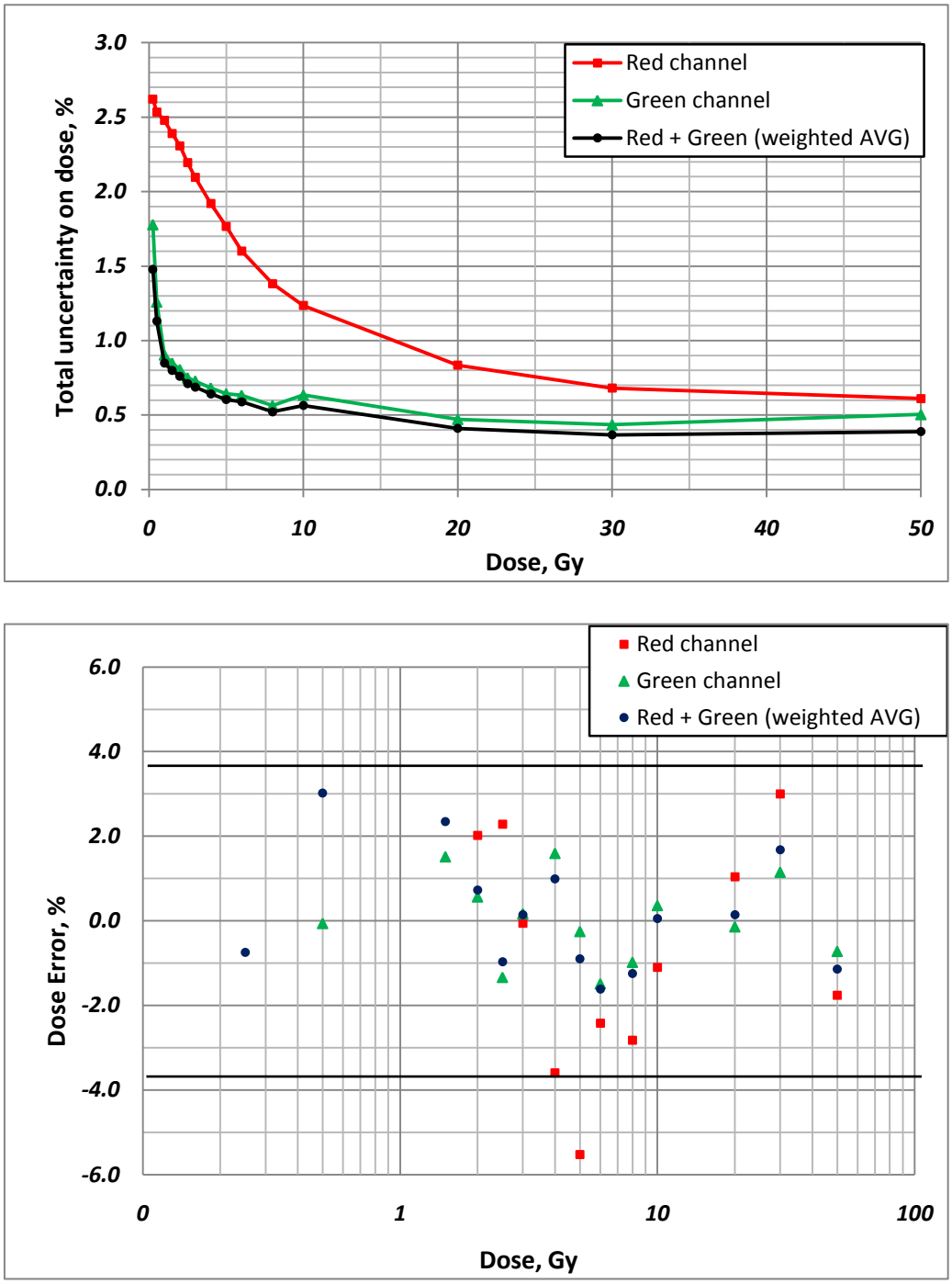


Fig. 5-6: (a) Uncertainty estimates of green, red and weighted average signal between both data for EBT-2 film irradiated by Ir-192 in the water setup for a dose range of 0 to 50 Gy , while (b) shows the justification of the uncertainty estimation analysis. Solid black lines indicate the 3.5% dose error line in (b).

It is evident from these figures that weighted average signal between both red and green channels does not reduce the uncertainty significantly in large dose ranges as it did for smaller dose range (Fig. 5-7). The one sigma uncertainty of green channel, red channel and weighted average signal is 1.7% for doses larger than 0.5 Gy, 3.6% for doses larger than 0.5 Gy and 1.5% for doses larger than 0.25 Gy; respectively. The gain in total uncertainty on dose from weighted signal as shown as minimal but still appreciated especially with in-water measurements. Red channel is not recommended solely for dosimetry in dose ranges larger than 8 Gy.

### 5.3.2 Uncertainty analysis for in-solid water measurements

The final uncertainty analysis achieved for dose measurements in solid water for doses larger than 0.5 Gy using EBT-2 GAFCHROMIC$^{TM}$ film is summarized in Table 5-2 and explicitly shown in Fig. 5-8a and Fig. 5-8b (Green Channel). These results show an estimate of uncertainties one will get assuming that precise nominal doses were delivered in the calibration phase and that uncertainty in position was overcame by dose homogeneity region where the uncertainty of our distance measurement tool (CT image) falls within the dose homogeneity region; a fact that was proven by the reproducibility of signal within the ±0.5% line. (See Table 3-1)

## 5.4 Importance of control film piece in dose measurements

It is well noticed from Tables 5-1, 5-2 and 5-3 that dose control introduces significant increase in total uncertainty. However, this is expected as the sole reason of introducing this principle was to gain accuracy in measurements. This might not be obvious if one sees only in-solid water measurements but if one considers measurements in water where we proved that there is an obvious dose error introduced by presence of water and such error is can be removed by the control film piece. A plausible justification of this claim is shown in Fig. 5-9 where measured signal from in-water measurements are compared to *netOD*

from solid water setup with both cases: Δ*netOD*, i.e. correcting for water presence (dose control principle, red circles) and *netOD* i.e. without correction (blue lozenges).

Table 5-2: Total uncertainty analysis for in-solid water dose measurements using EBT-2 model GAFCHROMIC™ film measurements in Ir-192 brachytherapy source. Data represents green channel for doses larger than 0.5 Gy.

| ***Source of uncertainty*** | ***Type*** | |
|---|---|---|
| | ***A*** | ***B*** |
| *Scanner homogeneity* | | *0.20%* |
| *Scanner reproducibility* | *0.11%* | |
| *Calibration curve fit* | | *0.70%* |
| *NOD measurement reproducibility* | *0.93%* | |
| *Dose control* | | *0.70%* |
| $(D_{SW}/D_W)^{Ir\text{-}192}$ *MC conversion factor* | *0.14%* | |
| **Total Uncertainty** | **1.38 %** | |

Table 5-3: Impact of control on total uncertainty analysis for in-solid water and in-water dose measurements using EBT-2 model GAFCHROMIC™ film measurements in Ir-192 brachytherapy source. Data represents doses larger than 0.5 Gy.

| ***Setup*** | ***Water Setup*** | | ***Solid water Setup*** | |
|---|---|---|---|---|
| ***Control \ Channel*** | ***Green Channel*** | ***Red Channel*** | ***Green Channel*** | ***Red Channel*** |
| ***Without control*** | *1.1%* | *3.6%* | *1.3%* | *3.1%* |
| ***With control*** | *1.3%* | *3.6%* | *1.7%* | *3.2%* |

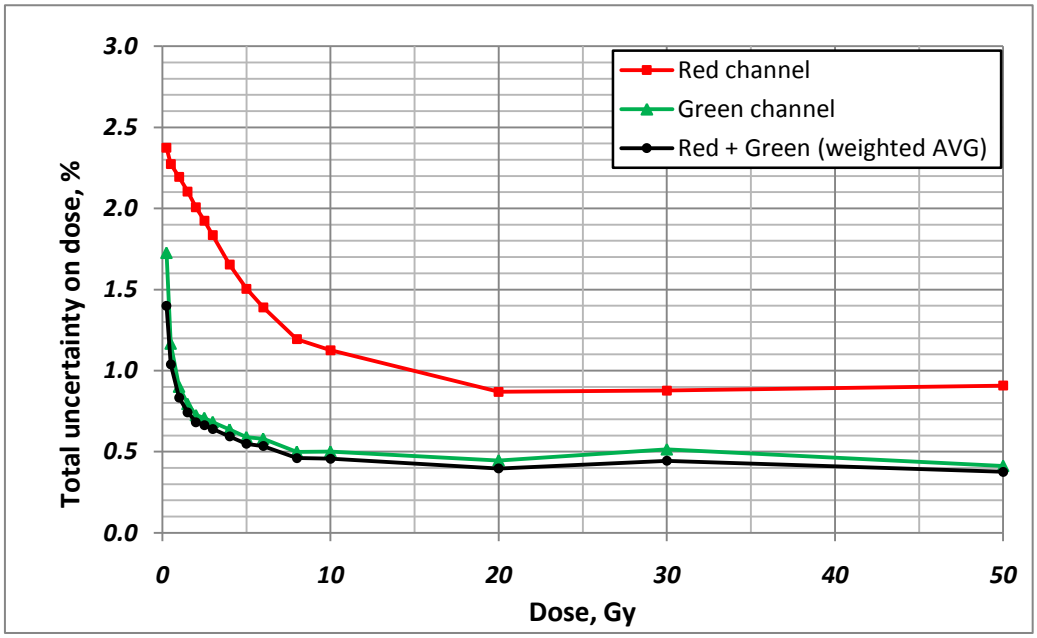


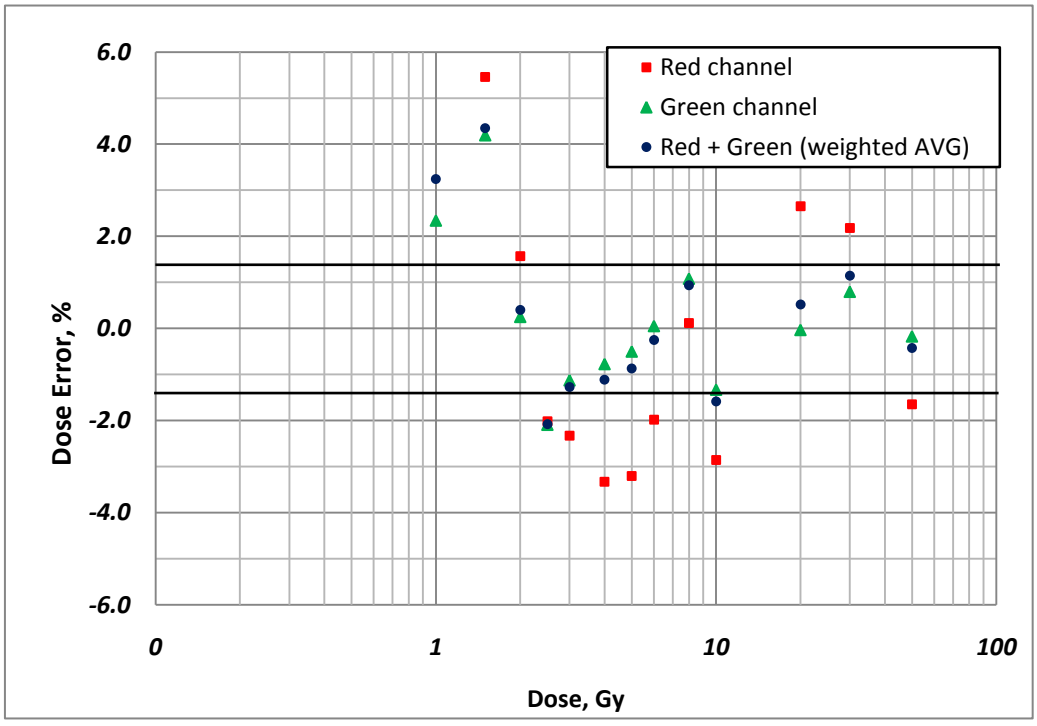


Fig. 5-8: (a) Uncertainty estimates of green, red and weighted average signal between both data for EBT-2 film irradiated by Ir-192 in the Solid Water setup for a dose range of 0 to 50 Gy , while (b) shows the justification of the uncertainty estimation analysis. Solid black lines indicate the 1.3% dose error line in (b).

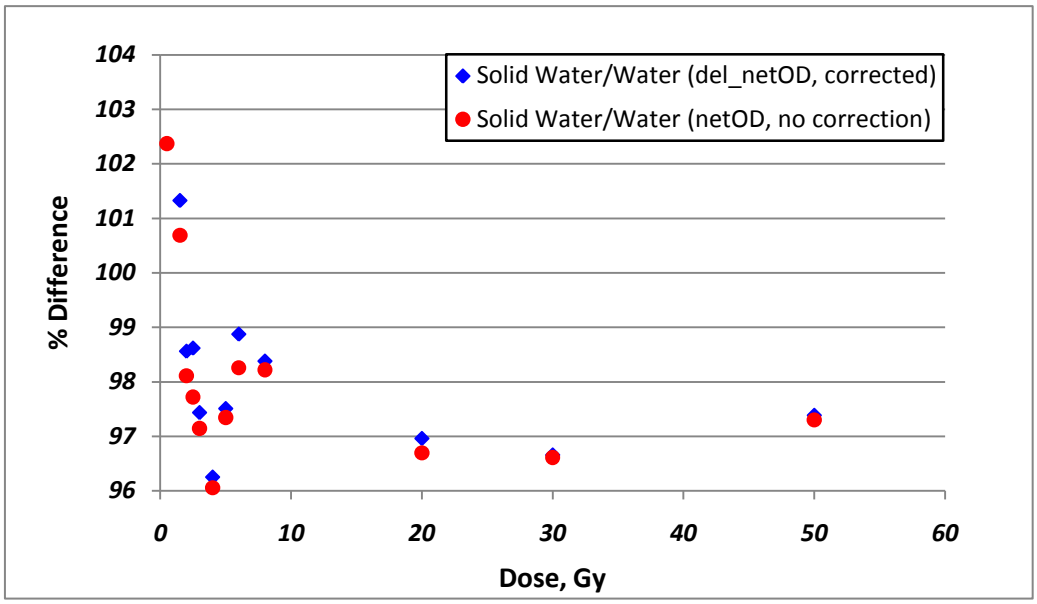


Fig. 5-9: Using control in water setup results in increased accuracy. Difference between Solid Water and water setups in signal is consistent with Monte Carlo results (2-3%).

## 5.5 Monte Carlo calculated ratios

The results of the Monte Carlo calculated conversion factor, $(D_{SW}/D_W)^{Ir\text{-}192}$, which converts the doses delivered from a dose to water in solid water to a dose to solid water in solid water without the presence of the film. The value of this factor was found to be 0.9808 ± 0.14% (1σ) in Ir-192 beam while it was 0.9777 ± 0.14% (1σ) in Co-60 beam. Including the film would change these values into 1.0099 ± 0.14% (1σ) in Ir-192 beam and 1.0079 ± 0.14% (1σ) in Co-60 beam where the scoring region is inside the active layer of the film. From these results, all doses delivered in the solid water setup will be decreased by 2%, refitted and then compared to water setup result.

## 5.6. Calibration curves

The final calibration curves from EBT-2 model GAFCHROMIC$^{TM}$ film and Ir-192 brachytherapy beam in water and Solid Water setups are plotted in Fig. 5-10.

These curves show explicitly the 2% difference that we calculated from Monte Carlo simulation and it is in agreement with data published by Seuntjens et al[102] in 2005 which shows a 3% difference between ratios of mass-energy absorption coefficient of water and solid water in Co-60 photon beam, where the 1% difference lies within the uncertainty of our dosimetry system. This could also be seen from Fig. 5-9 where the difference between the solid water and water is around the 1% and 3% lines.

From these curves and the uncertainty analysis previously discussed it is evident that one can use Solid Water in dose verification and avoid complexity associated with measurements in water which required accurate design of the film holder and accounting for the variable impact of water on the film pieces with different doses. However, reference doses to be delivered to the calibration film pieces must be downscaled by 2%, as calculated based on TG-43 protocol. In such a way, future measurements of *netOD* in Solid Water phantoms will provide a dose to water through the calibration curve established using reference dose scaled by 2%.

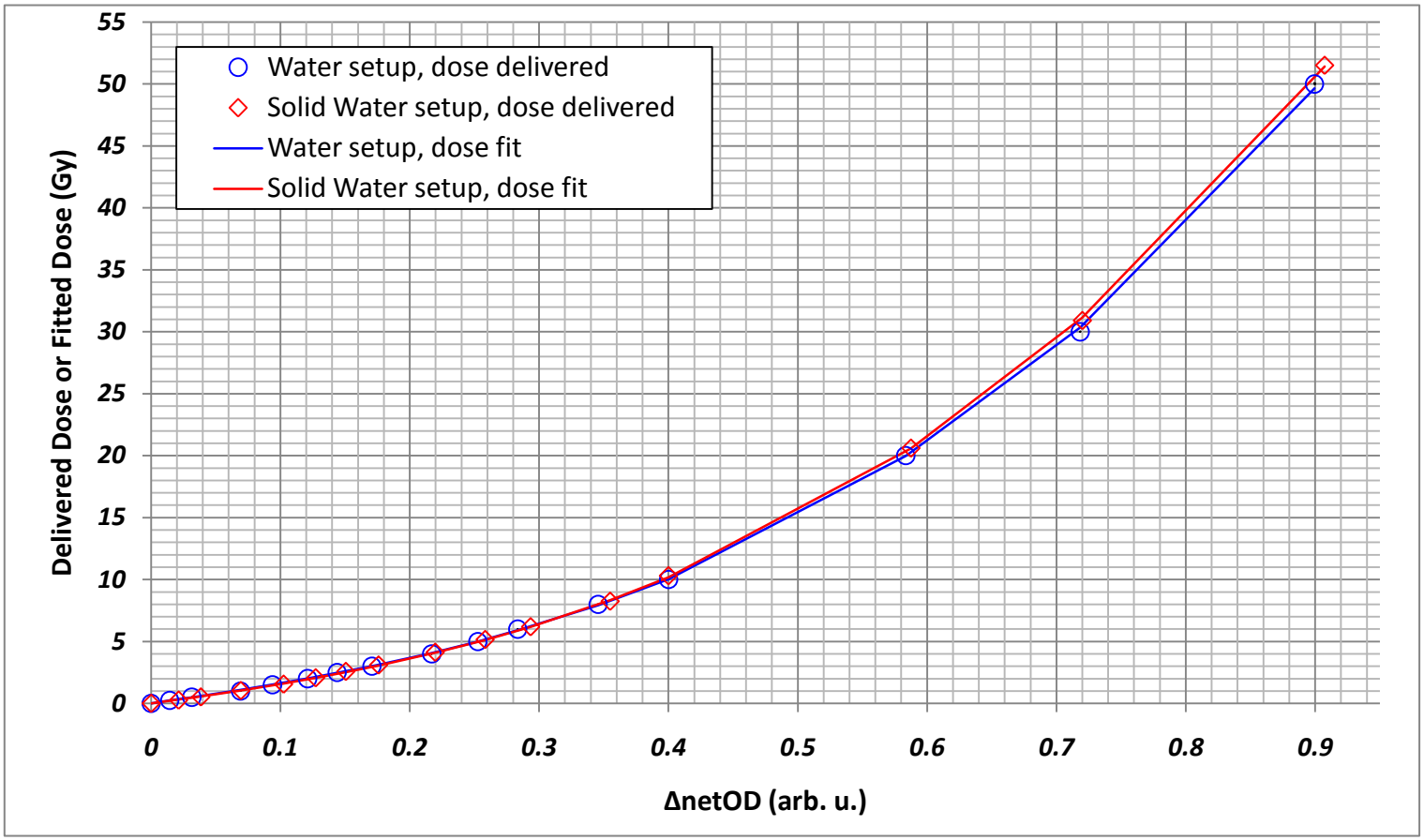


Fig. 5-10: Calibration curves from EBT-2 model GAFCHROMIC™ film and Ir-192 radiation beam in Water and Solid Water setups. Error bars are too small too small for this scale and thus neglected.

# Chapter.6: Conclusions

## 6.1 General conclusion

We have successfully established a reference dosimetry protocol for HDR Ir-192 using radiochromic film. An extensive review of the current status of radiochromic film dosimetry was discussed and optimized in order to develop this protocol. EBT-2 GAFCHROMIC film model was investigated as a precision dosimeter and shown to be a good alternative to EBT-1. Absorption spectra of EBT-2 were obtained for different doses and scanning time. The strong absorption band in blue region was observed and when we acquire the net absorbance signal, it has been shown that there is no radiation induced signal (or minimal) in the blue range. This strong absorption was caused by the addition of the yellow dye marker which was intended to correct for subtle changes in the active layer of the film.

A method has been described that can establish the time error constraints on the post-irradiation scanning time that will still provide an acceptable dose error for clinical applications if the protocol employing the shorter post-irradiation scanning time is implemented in the clinic. We show that for two post-irradiation scanning times of 30 minutes and 24 hours the 1% dose error can be granted if the scanning time window is less than ± 5 minutes and ± 2 hours, respectively.

We reported on an undoubted impact of radiochromic film immersion in water on the measured change in optical density that may lead to systematic errors in dose measurements if the film is kept in water for longer periods of time. Magnitude of the impact depends on many parameters: size of the film piece, initial optical density, post-immersion waiting time prior to scanning (defined by the current radiochromic film dosimetry protocol in place), and the time film was kept in water. We also suggested various approaches in correcting for the change in *netOD* due to water penetration into the film, but we believe that the use of the control film piece would be the most appropriate.

Two calibration curves have been established for EBT-2 film model. The first one was in a water setup, and the second is in Solid Water™. We reported a 2% difference between dose measured at Solid Water™ and water for the very same setups from Monte Carlo simulations with dose to Solid Water™ being less than dose to water. We confirmed this experimentally after incorporating this correction factor to Solid Water™ calibration curve. We plotted the difference between Water and Solid Water™ and we concluded that Solid Water™ is a viable alternative to water in HDR Ir-192 reference dosimetry.

### 6.2. Protocol summary

In order to calibrate a radiochromic film for dosimetry in Ir-192, the following steps are recommended (Fig. 6-1 summarizes the proposed protocol):

(i) A set of film pieces of the same size are cut and prepared for reference dosimetry irradiations in a deemed dose range including a zero dose (or control) film piece.

(ii) All unexposed pieces of film are scanned in a transmission mode using, preferably 48-bit, RGB color scanning mode with all the image enhancement filters turned off; five blank scans of the scanner bed are performed over the same scanning region, as for the unexposed film pieces, for defective pixel identification;

(iii) The film pieces are exposed in Solid Water™ to a series of known doses in an AP-PA approach that provides a homogenous dose distribution within a 4 mm × 4 mm volume in a source-to-film distance of 30 mm from a fresh source.

(iv) A time delay is introduced to allow the radiochromic film to self-develop; nominally 24 hours;

(v) Films are scanned and then another five blank scans of the scanner bed are performed over the same scanning region, as for the exposed film pieces, for defective pixel identification. At this point, measurement of the zero-light

transmitted intensity value - measured with an opaque piece of film - is recommended.

(vi) Images are firstly cropped to the films' area while preserving all RGB data. Then a region of interest is chosen to be fit with horizontal and vertical Gaussians where the maximum value of each fit is reported as the position of the maximum OD point. An average of the Gaussians' maxima is taken and then the position is reported back to the original RGB image and a small ROI is chosen around the maximum where care must be taken that this region should be consistent with the originally planned dose homogeneity region. RGB image are then split (Green Chanel is currently recommended) and faulty pixels are identified; within the average unexposed and exposed film images, the "bad" pixels are discarded or replaced by the average values of the neighboring pixels; a 2D Wiener filter is then applied to both resultant images, and the transmission scanner readings ($PV_{unexp}$ or $PV_{exp}$) as well as the standard deviations are determined for every film piece as a mean pixel value over the desired ROI;

(vii) For a given dose, ΔnetOD is acquired from equations 4-1 to 4-5 and then dose is plotted against ΔnetOD, weights are determined from equation 4-7 and the *D vs* Δ*netOD* relation is fitted with equation 4-13a and uncertainty on dose is calculated using equation 4-13b

(viii) Dose uncertainty assessment and verification of the calibration curve and dose uncertainty analysis, based on Fig. 5-8 are carried out.

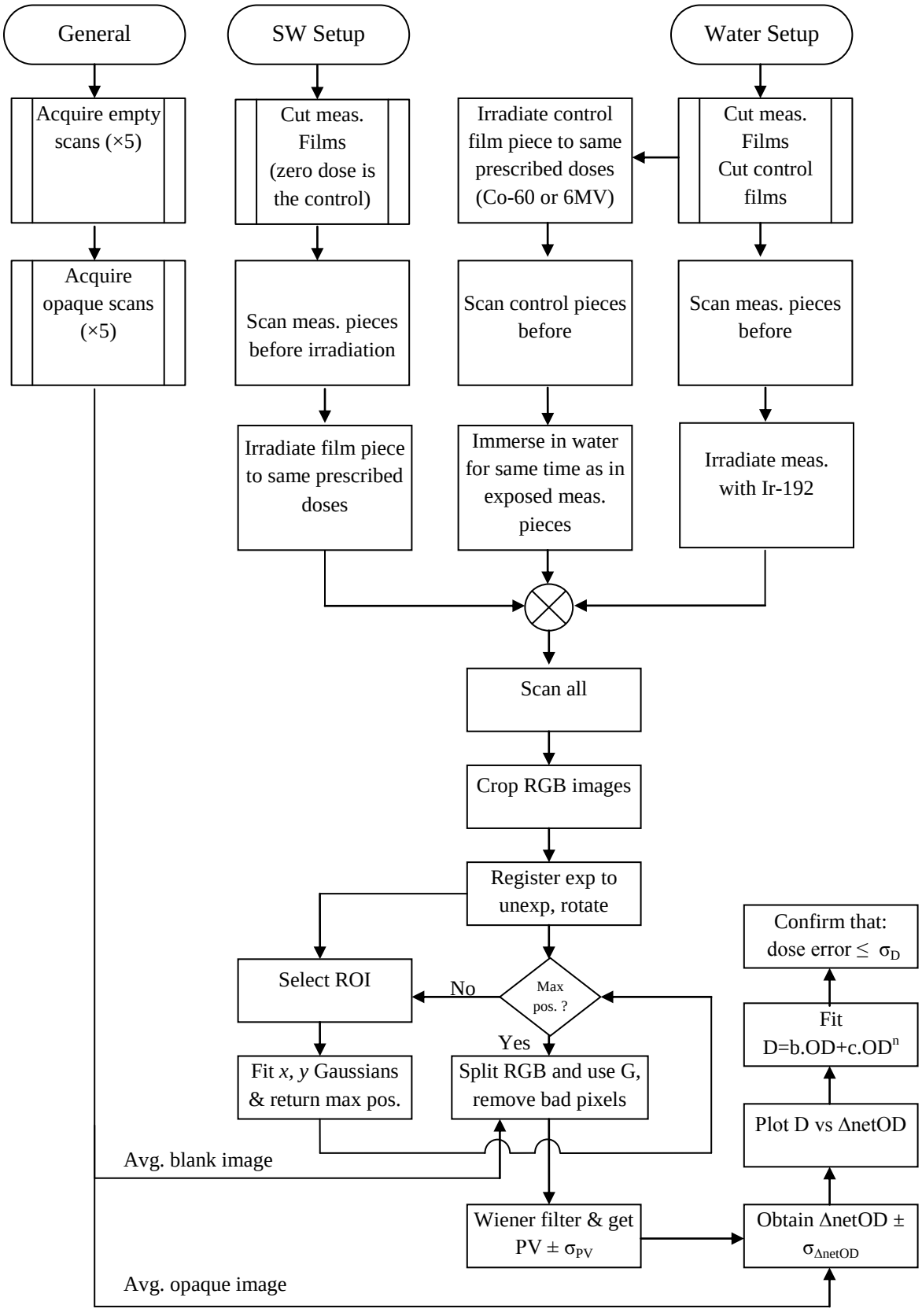


Fig. 6-1: Summary of HDR-192 reference dosimetry protocol using EBT-2 film model.

# Appendix I

## Main Matlab Code

```
clear
load Im_cor1
mean_unexp_r(1:5)=0;
stdev_unexp_r(1:5)=0;
mean_exp_r(1:5)=0;
stdev_exp_r(1:5)=0;

mean_unexp_g(1:5)=0;
stdev_unexp_g(1:5)=0;
mean_exp_g(1:5)=0;
stdev_exp_g(1:5)=0;

mean_unexp_rb(1:5)=0;
stdev_unexp_rb(1:5)=0;
mean_exp_rb(1:5)=0;
stdev_exp_rb(1:5)=0;

mean_unexp_gb(1:5)=0;
stdev_unexp_gb(1:5)=0;
mean_exp_gb(1:5)=0;
stdev_exp_gb(1:5)=0;

mean_unexp_b(1:5)=0;
stdev_unexp_b(1:5)=0;
mean_exp_b(1:5)=0;
stdev_exp_b(1:5)=0;

for kk=1:5
% read exposed films file
Im=imread('After_Ir-Water_001.tif');
Imw=imread('Before_Ir-Water_001.tif');

imagesc(Im)
axis image
tn=int2str(kk);

h2 = imcrop(ggg,[300 240 800 700]);
h1 = imcrop(Im,[300 240 800 700]);
% h1=imcrop;
imagesc(h1)
Title(['Take 2 points for rotation - take
points on the upper horizontal edge of the
film,',' Trial number: ',tn])
axis image
colorbar

[x_r,y_r,z_r]=impixel;
% Rotate image
if (y_r(2)-y_r(1))==0
    angle_r=0;
else a_r=(abs(y_r(2)-y_r(1))/(y_r(2)-
y_r(1)))*acos(sqrt((x_r(2)-
x_r(1))^2)/sqrt((x_r(2)-x_r(1))^2+(y_r(2)-
y_r(1))^2));
    angle_r=a_r*180/3.14;
end
angle_r;
```

```
clear b*
b1=imrotate(h1,angle_r,'crop');
b2=imrotate(h2,angle_r,'crop');
imagesc(b1)
axis image
colorbar
Title(['Take ONLY ONE point: in the upper
left corner -> to select origin of the
film piece,',' Trial number: ',tn])

[x_film,y_film,zc]=impixel;

imagesc(b1)
axis image
impixelinfo

ggg1=double(b2(:,:,1));
ggg2=double(b2(:,:,2));
ggg3=double(b2(:,:,3));

Title(['Take ONLY ONE point to isolate ROI
to be processed,',' Trial number: ',tn])

%%%%%%%%%%%%%%%%%%%%%%%%%%%%%%%%
%% Code for fitting gaussians %%
%%%%%%%%%%%%%%%%%%%%%%%%%%%%%%%%
[xcv,ycv,zcv]=impixel;
roi=b1(ycv-50:ycv+50,xcv-50:xcv+50);
imagesc(roi)
axis image
impixelinfo
% a profile per 10 pixels in x
x_profile_1=roi(10,:)';
x_profile_2=roi(20,:)';
x_profile_3=roi(30,:)';
x_profile_4=roi(40,:)';
x_profile_5=roi(50,:)';
x_profile_6=roi(60,:)';
x_profile_7=roi(70,:)';
x_profile_8=roi(80,:)';
x_profile_9=roi(90,:)';
x_profile_10=roi(100,:)';
% a profile per 10 pixels in y
y_profile_1=roi(:,10);
y_profile_2=roi(:,20);
y_profile_3=roi(:,30);
y_profile_4=roi(:,40);
y_profile_5=roi(:,50);
y_profile_6=roi(:,60);
y_profile_7=roi(:,70);
y_profile_8=roi(:,80);
y_profile_9=roi(:,90);
y_profile_10=roi(:,100);
ALL_x=[x_profile_1 x_profile_2 x_profile_3
x_profile_4 x_profile_5 x_profile_6
x_profile_7 x_profile_8 x_profile_9
x_profile_10];
```

```
ALL_y=[y_profile_1 y_profile_2 y_profile_3
y_profile_4 y_profile_5 y_profile_6
y_profile_7 y_profile_8 y_profile_9
y_profile_10];

ALL_x_1=(1/2^16).*double(ALL_x);
ALL_x_OD=-log10(ALL_x_1);

ALL_y_1=(1/2^16).*double(ALL_y);
ALL_y_OD=-log10(ALL_y_1);

max_x=0;
max_y=0;
figure;
for i=1:10
x=1:101;
sigma=15; mu=40; A=3;
yx=ALL_x_OD(:,i);
yy=ALL_y_OD(:,i);

hold all
subplot(1,2,1);plot(x,yx,'.');
hold all
subplot(1,2,2);plot(x,yy,'.');

%% fitting
[sigmaNew1,muNew1,Anew1]=mygaussfit(x,yx);
[sigmaNew2,muNew2,Anew2]=mygaussfit(x,yy);
yx1=Anew1*exp(-(x-
muNew1).^2/(2*sigmaNew1^2));
yy1=Anew2*exp(-(x-
muNew2).^2/(2*sigmaNew2^2));
hold all;

for j=1:101
    if yx1(j)>max_x
        max_x(i)=yx1(j);
        xx_position(i)=j;
    end
    if yy1(j)>max_y
        max_y(i)=yy1(j);
        xy_position(i)=j;
    end
end

subplot(1,2,1);plot(x,yx1,'r');title('x
position');
subplot(1,2,2);plot(x,yy1,'b');title('y
position');
end
y_roi=round(mean(xy_position))+ycv-50;
x_roi=round(mean(xx_position))+xcv-50;

delta_x=x_roi-x_film;
delta_y=y_roi-y_film;

Im_r=double(b1(:,:,1));
Im_r=wiener2(Im_r, [5 5]);
Im_r=Im_r.*ggg1;

Im_g=double(b1(:,:,2));
Im_g=wiener2(Im_g, [5 5]);
Im_g=Im_g.*ggg2;

Im_rb=double(b1(:,:,1))./double(b1(:,:,3))
;
Im_rb=wiener2(Im_rb, [5 5]);
Im_rb=Im_rb.*ggg1;

Im_gb=double(b1(:,:,2))./double(b1(:,:,3))
Im_gb=wiener2(Im_gb, [5 5]);
Im_gb=Im_gb.*ggg2;

Im_b=double(b1(:,:,3));
Im_b=wiener2(Im_b, [5 5]);
Im_b=Im_b.*ggg3;

Im_r=Im_r(y_roi-5:y_roi+5,x_roi-
5:x_roi+5);
Im_g=Im_g(y_roi-5:y_roi+5,x_roi-
5:x_roi+5);
Im_rb=Im_rb(y_roi-5:y_roi+5,x_roi-
5:x_roi+5);
Im_gb=Im_gb(y_roi-5:y_roi+5,x_roi-
5:x_roi+5);
Im_b=Im_b(y_roi-5:y_roi+5,x_roi-
5:x_roi+5);
v=5*2+1;
for k=1:v
    for l=1:v
        k1=(k-1)*v+l;
        Niz_1_r(k1)=Im_r(k,l);
        Niz_1_g(k1)=Im_g(k,l);
        Niz_1_rb(k1)=Im_rb(k,l);
        Niz_1_gb(k1)=Im_gb(k,l);
        Niz_1_b(k1)=Im_b(k,l);
    end
end
Niz_2_r=sort(Niz_1_r);
Niz_2_g=sort(Niz_1_g);
Niz_2_rb=sort(Niz_1_rb);
Niz_2_gb=sort(Niz_1_gb);
Niz_2_b=sort(Niz_1_b);
vv=v*v;
for i=1:vv
    Niz_3_r(i)=Niz_2_r(vv-i+1);
    Niz_3_g(i)=Niz_2_g(vv-i+1);
    Niz_3_rb(i)=Niz_2_rb(vv-i+1);
    Niz_3_gb(i)=Niz_2_gb(vv-i+1);
    Niz_3_b(i)=Niz_2_b(vv-i+1);
end
clear Niz_4
for i=1:vv
    while Niz_3_r(i)>0
        Niz_4_r(i)=Niz_3_r(i);
        break
    end
    while Niz_3_g(i)>0
        Niz_4_g(i)=Niz_3_g(i);
        break
    end
    while Niz_3_rb(i)>0
        Niz_4_rb(i)=Niz_3_rb(i);
        break
    end
    while Niz_3_gb(i)>0
        Niz_4_gb(i)=Niz_3_gb(i);
        break
    end
    while Niz_3_b(i)>0
        Niz_4_b(i)=Niz_3_b(i);
        break
    end
end
```

```
mean_exp_r(kk)=mean2(Niz_4_r);
stdev_exp_r(kk)=std2(Niz_4_r);
mean_exp_g(kk)=mean2(Niz_4_g);
stdev_exp_g(kk)=std2(Niz_4_g);
mean_exp_rb(kk)=mean2(Niz_4_rb);
stdev_exp_rb(kk)=std2(Niz_4_rb);
mean_exp_gb(kk)=mean2(Niz_4_gb);
stdev_exp_gb(kk)=std2(Niz_4_gb);
mean_exp_b(kk)=mean2(Niz_4_b);
stdev_exp_b(kk)=std2(Niz_4_b);

% read unexposed films file

clear Im_red
figure;
imagesc(Imw)
axis image

Title(['Select cropping region for the UN-
EXPOSED image,',' Trial number: ',tn]);
clear h1
h1 = imcrop;%(Imw,[340 280 720 580]);
imagesc(h1)
Title(['Take 2 points for rotation - take
points on the upper horizontal edge of the
film,',' Trial number: ',tn])
axis image
colorbar
[x_r,y_r,z_r]=impixel;

% Rotate image
if (y_r(2)-y_r(1))==0
    angle_r=0;
else a_r=(abs(y_r(2)-y_r(1))/(y_r(2)-
y_r(1)))*acos(sqrt((x_r(2)-
x_r(1))^2)/sqrt((x_r(2)-x_r(1))^2+(y_r(2)-
y_r(1))^2));
    angle_r=a_r*180/3.14;
end
angle_r;

clear b*
b1=imrotate(h1,angle_r,'crop');
imagesc(b1)
axis image
Title(['Take ONLY ONE point: in the upper
left corner -> to select origin of the
film piece,',' Trial number: ',tn])
[x_film,y_film,zc]=impixel;

Im_r=double(b1(:,:,1));
Im_r=wiener2(Im_r, [5 5]);
Im_g=double(b1(:,:,2));
Im_g=wiener2(Im_g, [5 5]);
Im_rb=double(b1(:,:,1))./double(b1(:,:,3))
Im_rb=wiener2(Im_rb, [5 5]);
Im_gb=double(b1(:,:,2))./double(b1(:,:,3))
Im_gb=wiener2(Im_gb, [5 5]);
Im_b=double(b1(:,:,3));
Im_b=wiener2(Im_b, [5 5]);
xcc=x_film+delta_x;
ycc=y_film+delta_y;

Im_r=Im_r(ycc-5:ycc+5,xcc-5:xcc+5);
Im_g=Im_g(ycc-5:ycc+5,xcc-5:xcc+5);
Im_rb=Im_rb(ycc-5:ycc+5,xcc-5:xcc+5);
Im_gb=Im_gb(ycc-5:ycc+5,xcc-5:xcc+5);
Im_b=Im_b(ycc-5:ycc+5,xcc-5:xcc+5);
```

```
for k=1:v
    for l=1:v
        k1=(k-1)*v+l;
        Niz_1_r(k1)=Im_r(k,l);
        Niz_1_g(k1)=Im_g(k,l);
        Niz_1_rb(k1)=Im_rb(k,l);
        Niz_1_gb(k1)=Im_gb(k,l);
        Niz_1_b(k1)=Im_b(k,l);
    end
end

Niz_2_r=sort(Niz_1_r);
Niz_2_g=sort(Niz_1_g);
Niz_2_rb=sort(Niz_1_rb);
Niz_2_gb=sort(Niz_1_gb);
Niz_2_b=sort(Niz_1_b);

for i=1:vv
    Niz_3_r(i)=Niz_2_r(vv-i+1);
    Niz_3_g(i)=Niz_2_g(vv-i+1);
    Niz_3_rb(i)=Niz_2_rb(vv-i+1);
    Niz_3_gb(i)=Niz_2_gb(vv-i+1);
    Niz_3_b(i)=Niz_2_b(vv-i+1);
end

clear Niz_4
for i=1:vv
    while Niz_3_r(i)>0
        Niz_4_r(i)=Niz_3_r(i);
        break
    end
    while Niz_3_g(i)>0
        Niz_4_g(i)=Niz_3_g(i);
        break
    end
    while Niz_3_rb(i)>0
        Niz_4_rb(i)=Niz_3_rb(i);
        break
    end
    while Niz_3_gb(i)>0
        Niz_4_gb(i)=Niz_3_gb(i);
        break
    end
    while Niz_3_b(i)>0
        Niz_4_b(i)=Niz_3_b(i);
        break
    end
end

mean_unexp_r(kk)=mean2(Niz_4_r);
stdev_unexp_r(kk)=std2(Niz_4_r);
mean_unexp_g(kk)=mean2(Niz_4_g);
stdev_unexp_g(kk)=std2(Niz_4_g);
mean_unexp_rb(kk)=mean2(Niz_4_rb);
stdev_unexp_rb(kk)=std2(Niz_4_rb);
mean_unexp_gb(kk)=mean2(Niz_4_gb);
stdev_unexp_gb(kk)=std2(Niz_4_gb);
mean_unexp_b(kk)=mean2(Niz_4_b);
stdev_unexp_b(kk)=std2(Niz_4_b);

close all
end

% save images in tabular format.
```

## II. Fitting function, spikes detection and dark signal codes

```
% fitting function

function [sigma,mu,A]=mygaussfit(x,y,h)
if nargin==2, h=0.2; end
ymax=max(y);
xnew=[];
ynew=[];
for n=1:length(x)
    if y(n)>ymax*h;
        xnew=[xnew,x(n)];
        ynew=[ynew,y(n)];
    end
end
ylog=log(ynew);
xlog=xnew;
p=polyfit(xlog,ylog,2);
A2=p(1);
A1=p(2);
A0=p(3);
sigma=sqrt(-1/(2*A2));
mu=A1*sigma^2;
A=exp(A0+mu^2/(2*sigma^2));

% dark signal
clear;
a1=imread('Dark_field_001.tif');
a2=imread('Dark_field_002.tif');
a3=imread('Dark_field_003.tif');
a4=imread('Dark_field_004.tif');
a5=imread('Dark_field_005.tif');

b1=a1(:,:,1);
b1=double(b1);
b2=a2(:,:,1);
b2=double(b2);
b3=a3(:,:,1);
b3=double(b3);
b4=a4(:,:,1);
b4=double(b4);
b5=a5(:,:,1);
b5=double(b5);

Im=(b1+b2+b3+b4+b5)/5;
clear b*
clear a*
Imagesc(Im)
axis image
[xc,yc,zc]=impixel
Im=Im(yc(1):yc(2),xc(1):xc(2));
Imagesc(Im)
axis image
impixelinfo
[m,n]=size(Im);
mm=mean2(Im);

% Find pixels which differe by more than
5% from mean of the image
```

```
for i=1:m
    for j=1:n
        if Im(i,j)<0.95*mm
            Imc(i,j)=(-1)*Im(i,j);
        else
            if Im(i,j)>1.05*mm
                Imc(i,j)=(-1)*Im(i,j);
            else
                Imc(i,j)=Im(i,j);
            end
        end
    end
end

% Set bad pixels to -1, and good onet to
+1
for k=1:m
    for l=1:n
        k1=(k-1)*n+l;
        Niz_1(k1)=Imc(k,l);
    end
end
Niz_2=sort(Niz_1);
v=m*n;
for i=1:v
    Niz_3(i)=Niz_2(v-i+1);
end
clear Niz_4
for i=1:v
    while Niz_3(i)>0
        Niz_4(i)=Niz_3(i);
        break
    end
end
mean2(Niz_4)
std2(Niz_4)

% for spike removal, similar approach as
dark signal but without transforming the
matrix into array. i.e. preserving the
image dimensions.
```

# Bibliography


[1] E. Poon, B. Reniers, S. Devic, T. Vuong, and F. Verhaegen, "Dosimetric characterization of a novel intracavitary mold applicator for Ir-192 high dose rate endorectal brachytherapy treatment," Med. Phys. 33, 4515-4526 (2006).

[2] S. Chiu-Tsao, J. Hanley, J. Napoli, S. Davis, T. Pike, and L. DeWerd, "Determination of TG43 parameters for Cs-131 model CS-1R2 seed using radiochromic EBT film dosimetry," Med. Phys. 34, 2434-2435 (2007).

[3] Y. Le, E. Armour, and J. Wong "Evaluation of heterogeneity effect in intra-operative HDR (IOHDR) brachytherapy dose calculation using Monte Carlo simulation and GAFCHROMIC EBT film measurement," Med. Phys. 34, 2450-2450 (2007).

[4] M. Evans, S. Devic, and E. B. Podgorsak, "High dose-rate brachytherapy source position quality assurance using radiochromic film," Medical Dosimetry 32, 13-15 (2007).

[5] A. Bufacchi, A. Carosi, N. Adorante, S. Delle Canne, T. Malatesta, R. Capparella, R. Fragomeni, A. Bonanni, M. Leone, L. Marmiroli, and L. Begnozzi, "In vivo EBT radiochromic film dosimetry of electron beam for Total Skin Electron Therapy (TSET)." Phys. Med. 23, 67-72 (2007).

[6] D. Lightfoot, "Total skin electron beam commissioning with EBT film," Med. Phys. 33, 2146-2146 (2006).

[7] F.C. Su, Y. Liu, S. Stathakis, C. Shi, C. Esquivel, and N. Papanikolaou, "Dosimetry characteristics of GAFCHROMIC (R) EBT film responding to therapeutic electron beams," Appl. Rad. Isotop. 65, 1187-1192 (2007).

[8] B.J. Gerbi, and E.Y. Han, "The response of RadioChromic EBT film in high-energy electron beams," Med. Phys. 33, 2144-2144 (2006).

[9] M.J. Butson, T. Cheung, and P. K. N. Yu, Megavoltage x-ray skin dose variation with an angle using grid carbon fibre couch tops," Phys. Med. Biol. 52, N485-N492 (2007).

[10] S. Devic, J. Seuntjens, W. Abdel-Rahman, M. Evans, M. Olivares, E. B. Podgorsak, T. Vuong, and C. G. Soares, "Accurate skin dose measurements using radiochromic film in clinical applications," Med. Phys. 33, 1116-1124 (2006).

[11] F. C. Su, C. Y. Shi, and N. Papanikolaou "Clinical application of GAFCHROMIC (R) EBT film for in vivo dose measurements of total body irradiation radiotherapy." Appl. Rad. Isotop. 66, 389-394 (2008).

[12] E. Nioutsikou, Y. Seppenwoolde, J. R. Symonds-Tayler, B. Heijmen, P. Evans, and S. Webb, "Dosimetric investigation of lung tumor motion compensation with a robotic respiratory tracking system: An experimental study," Med. Phys. 35, 1232-1240 (2008).

[13] E. E. Wilcox, and G. Daskalov, "Use of EBT film for dose measurement in heterogeneous phantoms containing lung and bone equivalent materials for 6 MV photon fields in the range 0.5 to 4cm diameter produced by Cyberknife," Radiother. Oncol. 84, S53-S53 (2007).

[14] M. Polednik, Y. Abo Madyan, F. Schneider, D. Wolff, B. Bannach, U. Lambrecht, A. Wallin, M. Cwiekala, K. Maurer, F. Reif, F. Lohr, and F. Wenz, "Evaluation of calculation algorithms implemented in different commercial planning systems on an anthropomorphic breast phantom using film dosimetry," Strahlen. Onkol. 183, 667-672 (2007).

[15] E. E. Wilcox, and G. M. Daskalov "Evaluation of GAFCHROMIC (R) EBT film for CyberKnife (R) dosimetry," Med. Phys. 34, 1967-1974 (2007).

[16] E. E. Wilcox, and G. M. Daskalov, "Accuracy of dose measurements and calculations within and beyond heterogeneous tissues for 6 MV photon fields smaller than 4 cm produced by Cyberknife," Med. Phys. 35, 2259-2266 (2008).

[17] E. Sturtewagen, M. Fuss, L. Paelinck, C. De Wagter, and D. Georg, "Multi-dimensional dosimetric verification of stereotactic radiotherapy for uveal melanoma using radiochromic EBT film, Zeitschr. Med. Phys. 18, 27-36 (2008).

[18] G. Ciangaru, J.N. Yang, P.J. Oliver, M. Bues, M. Zhu, F. Nakagawa, H. Chiba, S. Nakamura, H. Yoshino, M. Umezawa, and A.R. Smith, "Verification procedure for isocentric alignment of proton beams," J. Appl. Clin. Med. Phys. 8, 65-75 (2007).

[19] N. Tomic, M. Gosselin, J. F. Wan, U. Saragovi, E. B. Podgorsak, M. Evans, and S. Devic, "Verification of Cell Irradiation Dose Deposition Using Radiochromic Film," Phys. Med. Biol. 52, 3121-3131 (2007).

[20] Radiation Oncology Physics: A Handbook for Teachers and Students, IAEA, 2005.

[21] R.D. Ashpole, H. Snyman, J.A. Bullimore, H.J. Appleby, B.H. Cummins, H.B. Coakham, A new technique of brachytherapy for malignant gliomas with caesium-137: A new method utilizing a remote afterloading system, Clinical Oncology, Volume 2, Issue 6, November 1990, Pages 333-337, ISSN 0936-6555, DOI: 10.1016/S0936-6555(05)80996-3

[22] Wang X, Liu R, Ma B, Yang K, Tian J, Jiang L, Bai ZG, Hao XY, Wang J, Li J, Sun SL, Yin H. High dose rate versus low dose rate intracavity brachytherapy for locally advanced uterine cervix cancer. Cochrane Database of Systematic Reviews 2010, Issue 7. Art. No.: CD007563. DOI: 10.1002/14651858.CD007563.pub2

[23] Ranjan K. Sur, C. Victor Levin, Bernard Donde, Vinay Sharma, Leszek Miszczyk, Subir Nag, Prospective randomized trial of HDR brachytherapy as a sole modality in palliation of advanced esophageal carcinoma--an International Atomic Energy Agency study, International Journal of Radiation Oncology*Biology*Physics, Volume 53, Issue 1, 1 May 2002, Pages 127-133, ISSN 0360-3016, DOI: 10.1016/S0360-3016(02)02702-5

[24] C G Soares, G Douysset and M G Mitch, "Primary standards and dosimetry protocolos for brachytherapy sources," Metrologia 46, S80–S98 (2009)

[25] R. Nath, L.L. Anderson, G. Luxton, K.A. Weaver, J.F. Williamson and A.S. Meigooni , Dosimetry of interstitial brachytherapy sources: Recommendations of the AAPM Radiation Therapy Committee Task Group No. 43. Med. Phys. 22 (1995), pp. 209–234.

[26] L.L. Anderson, R. Nath, K.A. Weaver (ICWG), Interstitial brachytherapy: Physical, biological, and clinical considerations. New York: Raven; 1990

[27] J. A. Meli, A. S. Meigooni, R. Nath, "On the choice of phantom material for the dosimetry of sources." International journal of radiation oncology, biology, physics 14(1988):587.

[28] L. L. Meisberger, R. J. Keller, and R. J. Shalek, "The effective attenuation in water of the γ-rays of gold-198, iridium-192, cesium-137, radium-226, and cobalt-60," Radiology 90, 953–957 (1968)

[29] M. J. Berger, "Energy deposition in water by photons from point isotropic sources MIRD/Pamphlet No 2", J. Nucl. Medicine Suppl. 1 (1968)

[30] S. Webb and R. A. Fox, "The dose in water surrounding point isotropic gamma-ray emitters", Br. J. Radiol. 52482-4 (1979)

[31]AL Boyer, PD Cobb, K. R, Kase and TS Chen, 102ir Hospital Cali- bration Procedures, In Recent Advances in Brachytherapy Physics, edited by D. A. Shearer, AAPM Monograph 7 (American Institute of Physics, New York, 1981).

[32] D C Kocher, "Radioactive decay tables US Department of Energy Technical Information Center Report DOE/TIC-1102C" (1981)

[33] Glasgow G P 1981 Exposure rate constants for filtered 192Ir sources Med. Phys. 8 502-3

[34] RG. Dale, "A Monte Carlo Derivation of parameters for use in the tissue dosimetry if medium and low-energy nuclides", British J Radiol. 55:748-757 (1982).

[35] R. Nath, L. Anderson, D. Jones, C. Ling, R. Loevinger, J. Williamson and W. Hanson, "Specification of brachytherapy source strength: A report by Task Group 32 of the American Association of Physicists in Medicine". AAPM Report No. 21 (NY: American Institute of Physics) (1987).

[36] C. Thomason, T. R. Mackie, and M. J. Lindstrom, Effect of source encapsulation on the energy spectra of 192Ir and 137Cs seed sources, Phys. Med. Biol. 36, 495 – 505 (1991).

[37] J. F. Williamson, "Comparison of measured and calculated dose rates in water near I-125 and Ir-192 seeds". Med. Phys. 18, 776–786 (1991).

[38] S. J. Goetsch, F. H. Attix, D. W. Pearson, B. R. Thomadsen; "Calibration of 192 Ir high-dose-rate afterloading systems"; Medical Physics 18, 462-467 (1991).

[39] J. F. Williamson, B. M. Coursey, L. A. DeWerd, W. F. Hanson, and R. Nath, "Dosimetric prerequisites for routine clinical use of new low energy photon interstitial brachytherapy sources," Med. Phys. 25, 2269–2270 (1998).

[40] G. M. Daskalov, E. Löffler, and J. F. Williamson, "Monte Carlo-aided dosimetry of a new high dose-rate brachytherapy source," Med. Phys. 25, 2200–2208 (1998)

[41] N. Reynaert, F. Verhaegen, and H. Thierens "In-water calibration of PDR 192Ir brachytherapy sources with an NE2571 ionization chamber.", Phys. Med. Biol. 43 2095 (1998);

[42] N Reynaert, M Van Eijkeren, Y Taeymans and H Thierens "Dosimetry of Ir-192 sources used for endovascular brachytherapy", Phys. Med. Biol. 46 499–516 (2001)

[43] M. J. Rivard, B. M. Coursey, L. A. DeWerd, W. F. Hanson, M. S. Huq, G S. Ibbott, M. G. Mitch, R. Nath, and J. F. Williamson, "Update of AAPM Task Group No. 43 Report: A revised AAPM protocol for brachytherapy dose calculations," Med. Phys. **31**, 633–674 _2004_.

[44] J.A. Sayeg and R.C. Gregory, "A new method for characterizing beta-ray ophthalmic applicator sources." Med. Phys. 18 (1991)

[45] C. G. Soares,. "Calibration of ophthalmic applicators at NIST: A revised approach." Med Phys 18:787–793. (1991)

[46] C. G. Soares, S. Vynckier, H. Järvinen, W. G. Cross, J. Hokkanen, P. Sipilä, D. Flühs, B. Schaeken, F. A. Mourtada, G. A. Bass, and T. T. Williams. "Dosimetry of beta-ray ophthalmic applicators: Comparison of different measurement methods." Med. Phys 28:1373–1384. (2001)

[47] S. T. Chiu-Tsao, , T. L. Duckworth, N. S. Patel, J. Pisch, and L. B. Harrison.. "Verification of Ir-192 near source dosimetry using GAFCHROMIC® film." Med Phys 31:201–207. (2004)

[48] S D Sharma, C Bianchi, L Conte, R Novario and B C Bhatt, "Radiochromic film measurement of anisotropy function for high-dose-rate Ir-192 brachytherapy source." Phys Med Biol. Sep 7;49(17):4065-72. (2004)

[49] D Baltas, R Kramer and E Loffler, "Measurements of the anisotropy of the new Ir-192 source for the microSelectron-HDR International Brachytherapy: Programme and Abstracts", 7th Int. Brachytherapy Working Conf. (Baltimore, MD) (Veenendal, The Netherlands: Nucletron International B V) pp 290–306 (1992)

[50] J C Anctil, B G Clark and C J Arsenault, "Experimental determination of dosimetry functions of Ir-192 sources", Med. Phys. 25 2279–87 (1998)

[51] J. F. Williamson and Z. Li, ''Monte Carlo aided dosimetry of the microSelectron pulsed and high dose rate 192Ir sources,'' Med. Phys. **22**, 809–819 (1995)

[52] S. T. Chiu-Tsao, D. Medich, J. Munro 3rd, "The use of new GAFCHROMIC EBT film for $^{125}I$ seed dosimetry in Solid Water phantom". Med. Phys. 35, 3787 (2008).

[53] Y Yang, MJ Rivard."Monte Carlo simulations and radiation dosimetry measurements of peripherally applied HDR 192Ir breast brachytherapy D-shaped applicators." Med Phys. Mar; 36(3):809-15. (2009)

[54] P. Sellakumar, A. Sathish Kumar, Sanjay S. Supe, M.R. Anand, K. Nithya, S. Sajitha,"Evaluation of dosimetric functions for Ir-192 source using radiochromic film." Nuclear Instruments and Methods in Physics Research B 267 1862–1866 (2009)

[55] A. Sarfehnia, I. Kawrakow, J. Seuntjens,"Direct measurement of absorbed dose to water in HDR 192Ir brachytherapy: Water calorimetry, ionization chamber, Gafchromic Film, and TG-43." Med Phys Vol. 37, No. 4, April (2010)

[56] D. M. Duggan, C. W. Coffey II, J. L. Lobdell, and M. C. Schell, "Radiochromic film dosimetry of a high dose rate beta source for intravascular brachytherapy," Med. Phys. 26, 2461–2464 (1999)

[57] W. L. McLaughlin and M.F.Desrosiers, "Dosimetry systems for radiation processing," Radiat. Phys. Chem. 46, 1163–1174 (1995)

[58] L. E. Reinstein, G. R. Gluckman, and H. I. Amols, ''Predicting optical densitometer response as a function of light source characteristics for radiochromic film dosimetry,'' Med. Phys. 24, 1935–1942 (1997).

[59] S. Devic, J. Seuntjens, G. Hegyi, E. B. Podgorsak, C. G. Soares, A. S. Kirov, I. Ali, J. F. Williamson, A. Elizondo, "Dosimetric properties of improved GafChromic films for seven different digitizers," Med. Phys. 31, 2392-2401 (2004).

[60] S. Devic, N. Tomic, Z. Pang, J. Seuntjens, E. B. Podgorsak, and C. G. Soares, "Absorption spectroscopy of EBT model GAFCHROMIC (TM) film," Med. Phys. 34, 112-118 (2007).

[61] B. Lynch, M. Ranade, J. Li, and J. Dempsey, "Characteristics of a new very high sensitivity radiochromic film," Med. Phys. 31, 1873-1873 (2004).

[62] M. J Butson, P. K N Yu, T. Cheung and P. Metcalfe, "High sensitivity radiochromic film dose comparisons", Phys. Med. Biol. 47, N291-N295 (2002).

[63] R. D. H. Chu, G. VanDyke, D. F. Lewis, K. P. J. O'Hara, B. R'. Buckland, and F. Dinelle, "GafChromic Dosimetry Media: A New High Dose Rate Thin Film Routine Dosimeter and Dose Mapping Tool," Radiat. Phys. Chem. 35, 767-773 (1990).

[64] W. L. McLaughlin, Y. D. Chen, C. G. Soares, A. Miller, G. Van Dyke, and D. F. Lewis, "Sensitometry of the response of a new radiochromic film dosimeter to gamma radiation and electron beams," Nucl. Instrum. Methods Phys. Res. A 302, 165–176 (1991)

[65] M. J Butson, T. Cheung and, P. K N Yu "Absorption spectra variations of EBT radiochromic film from radiation exposure," Phys. Med. Biol. 50, N135-N140 (2005).

[66] S. Devic, J. Seuntjens, E. Sham, E. B. Podgorsak, A. S. Kirov, R. C. Schmidtlein, C. G. Soares, "Precise radiochromic film dosimetry using a flat-bed document scanner," Med. Phys. 32, 2245-2253 (2005).

[67] L. Xu, M. McEwen, C. Cojocaru, and B. Faddegon, "Measurement of Lateral Dose Distributions Using GafChromic EBT Films and PTW Starcheck 2-D Array," Med. Phys. 36, 2624-2624 (2009).

[68] S. Devic, S. Aldelaijan, H. Mohammed, N. Tomic, L. Liang, F. DeBlois, J. Seuntjens, "Absorption spectra time evolution of EBT-2 model GAFCHROMIC$^{TM}$ film." Med Phys 37(5)

[69] M. J. Butson, T. Cheung, P. K. N. Yu and H. Alnawaf, "Dose and absorption spectra response of EBT2 Gafchromic film to high energy x-rays," Australas. Phys. Eng. Sci. Med. Vol. 32, No 4, (2009)

[70] S. T.Chiu-Tsao, Y. Ho, R. Shankar, L. Wang, and L. B. Harrison.. "Energy dependence of response of new high sensitivity radiochromic films for megavoltage and kilovoltage radiation energies." Med Phys 32:3350–3354. (2005)

[71] M. J Butson, T. Cheung, P. K.N. Yu, "Weak energy dependence of EBT gafchromic film dose response in the 50 kVp-10 MVp X-ray range", Applied Radiation and Isotopes, Volume 64, Issue 1, Pages 60-62, ISSN 0969-8043, DOI: 10.1016/j.apradiso.2005.07.002. (2006)

[72] M. A. Ebert, A. H. Asad, and S. A. Siddiqui, "Suitability of radiochromic films for dosimetry of very-low energy x-rays," J. Appl. Clin. Med. Phys. 10, 232–240 (2009)

[73] J. G. H. Sutherland and D. W. O. Rogers, "Monte Carlo calculated absorbed-dose energy dependence of EBT and EBT2 film", Med. Phys. 37, 1110 (2010).

[74] J. F. Dempsey, D. A. Low, A. S. Kirov, and J. F. Williamson, "Quantitative optical densitometry with scanning-laser film digitizers," Med. Phys. 26, 1721-1731 (1999).

[75] N. Klassen, L. Zwan, and J. Cygler, ''GafChromic MD-55: investigated as a precision dosimeter,'' Med. Phys. 24, 1924-1934 (1997).

[76] M. J. Butson, P. K. N. Yu, T. Cheung and D. Inwood, "Polarization effects on a high-sensitivity radiochromic film," Phys. Med. Biol. 48, N207-N211 (2003).

[77] B C Ferreira, M C Lopes and M Capela, "Evaluation of an Epson flatbed scanner to read Gafchromic EBT films for radiation dosimetry." Phys. Med. Biol. 54 1073–1085 (2009)

[78]L. Paelinck, W. De Neve and C. De Wagter, "Precautions and strategies in using a commercial flatbed scanner for radiochromic film dosimetry", Phys Med Biol 52 (1), pp. 231–242. (2007)

[79] B. D. Lynch, J. Kozelka, M. K. Ranade and J. G. Li, W. E. Simon, J. F. Dempsey, "Important considerations for radiochromic film dosimetry with flatbed CCD scanners and EBT GAFCHROMIC® film", Med. Phys. 33, 4551 (2006).

[80] M Martisikova, B Ackermann, S Klemm and O Jakel "Use of Gafchromic R_ EBT films in heavy ion therapy", Nucl. Instrum. Methods Phys. Res. A 591 171–3 (2008)

[81] M. Fuss, E. Sturtewagen, C. De Wagter, and D. Georg, "Dosimetric characterization of GafChromic EBT film and its implication on film dosimetry quality assurance," Phys. Med. Biol. 52, 4211-4225 (2007).

[82] S. Devic, Y. Wang, N. Tomic, and E. B. Podgorsak, "Sensitivity of linear CCD array based film scanners used for film dosimetry," Medical Physics, 33, 3993-3996 (2006).

[83] L. Menegotti, A. Delana, and A. Martignano, "Radiochromic film dosimetry with flatbed scanners: A fast and accurate method for dose calibration and uniformity correction with single film exposure," Med. Phys. 35, 3078–3085 (2008).

[84] A. Rink, I.A. Vitkin, and D.A. Jaffray, "Energy dependence (75 kVp to 18 MV) of radiochromic films assessed using a real-time optical dosimeter," Med. Phys. 34, 458-463 (2007).

[85] S. Aldelaijan, S. Devic, H. Mohammed, N. Tomic, . Liang, F. DeBlois, J. Seuntjens "Evaluation of EBT-2 Model GAFCHROMIC$^{TM}$ Film Performance in Water," Med. Phys. (2010), in press.

[86] J. Kalef-Ezra and K. Karava, "Radiochromic film dosimetry: Reflection vs transmission scanning". DOI: 10.1118/1.2919092

[87] L Richley, A C John, H Coomber and S Fletcher, "Evaluation and optimization of the new EBT2 radiochromic film dosimetry system for patient dose verification in radiotherapy", Phys. Med. Biol. 55 2601–2617 (2010)

[88] M. J. Butson, T. Cheung, and P. K. N. Yu, "Radiochromic film dosimetry in water phantoms," Phys. Med. Biol. 46, N27-N31 (2001).

[89] L. J. van Battum, D. Hoffmans, H. Piersma, and S. Heukelom. "Accurate dosimetry with GafChromic (TM) EBT film of a 6 MV photon beam in water: What level is achievable?" Med. Phys. 35, 704-716 (2008).

[90] A. Rink, D. F. Lewis, S. Varma, I. A. Vitkin, and D. A. Jaffray, " Temperature and hydration effects on absorbance spectra and radiation sensitivity of a radiochromic medium," Med. Phys. 35, 4545-4555 (2008).

[91] H. Bouchard, F. Lacroix, G. Beaudoin, J. Carrier, and I. Kawrakow, "On the characterization and uncertainty analysis of radiochromic film dosimetry," Med. Phys. 36, 1931–1946 (2009)

[92] S. Devic, N. Tomic, C. G. Soares, and E. B. Podgorsak, "Optimizing the Dynamic Range Extension of a Radiochromic Film Dosimetry System," Med. Phys. 36, 429-437 (2009).

[93] M. J. Butson, T. Cheung, and P. K. N. Yu, "Radiochromic film dosimetry in water phantoms," Phys. Med. Biol. 46, N27-N31 (2001).

[94] P. R. Bevington and D. K. Robinson, "Data Reduction and Error Analysis for the Physicsal Sciences", WCB/McGraw-Hill, Boston (1992)

[95] Silberstein J. Opt. Soc. Am. 35, 93–107, (1945)

[96] F. del Moral,a J. A. Vázquez, and J. J. Ferrero, P. Willisch and R. D. Ramírez, A. Teijeiro, A. López Medina, B. Andrade, J. Vázquez, F. Salvador, D. Medal, and M. Salgado, V. Muñoz, "From the limits of the classical model of sensitometric curves to a realistic model based on the percolation theory for GafChromic™ EBT films", DOI: 10.1118/1.3187226

[97] X. R. Zhu, S. Yoo, P. A. Jursinic, D. F. Grimm, F. Lopez, J. J. Rownd, and M. T. Gillin, "Characteristics of sensitometric curves of radiographic films", DOI: 10.1118/1.1568979

[98] C. Fiandra, U. Ricardi, R. Ragona, S. Anglesio, F. R. Giglioli, E. Calamia, and F. Lucio, "Clinical use of EBT model Gafchromic™ film in radiotherapy," Med. Phys. 33, 4314–4319 (2006)

[99] F Crop, B Van Rompaye, L Paelinck, L Vakaet, H Thierens and C De Wagter, "On the calibration process of film dosimetry: OLSinverse regression versus WLS inverse prediction", Phys. Med. Biol. 53 3971–3984 (2008)

[100] M. A. Stevens, J. R. Turner, R. P. Hugtenburg, and P.H. Butler, "High-resolution dosimetry using radiochromic film and a document scanner," Phys. Med. Biol. 41, 2357-2365 (1996).

[101] A. S. Aydarous, P. J. Darley and M. W. Charles, A wide dynamic range, high-spatial-resolution scanning system for radiochromic dye films, Phys. Med. Biol. 46, 1379–1389 (2001).

[102] J. Seuntjens, M. Olivares, M. Evans, E. Podgorsak, "Absorbed dose to water reference dosimetry using solid phantoms in the context of absorbed-dose protocols" (Med Phys. 2005 Sep;32(9):2945-53.)